UNIVERSIDADE ESTADUAL DE CAMPINAS
FACULDADE DE ENGENHARIA MECÂNICA
E INSTITUTO DE GEOCIÊNCIAS

FABIÁN ANDRÉS TAPIAS HERNÁNDEZ

SURFACTANT-POLYMER FLOODING IN SANDSTONES EVALUATED BY COMPUTED TOMOGRAPHY

INJEÇÃO DE SURFACTANTE-POLÍMERO EM ARENITOS AVALIADA COM TOMOGRAFIA COMPUTADORIZADA

CAMPINAS
2018

FABIÁN ANDRÉS TAPIAS HERNÁNDEZ

SURFACTANT-POLYMER FLOODING IN SANDSTONES EVALUATED BY COMPUTED TOMOGRAPHY

INJEÇÃO DE SURFACTANTE-POLÍMERO EM ARENITOS AVALIADA COM TOMOGRAFIA COMPUTADORIZADA

Dissertation presented to the Mechanical Engineering Faculty and Geosciences Institute of the University of Campinas in partial fulfillment of the requirements for the degree of Master in Petroleum Sciences and Engineering in the area of Reservoirs and Management.

Dissertação apresentada à Faculdade de Engenharia Mecânica e Instituto de Geociências da Universidade Estadual de Campinas como parte dos requisitos exigidos para a obtenção do título de Mestre em Ciências e Engenharia de Petróleo na área de Reservatórios e Gestão.

Orientador: Profa. Dra Rosângela Barros Zanoni Lopes Moreno.

Este exemplar corresponde à versão final da Dissertação defendida pelo aluno Fabián Andrés Tapias Hernández e orientada pela Profa. Dra Rosângela Barros Zanoni Lopes Moreno.

_____

Assinatura do Orientador

CAMPINAS

2018

FICHA CATALOGRÁFICA

Agência(s) de fomento e nº(s) de processo(s): CAPES, 33003017

Ficha catalográfica
Universidade Estadual de Campinas
Biblioteca da Área de Engenharia e Arquitetura
Luciana Pietrosanto Milla - CRB 8/8129

T162s

Tapias Hernández, Fabián Andrés, 1991-
Surfactant-polymer flooding in sandstones evaluated by computed tomography / Fabián Andrés Tapias Hernández. – Campinas, SP : [s.n.], 2018.

Orientador: Rosangela Barros Zanoni Lopes Moreno.
Dissertação (mestrado) – Universidade Estadual de Campinas, Faculdade de Engenharia Mecânica.

1. Surfactantes. 2. Polímeros. 3. Tomografia computadorizada. 4. Comportamento de fases. 5. Recuperação avançada de petróleo. I. Moreno, Rosangela Barros Zanoni Lopes, 1966-. II. Universidade Estadual de Campinas. Faculdade de Engenharia Mecânica. III. Título.

Informações para Biblioteca Digital

Título em outro idioma: Injeção de surfactante-polímero em arenitos avaliada com tomografia computadorizada
Palavras-chave em inglês:
Surfactant
Polymer
Computed tomography
Phase behavior
Enhanced oil recovery
Área de concentração: Reservatórios e Gestão
Titulação: Mestre em Ciências e Engenharia de Petróleo
Banca examinadora:
Rosangela Barros Zanoni Lopes Moreno [Orientador]
Maria Aparecida de Melo
Watson Loh
Data de defesa: 24-01-2018
Programa de Pós-Graduação: Ciências e Engenharia de Petróleo

UNIVERSIDADE ESTADUAL DE CAMPINAS
FACULDADE DE ENGENHARIA MECÂNICA
E INSTITUTO DE GEOCIÊNCIAS

DISSERTAÇÃO DE MESTRADO ACADÊMICO

SURFACTANT-POLYMER FLOODING IN SANDSTONES EVALUATED BY COMPUTED TOMOGRAPHY

INJEÇÃO DE SURFACTANTE-POLÍMERO EM ARENITOS AVALIADA COM TOMOGRAFIA COMPUTADORIZADA

Autor: Fabián Andrés Tapias Hernández
Orientador: Profa. Dra Rosângela Barros Zanoni Lopes Moreno.

A Banca Examinadora composta pelos membros abaixo aprovou esta Dissertação:

Profa. Dra Rosângela Barros Zanoni Lopes Moreno, Presidente
DE / FEM / UNICAMP

Prof. Dr Watson Loh.
IQ / UNICAMP

Dra. Maria Aparecida de Melo
PETROBRAS

A Ata de defesa com as respectivas assinaturas dos membros encontra-se no processo de vida acadêmica do aluno.

Campinas, Janeiro 24 de 2018.

DEDICATION

To my beloved parents, Yaneth and Gustavo, whose immense love inspired my path far and beyond.

ACKNOWLEDGMENTS

I thank God for guidance and to give me the constancy to accomplish my dreams.

To my family, who have always been available to listen and give me a word of encouragement.

To my beloved companion of life, always patient and willing to be a support in the difficult days.

I also express my gratitude to Profa.Dra. Rosângela Barros Zanoni Lopes Moreno, for her teachings in this research and sharing her knowledge and experience with me.

To my dear friends for life, Ricardo V, and Leandro F, their friendship and help were essential to complete this work. I will always remember our life experiences together.

A special note of gratitude to my old and dear friends: Alba, Silvia, Catalina, Maria Libia, Nicolas, and Edwar. Love you all.

To all my friends and colleagues from LABORE, CEPETRO, and FEM at UNICAMP, for their friendship and help in the details of this dissertation.

Finally, I would like to thank the Coordenação de Aperfeiçoamento de Pessoal de Nível Superior (CAPES), the Department of Energy DE-FEM-UNICAMP, and to the project "Advanced image techniques for the reservoir characterization and improvement the oil recovery factor", developed for Universidad Industrial de Santander (UIS), Ecopetrol S.A and Colciencias for their information and support of this work.

RESUMO

O processo de Surfactante-Polímero (SP) faz parte dos métodos de recuperação melhorada com químicos (CEOR) reconhecidos por atingir maiores fatores de recuperação. Esses métodos tornaram-se atraentes novamente devido à crescente demanda global por energia. Entretanto, ainda caracterizam-se como um desafio para à indústria petrolífera principalmente pela dificuldade para planejar e prever seu comportamento em escala de campo. A compreensão dos fenômenos associados ao processo CEOR é de vital importância. Por estas razões, este trabalho apresenta uma avaliação do processo Surfactante-Polímero (SP) incluindo tomografia computadorizada (CT). O estudo abrange o desenvolvimento do processo em escala de laboratório e descreve as interações químicas e a dinâmica dos fluidos no meio poroso. A pesquisa começa com uma extensa revisão da literatura para determinar as condições gerais de aplicação do processo SP. Além disso, são propostos alguns critérios de seleção para escolher ou avaliar um campo de referência e reproduzir suas propriedades petrofísicas e de fluidos experimentalmente. A primeira etapa experimental deste trabalho consistiu de um estudo detalhado sobre as interações entre os fluidos e os produtos químicos. Esta etapa visou determinar a influência de variáveis tais como temperatura, conteúdo de íons monovalentes e divalentes, e concentração de surfactante no comportamento reológico e viscoelástico das soluções poliméricas. As interações entre as soluções aquosas e a fase oleica foram estudadas por meio de testes de tensão interfacial e comportamento de fases. Além disso, a lei de Bancroft foi empregada como uma ferramenta qualitativa para verificar o tipo de microemulsão obtido. Como resultado, as soluções a serem usadas nos testes de deslocamento foram escolhidas. A segunda parte do estudo abordou atividades previas aos testes de deslocamento. Para isso, amostras de arenito foram selecionadas e caraterizadas de acordo com os critérios de seleção propostos. Em seguida, uma bancada experimental, incluindo um tomógrafo, foi planejada e montada com o objetivo de avaliar a recuperação de óleo por injeção convencional de água e por injeção de surfactante-polímero como método secundário e terciário. O estudo desenvolvido permitiu conhecer o comportamento reológico e viscoelástico da mistura de surfactante-polímero a ser injetada, avaliar o perfil de porosidade e saturação ao longo da amostra de rocha através de imagens de CT e avaliar a eficiência de ambos métodos de recuperação por injeção convencional de água e recuperação melhorada por injeção de surfactante-polímero. A análise comparativa dos resultados de razão agua-óleo (WOR) e corte de agua (Wcut) mostraram a melhoria da mobilidade e a redução da saturação de óleo residual devido à injeção de uma

mistura SP sobre a água convencional. Além disso, os resultados comparativos do fator de recuperação de óleo (FR) obtidos através do balanço volumétrico de material e da tomografia computadorizada apresentaram um aumento de FR de 17 e 10 pontos percentuais para esquemas de injeção secundária e terciária, respectivamente. Finalmente, discute-se a eficácia da técnica de imagem e suas vantagens como uma poderosa ferramenta para visualizar imagens 2D e 3D durante os testes de deslocamento. Com isso, pode-se melhorar o entendimento sobre o escoamento de fluidos em meios porosos.

Palavras Chave: Surfactante, Polímero, Comportamento Reológico, Comportamento de fases, Testes de Deslocamento, Tomografia Computadorizada.

ABSTRACT

The Surfactant-Polymer (SP) process is a type of Chemical Enhanced Oil Recovery (CEOR) methods known for the possibility of reaching higher oil recovery factors. These methods have become attractive again due to the growing global demand for energy. However, they are still a challenge for the petroleum oil industry mainly because of the difficulty in designing and forecasting the process behavior in the field scale. The understanding of the phenomena associated with a CEOR process is of vital importance. For these reasons, this work presents the assessment of a Surfactant-Polymer (SP) process evaluated by computed tomography (CT). The study covers the development of the process on a laboratory scale and describes the chemical interactions and fluid dynamics in the porous media. The research begins with an extensive literature review that allows the determination of general conditions to apply an SP process. Furthermore, some screening criteria are proposed aims to select a reference field to recreate their petrophysical and fluids properties experimentally. The first experimental stage of this research consists of a detailed study to understand the interactions between the fluids and chemical products (Brine, Oil, Polymer, and Surfactant). This step aims to determine the influence of variables such as temperature, monovalent and divalent ions content, and surfactant concentration on the rheological and viscoelastic behavior of the polymer solutions. The interactions between the aqueous solutions and oil phase were studied through interfacial tension and phase behavior tests. Besides that, the Bancroft Rule's was employed as a qualitative tool to verify the type of the microemulsion obtained. As a result, the solutions to be used in core flooding tests were selected. The second part of the study covered the laboratory activities conducted previously to the core flooding tests. For this, sandstone samples were previously characterized and chosen according to the screening criteria. Afterward, an experimental workbench including the CT scan was assembled aiming to evaluate the oil recovery by conventional waterflooding and by SP floodings as secondary and tertiary oil recovery methods. The developed study allowed to know the rheological and viscoelastic behavior of the tailor-made surfactant-polymer blend, evaluate the porosity and saturation profiles along the rock sample through CT images and assess the efficiency of both recovery methods - the conventional waterflooding and the advanced SP. Comparative analysis of the water-oil ratio (WOR) and water cut (Wcut) results elucidated the mobility ratio improvement and oil residual saturation reduction due to the injection of an SP blend over conventional water. Also, comparative results of oil recovery factor (FR) obtained through the volumetric material

balance and CT scan show an FR increases of 17 and 10 percentage points for secondary and tertiary injection schemes, respectively. Finally, this work includes a discussion about the effectiveness of the imaging technique and its advantages as a powerful tool to visualize 2D and 3D images during core flooding tests and understanding of fluid flow through a porous media.

Key Word: Surfactant, Polymer, Rheological Behavior, Phase Behavior, Core flooding tests, Computed Tomography.

FIGURES LIST

TABLES LIST

ABBREVIATIONS AND ACRONYMS LIST

ACN	Alkane carbon number
ASP	Alkali/Surfactant/Polymer
AST	Amplitude sweep tests
BT	Breakthrough
CEOR	Chemical Enhanced Oil Recovery
CMC	Critical Micellar Concentration
CT	Computed Tomography
CT 1	First method used to estimate the saturation profile through CT
CT 2	Second method used to estimate the saturation profile through CT
CT 3	Third method used to estimate the saturation profile through CT
DP	Differential Pressure
EACN	Effective Alkane Carbon Number
EOR	Enhanced Oil Recovery
FR	Oil Recovery Factor
FST	Frequency sweep tests
HPAM	Partially Hydrolyzed Polyacrylamide
IFT	Interfacial Tension
LVR	Linear Viscoelastic Region
MB	Material Balance
PAM	Polyacrylamide
PF	Polymer Flooding
SB	Synthetic Brine
SDS	Sodium Dodecyl Sulfate
SEM	Scanning Electron Microscope
SF	San Francisco
SP	Surfactant-Polymer
STOOIP	Stock Tank Original Oil in Place
TDS	Total Dissolved Solids
Test 1	Waterflooding
Test 2	Surfactant-polymer flooding as secondary oil recovery method
Test 3	Surfactant-polymer flooding as tertiary oil recovery method

TMO	Total Mobilized oil
PV	Pore Volume
PVInj	Injected Pore Volume
WF	Waterflooding
Wcut	Water Cut
WOR	Water-oil-Ratio
XG	Xanthan Gum

SYMBOLS LIST

θ	Contact angle
σ	Interfacial tension
σ_{so}	Interfacial tension between the solid and oil.
σ_{sw}	Interfacial tension between the solid and water.
σ_{wo}	Interfacial tension between the water and oil.
σ_{om}	Interfacial tension between the oil and microemulsion phases.
σ_{wm}	Interfacial tension between the water and microemulsion phases.
γ	Shear rate
γ_c	Critical shear rate
v	Pore flow velocity of displacing fluid
μ	Apparent fluid viscosity
λ	Mobility
τ	Linear attenuation coefficient
ρ	Bulk density
ΔP	Differential Pressure
ΔE_η	Viscous activation energy
o/w	Oil in water
w/o	Water in oil
A	Aqueous level
A_{cs}	Rock Sample Cross Section
D	Constant characteristic of the polymer solution
C	Height of Mercury Column
C_y	Optimum salinity
C_s^o	Concentration of the solute in the oleic phase
C_s^w	Concentration of the solute in the aqueous phase
cm	Centimeter
cp	Centipoise
F_v	Viscous forces
F_c	Capillary forces
g	Gravity

G’	Elastic modulus
G’’	Viscous modulus
h	Thickness
h_w	Height of Water Column
H	Hounsfield units
I_o	Incident X-Ray intensity
I	Intensity remaining
I_{10}	Iododecane
K_a	Absolute permeability of the porous media.
K_e	Partitioning coefficient
K_g	Gas Permeability
K_i	Effective permeability of the porous media for fluid i
K_{ri}	Relative permeability of the porous media to fluid i
L	Rock sample Length
L_i	Stretch of Rock sample length
M_r	Mobility ratio
M_e	Microemulsions
N_c	Capillary Number
N_p	Oil produced
NaCl	Sodium Chloride
NaI	Sodium Iodide
O	Oil
P_c	Capillary pressure
P_{nw}	Pressure non-wetting phase
P_w	Pressure wetting phase
ppm	Parts Per Million
P4	Pressure tap 4
P5	Pressure tap 5
Q_g	Gas Rate
R	Universal gas constant
S_o	Oil Saturation
S_{or}	Oil residual saturation
S_w	Water Saturation

S_{wi}	Initial Water Saturation
S_t^w	Saturation of water at any time in a pixel of tomographic image
S_t^o	Saturation of oil at any time in a pixel of tomographic image
S_t^{me}	Saturation of microemulsion at any time in a pixel of tomographic image
T	Absolute temperature
V_o	Oil solubilized volume
V_w	Water solubilized volume
V_s	Surfactant volume in the microemulsion phase
V_{om}	Oil solubilization parameter
V_{wm}	Water solubilization parameter
W	Water
W_p	Water produced
Z	Atomic number

SUMMARY

1 INTRODUCTION

1.1 Scope

Nowadays, the growing global energy demand and the gradual revitalization of the oil prices (BRITISH PETROLEUM, 2017) stimulate the reactivation of oil fields that in the past were considered non-profitable. These fields are known as mature oil fields, and according to TELES et al. (2015), they are defined as those fields that already produced 40% of the recoverable oil volume based on initial studies. Usually, after the depletion of the natural energy of the reservoir (primary recovery methods) and the application of water or gas injection (secondary recovery methods) to pressure maintenance, mature fields require the implementation of some Enhanced Oil Recovery (EOR) technique. Nevertheless, despite the usual application of EOR methods in the advanced stage of the reservoirs life cycle, they also can be utilized at any time during the field development aiming to improve the oil recovery factor.

Several authors (LAKE, 1991; SHANDRYGIN; LUTFULLIN, 2008; SHENG, 2013; TABER; MARTIN; SERIGHT, 1997) have presented a classification of EOR methods dividing them into three broad categories: thermal, miscible and chemical processes. The last group consists of adding chemical products to the fluids injected. One of these methods includes the addition of surfactant products, whose goal is to reduce the interfacial tension, increasing the capillary number and, therefore, decreasing the oil saturation. The method can be applied combined with a polymer solution, as control mobility agent, looking for an increase in displacement efficiency (HEALY; REED, 1974). This combination of chemical products and methods is known as surfactant-polymer (SP) process.

Surfactants are organic compounds with a hydrophilic (polar) and a hydrophobic (apolar) group. Thus, they are soluble in water and oil (ROSEN, 1989). Surfactants are classified according to the charge of the polar group in the molecule head as anionic, cationic, non-ionic and Zwitterionic. Surfactants properties are related to their molecular structure and behavior in solution. For this reason, it is essential to know some physical and chemical properties of the surfactant solutions to be used, such as interfacial tension, critical micelle concentration, phase behavior and adsorption on solid superficies. A determinant factor in an SP process is the characterization of the interaction between the selected chemical products to be injected (LLAVE et al., 1992; LORENZ; BROCK, 1987).

There are two kinds of polymers potentially used in EOR process, the synthetic polymers, such as Partially Hydrolyzed Polyacrylamide (HPAM), and the biopolymers such as Xanthan Gum (XG). The term Partially Hydrolyzed is associated with the conversion of some amide groups ($CONH_2$) to carboxyl groups (COOH) of the Polyacrylamide (PAM). In other words, HPAM is a flexible polyelectrolyte with negative charges on the carboxylate groups, which generate a strong interaction between the polymer chains and any cation present in the water (LOPES; SILVEIRA; MORENO, 2014). Chemical Enhanced Oil Recovery (CEOR) process including polymer requires the determination of the effects of the formation water salinity and surfactant concentration on the rheological polymer solution properties (SAMANTA et al., 2010).

Core flooding tests allow assessing the performance of these chemical products through porous media and their capability to improve the oil recovery factor in laboratory scale. These tests also can be used as a calibration tool of numerical simulation models used to forecast the flow through porous media.

The detailed visualization of the in-situ fluids dynamics and the spatial distribution of fluids injected during core-flooding tests is an issue for research on this topic. For this reason, several authors have presented results including computed tomography (CT). This technique allows observing the in-situ fluids flow during the core flooding test and improves the evaluation of the EOR methods. (BATENBURG et al., 2015; HOVE; NILSEN; LEKNES, 1990; HUNT; ENGLER; BAJSAROWICZ, 1988; LONDON et al., 2014; VINEGAR; WELLINGTON, 1987; WANG; AYRAL; GRYTE, 1984; WELLINGTON; VINEGAR, 1987; WITHJACK, 1988; WITHJACK; DEVIER; MICHAEL, 2003).

1.2 Motivation

The Chemical Enhanced Oil Recovery (CEOR) processes have been revitalized globally after two decades of relative calm (STOLL *et al*., 2011). Among those processes, polymer flooding (PF) is the most used method on a field scale, whereas, the Surfactant-Polymer (SP) and alkali/surfactant/polymer (ASP) applications are limited due to technical reasons. Limiting factors include the difficulty in designing and forecasting the processes behavior in the field, the excessive formation of carbonate or silicate scale and the formation of strong emulsions in the production facilities. Therefore, these processes still are a challenge for the petroleum industry.

1.3 Objectives

The present work aims to use computed tomography as a tool to evaluate the flooding potential of surfactant-polymer flooding in sandstones at laboratory scale encompassing: the selection and characterization of the chemical products (polymer and surfactant), the design of an SP process and conducting core-flooding tests supported by CT. As secondary objectives, the following steps can be highlighted:

- Characterize the rheological behavior of the polymer solution to be used.
- Design the surfactant solution to be employed during the core flooding tests.
- Design surfactant-polymer flooding and to evaluate its performance with core flooding tests supported by computed tomography.
- Evaluate and analyze the results through core flooding tests and compare the material balance with the computed tomography results.

1.4 Work Description

This work is composed of six chapters, where:

Chapter 1 presents the introduction, the knowledge gap that motivated this work and the objectives aiming to contribute to different topics of existent knowledge.

Chapter 2 covers the basic concepts and theories for surfactant-polymer flooding. Besides that, fundaments of computed tomography are included.

Chapter 3 includes a detailed literature review about of Surfactant-Polymer process, oil mobilization mechanisms, phase behavior, rheological behavior of polymer solutions and the influence of salts, temperature and surfactants; and finally, use of CT for EOR process.

Chapter 4 introduces the materials, devices and equipment, and a detailed explanation of the experimental methods used to develop this research.

Chapter 5 shows the results obtained in each methodology step of this research related to an experimental assessment of a surfactant-polymer process as a secondary and tertiary oil recovery method in sandstones evaluated by computed tomography.

Finally, Chapter 6 exhibits the main conclusions obtained throughout this research.

2 CONCEPTS AND THEORY BASIS

This chapter covers the basic concepts and theories for surfactant-polymer flooding, which includes interfacial tension, wettability, capillary pressure, capillary number, relative permeability, rock and fluid properties, types of surfactant and polymers, types of microemulsions and phase behavior. Besides that, basic concepts of computed tomography are included.

2.1 Multiphase Flow Key-Parameters

2.1.1 Surface and interfacial tension

When two immiscible fluids are in contact, they stay separated by a well-defined interface of only a few molecular diameters thick. The internal molecules of fluid (See Figure 2.1) exert an attractive force on each other in all directions (a). At the interface, there is an inward directed force attempting to minimize the surface by pulling it into the shape of a sphere (b). The molecular activity at the surface creates a film of molecules that are in tension, which is a function of the specific free energy of the interface (TIAB; DONALDSON, 2004).

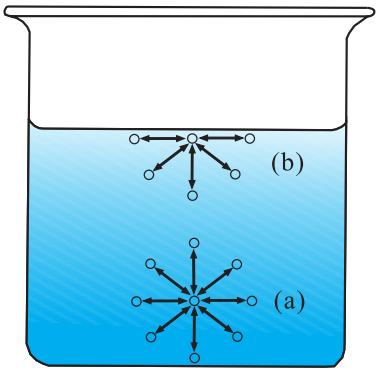

Figure 2.1 Interaction of attractive molecular forces in (a) the liquid and (b) at the surface.
Adapted from DONALDSON; WAQI (2008).

Some authors, such as HOLMBERG; JÖNSIN; KRONBERG (1998); ROSEN (1989); SHENG (2011); TIAB; DONALDSON (2004), have called this forces balance as surface tension or interfacial tension. The use of these terms is related to the nature of fluids in contact, i.e., the surface tension is used when the interaction occurs between air and liquid, whereas, the interfacial tension (IFT) is commonly used for liquid-liquid.

Having said that, the IFT is the surface energy per unit area required to develop the interface between two immiscible fluids (DONALDSON; WAQI, 2008). It is considered as a condition of mechanical equilibrium at an interface (GREEN; WILLHITE, 1998) The interfacial tension is commonly expressed in dynes/cm as a unit of measurement, which is numerically equal to milliNewton/m, [(N x 10^{-3})/m or mN/m].

The IFT behavior between an aqueous surfactant solution and a hydrocarbon phase is a function of several parameters, for example, type and concentration of salts, temperature, surfactant concentration, surfactant type and purity, water-oil ratio and the nature of the hydrocarbon phase (HEALY; REED; STENMARK, 1976).

2.1.2 Wettability

The measure of the preferential tendency of a fluid to spread, wet or adhere to the interstitial surfaces of the porous medium in the presence of other fluids is known as wettability (DONALDSON; WAQI, 2008). The most common method of determining rock wettability is by measurement of the contact angle (θ) between the rock surface and the fluid system. For an oil-water system in contact with a solid surface, θ, is the angle between the fluid and solid interface measured through the water phase (EZEKWE, 2011). This angle is mathematically represented by Young's equation:

$$Cos\ \theta = \frac{\sigma_{so} - \sigma_{sw}}{\sigma_{wo}} \qquad (2.1)$$

Where,

σ_{so} = interfacial tension between the solid and oil.

σ_{sw} = interfacial tension between the solid and water.

σ_{wo} = interfacial tension between the water and oil.

The above relationship between the contact angle and the interfacial tension expressed by the Young equation are shown in Figure 2.2.

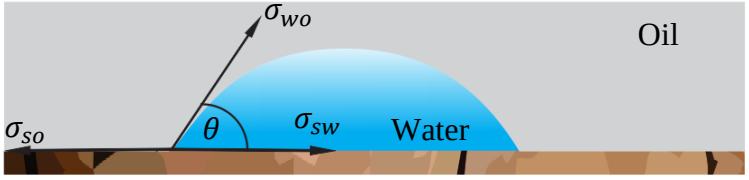

Figure 2.2 Relationships between the contact angle and the interfacial tension.

Adapted from TIAB; DONALDSON (2004).

The rock surface is considered to be water-wet when $0 < \theta < 70°$, oil-wet when $110 < \theta < 180°$. When $70 < \theta < 110°$, the rock surface is considered to be intermediate or neutral wet (TIAB; DONALDSON, 2004).

2.1.3 Capillary pressure

If two immiscible fluids are in contact within a capillary, one of them tends to wet the capillary walls (wetting phase), and the other is resting on a thin film of the wetting fluid (non-wetting). The pressure within the non-wetting phase is higher than the pressure of the wetting phase. This pressure difference creates a curvature between both fluids that relates to the preferential wettability of the capillary walls by one of the phases. For example, in a water-oil system, where the water is the wetting phase, the interface between the fluids is curved convex concerning to the oil (TIAB; DONALDSON, 2004). The capillary pressure (P_c) is defined as the pressure difference between the non-wetting (P_{nw}) and wetting (P_w) phases:

$$P_c = P_{nw} - P_w \tag{2.2}$$

The magnitude of capillary pressure depends on the saturation of each phase, the nature of the continuous phase, and the distribution, shape, and size of the pores and the pore throats (EZEKWE, 2011). For a capillary tube, P_c is represented by:

$$P_c = \frac{2\sigma cos\theta}{r} \tag{2.3}$$

where σ is the interfacial tension between the fluids; θ is the contact angle which denotes the wettability of the capillary tube, and r is the radius of the capillary tube.

An expression given by the Laplace equation, for calculating the capillary pressure at any point on an interface between oil and water, within two spherical sand grains (Figure 2.3), in a wet-water reservoir (DAKE, 2008), is presented by the Equation (2.4).

$$P_c = P_{nw} - P_w = \sigma\left(\frac{1}{r_1} + \frac{1}{r_2}\right) \tag{2.4}$$

In the Equation (2.4), r_1 and r_2 are the principal radii of curvature at any point on the interface between oil and water, respectively.

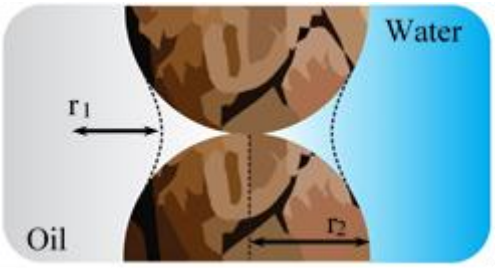

Figure 2.3 Water entrapment between two spherical sand grains in a water-wet reservoir. Adapted from DAKE (2008).

2.1.4 Capillary number

Two main forces are acting on the residual oil drops within the interstices or pores of rock, viscous and capillary forces. The transition between a displacement process dominated by capillary forces and one dominated by viscous forces is assessed with a dimensionless parameter (MELROSE, 1974), named Capillary Number (N_c) and is defined as follows.

$$N_C = \frac{F_v}{F_c} = \frac{v\mu}{\sigma cos\theta} \tag{2.5}$$

Here, F_v and F_c are viscous and capillary forces, respectively; v is the pore flow velocity of displacing fluid; μ is the displacing fluid viscosity; σ is the interfacial tension between the displacing and displaced phases and θ is the contact angle. A set of consistent units must be used. For example, v is in m/s, μ in mPas, and σ in mN/m.

The Equation (2.5) shows that the capillary number increases when the IFT decreases. The increase of one order of magnitude of the Nc is related to an additional reduction in residual oil saturation (MOORE; SLOBOD, 1955; MORROW, 1979; SHENG, 2011).

2.1.5 Permeability and relative permeability

According to EZEKWE (2011), the measure of the capability to transmit fluids through of porous media whose pore spaces are an interconnected system is named permeability. In addition, when the porous media is wholly saturated with a single fluid, the measured permeability is known as absolute permeability, which is independent of the type of the fluid in the pore spaces. On the other hand, when two or more fluids are occupying the porous media, the measured permeability is the effective permeability of that particular fluid in the pore

spaces. Finally, the ratio of the effective permeability to the absolute permeability of the porous media is designated as relative permeability. Mathematically, the relative permeability is represented by the Equation (2.6):

$$K_{ri} = \frac{K_i}{K_a} \tag{2.6}$$

In Equation (2.6), $K_{ri} =$ relative permeability of the porous media to fluid i; $K_i =$ effective permeability of the porous media to fluid i; $K_a =$ absolute permeability of the porous media.

2.1.6 Mobility and mobility ratio

Mobility control is one of the most important concepts in all EOR process. It can be achieved through injection of chemicals to change displacing fluid viscosity, to reduce specific fluid relative permeability, or even though to modify wettability.

The mobility (λ) is defined as the relationship between the effective permeability (K_i) and the viscosity of the phase (μ). If K_i is changed by the relative permeability (K_{ri}), it is named relative mobility (λ_r).

The term mobility ratio (M_r) is the ratio between displacing phase mobility and the displaced phase mobility. It is mathematically defined as:

$$M_r = \frac{\lambda_{displacing\ phase}}{\lambda_{displaced\ phase}} = \frac{\frac{k_i}{\mu_i}}{\frac{k_j}{\mu_j}} \tag{2.7}$$

In the Equation (2.7) the subscripts *i* and *j* represents the displacing and displaced phases, respectively. Besides that, *i, j = w, o;* for water and oil phase.

Several authors (ABIDIN; PUSPASARI; NUGROHO, 2012; GREEN; WILLHITE, 1998; SHENG, 2011; SORBIE, 2013) have proposed that a mobility ratio equal to or less than one ($M_r \leq 1$) is favorable and $M_r > 1$ is unfavorable.

This investigation work includes the modification of the mobility ratio through the addition of polymers products to change displacing fluid mobility and reducing the effective water permeability of the porous media.

2.2 Surfactants

Surfactants are organic compounds whose chemical structure makes it favorable to reside at the interfaces. As maintained by GREEN; WILLHITE (1998), surfactants are chemical

substances that adsorb or concentrate at a fluid/fluid surface or interface when present at low concentrations in a system. They decrease the interfacial tension (IFT). Hence, they are termed surface-active agents (GOODWIN, 2004).

Surfactants are amphiphilic molecules, that is, they have both hydrocarbon portion (nonpolar) and other ionic portion (polar). The hydrocarbon portion is often called hydrophobic portion or "tail," and the ionic portion is named hydrophilic portion or "head" of the molecule (SHENG, 2011). Therefore, they are soluble in both, organic solvents and water (Figure 2.4).

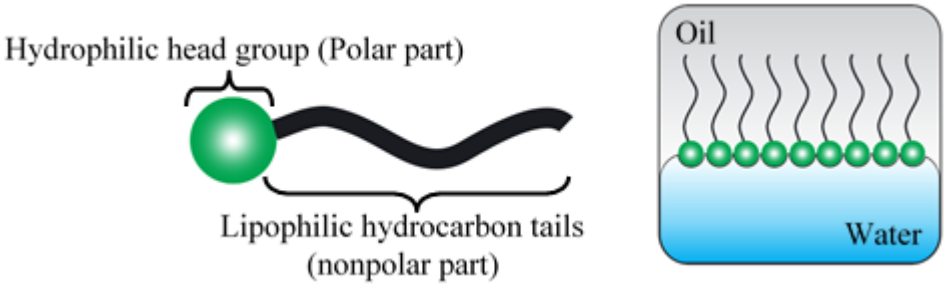

Figure 2.4 Surfactant molecule and surfactant orientation in a solution.
Adapted from Sandersen (2012).

2.2.1 Surfactants classification

The most common classification of surfactants is based on the ionic nature of the head group. Thus, they can be classified as anionic, cationic, nonionic and zwitterionic. Each kind of surfactant depends on how the molecules ionize in aqueous solution (Table 2.1).

Table 2.1 List of typical surfactant molecules with different types of charge.

ANIONIC	
Sodium dodecyl sulfate (SDS)	$CH_3(CH_2)_{11}SO_4^-Na^+$
Sodium dodecyl benzene sulfonate	$CH_3(CH_2)_{11}C_6H_4SO_3^-Na^+$
CATIONIC	
Cetyltrimethylammonium bromide (CTAB)	$CH_3(CH_2)_{15}N(CH_3)_3^+Br^-$
Dodecylamine hydrochloride	$CH_3(CH_2)_{11}NH_3^+Cl^-$
NON-IONIC	
Alcohol Ethoxylates	$CH_3(CH_2)_7(O.CH_2CH_2)_8OH$
ZWITTERIONIC	
Dodecyl betaine	$C_{12}H_{25}N^+<^{(CH_3)_2}_{CH_2COO^-}$

Adapted from HOLMBERG; JÖNSIN; KRONBERG (1998).

Anionic and nonionic surfactants have been used in EOR process (GREEN; WILLHITE, 1998; SANABRIA, 2013). As stated by SHENG (2011), the type of surfactants most used in CEOR process is the anionic, because they exhibit relatively low adsorption on a

sandstone rock whose surface charge is negative. Moreover, non-ionic surfactants have been used primarily as co-surfactants to improve phase behavior system.

2.2.2 Partitioning coefficient

When the surfactant is dissolved in either water or oil phase, it tends to partition in some degree into the other phase depending on its capability of being solubilized between the phases. In other words, a hydrophilic surfactant tends to solubilize preferably into the water, without meaning that part of it can be into the oil, too. The partitioning can be characterized by the partitioning coefficient (K_e), which is defined as:

$$K_e = \frac{C_s^o}{C_s^w} \tag{2.8}$$

where C_s^o and C_s^w are the concentrations of the solute in the oleic and aqueous phase, respectively.

GHOULAM et al., (2004) and POLLARD; SHI; GÖKLEN (2006) affirm that the partitioning coefficient depends on the temperature, surfactant composition at the interface, ionic strength, pH, oil type and cosolvents used.

2.2.3 Surfactant micellization

Surfactants can adsorb at interfaces due to the capability of forming a colloidal-sized cluster in solution. This property is usually named micelle formation or micellization (ROSEN, 1989).

Initially, when the surfactant is added to a solvent, its molecules are dispersed as monomers. Then, as the surfactant concentration increases the molecules tend to aggregate and, when a specific concentration of surfactant is reached, the spontaneous micelles formation starts. This particular concentration is called critical micellar concentration (CMC). By considering this, it is possible to define a micelle as an aggregate of monomers (Figure 2.5). For example, in a system whose solvent is water, the micelles are formed with the tail portion directed inward and the head portion outward.

In EOR process, some solution properties change as a function of surfactant concentration at the CMC. SAMANTA et al. (2011) showed the interaction between an anionic surfactant (Sodium Dodecyl Sulfate - SDS) and HPAM. They reported an increase in the surface tension with the polymer presence. Whereas CMC had not changed significantly, i.e., the micelle formation is not heavily influenced by the polymer concentration depends mainly on the surfactant concentration.

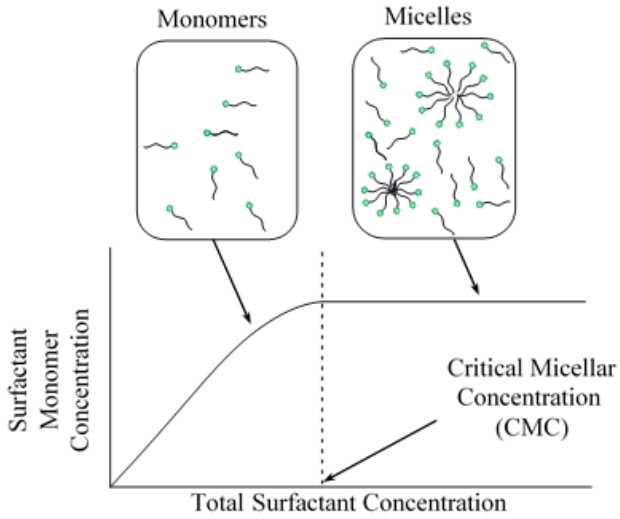

Figure 2.5 Micelle formation.
Adapted from LAKE (1991).

The present research study is focused on the analysis of the interfacial tension, which is the most commonly measured property of surfactants in solution (RICHARD PASHLEY; KARAMAN, 2004). It depends directly on the replacement of molecules of solvent at the interface by molecules of surfactant, i.e., the micelles solubilize the phase that is immiscible with the solvent. These aggregates into the solutions are named microemulsions (M_e). According to GREEN; WILLHITE (1998), in EOR process a microemulsion is a stable, translucent micellar solution of oil and water that may contain electrolytes and one or more amphiphilic compounds.

2.3 Types of Microemulsions

Several authors, such as ELMOFTY (2012); GREEN; WILLHITE (1998); LAKE (1991); ROSEN (1989) and ZHANG et al. (2006) have proposed that for a displacement of the oil in the pores and capillaries of petroleum reservoir rock, ultralow IFT (about a 10^{-3} mN/m) values are required for aqueous-oil solutions. The microemulsions with high solubilization of oil and water have been correlated with these ultralow IFT values.

The phase behavior of these microemulsions is usually represented by ternary diagrams, in which the top apex represents the surfactant pseudo component, the lower left represents water, and the lower right represents the oil (LAKE, 1991). As presented by GREEN; WILLHITE (1998); HEALY; REED (1974) and HEALY; REED; STENMARK (1976) the phase behavior is strongly affected by the brine salinity, temperature, co-solvent type and other factors. Based on this statement, three types of a microemulsion are essential in CEOR process, and they are explained below.

2.3.1 Lower-phase microemulsion

When surfactant exhibits good aqueous-phase solubility, and a small quantity of oil will be solubilized in the cores of the micelles, the resultant system (Figure 2.6) will have two phases: an excess oil phase without surfactant and a water-external microemulsion phase. This microemulsion is called lower-phase Microemulsion (due to it is denser than the excess oil phase) or microemulsion type II (-). The II means that no more than two phases can form, and the (-) implies that the tie lines within the two-phase region have a negative slope. Also, as mentioned by GREEN et al. (2011), this microemulsion can be named as Winsor type I.

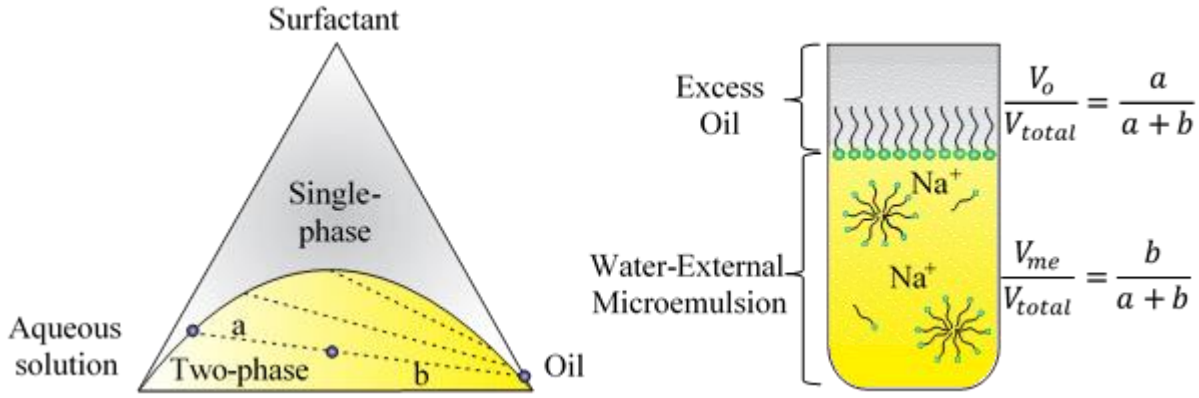

Figure 2.6 Lower-phase Microemulsion.
Adapted from LAKE (1991) and SHENG (2011).

2.3.2 Upper-phase microemulsion

The upper-phase microemulsion corresponds to the opposite behavior mentioned in the previous Item 2.3.1. In this case, the system separates into an oil-external microemulsion containing some solubilized water (Figure 2.7) and an excess of the water phase. Therefore, the microemulsion is called an upper-microemulsion, type II (+) or Winsor type II.

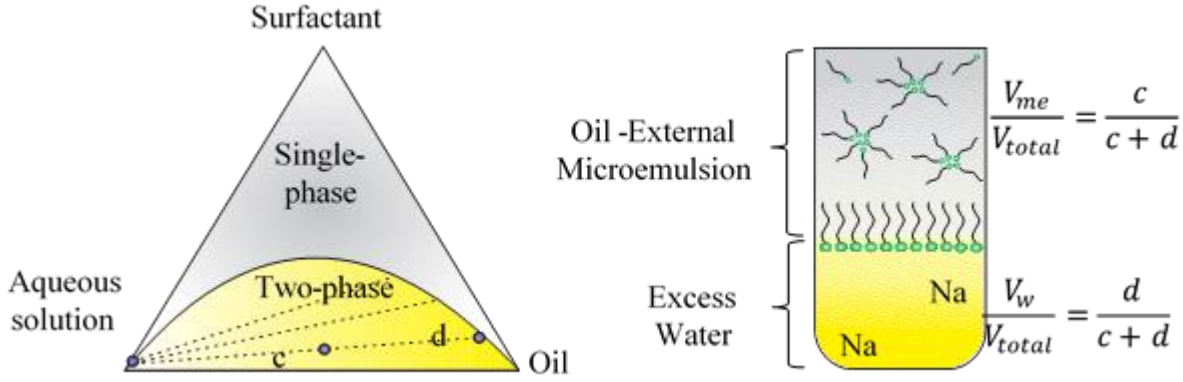

Figure 2.7 Upper-phase Microemulsion.
Adapted from LAKE (1991) and SHENG (2011).

2.3.3 Middle-phase or bicontinuous microemulsion

A more complex system occurs when the three-phase region exists, i. e., excess oil, microemulsion, and excess water (HEALY; REED; STENMARK, 1976). In this case, the kind of microemulsion is called middle-phase or bicontinuous microemulsion, Type III or Winsor type III. A middle-phase microemulsion is saturated with both oil and water at the specified temperature and overall composition of the system, and it is vital because ultralow IFT's values are usually found in this region (GREEN; WILLHITE, 1998).

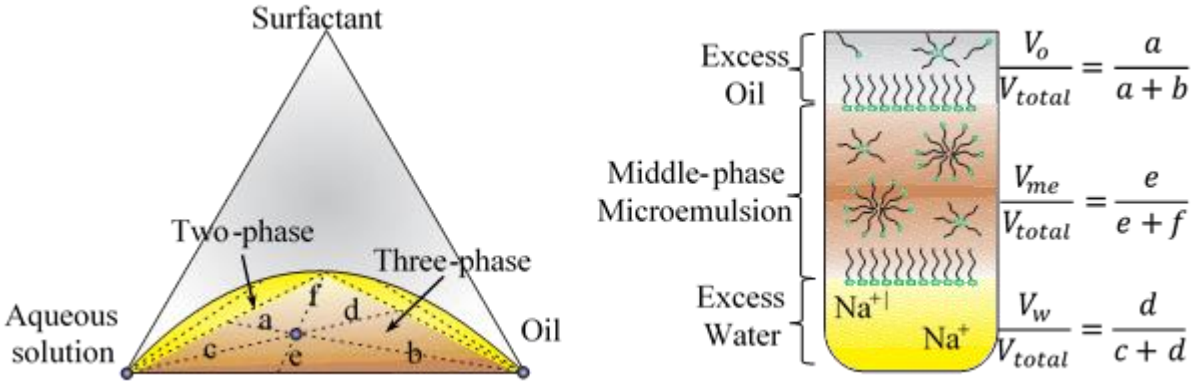

Figure 2.8 Middle-phase Microemulsion.
Adapted from LAKE (1991) and SHENG (2011).

2.4 Methods to Characterize Surfactants

The success of a CEOR process depends on the chemical interaction between the used products and porous media. For this reason, carrying out a proper characterization of this performance is necessary before evaluating the process in a laboratory scale using core-flooding tests (SHENG; LEONHARDT; AZRI, 2015). In this investigation, the chemical interactions between the interest fluids are experimentally studied through aqueous stability tests, solubilization ratio parameters, phase behavior tests, optimum salinity and IFT measurements.

2.4.1 Bancroft's rule

The Bancroft's Rule is an entirely qualitative method based on the idea that the phase, in which an emulsifier is soluble, constitutes the continuous phase (HOLMBERG; JÖNSIN; KRONBERG, 1998). Therefore, hydrophilic surfactants tend to generate oil in water (o/w) emulsion whereas lipophilic surfactants produce water in oil (w/o) emulsion. The use of this rule has been recently reported (ALMEIDA, 2014). Although this rule was developed for

emulsions, Ruckenstein (1996) showed that for surfactant concentrations higher than the CMC, the macroemulsion type corresponds to that of the microemulsion.

2.4.2 Aqueous stability tests

Aqueous stability tests consist of checking if the aqueous solution (Brine, Polymer, surfactant, and others) is transparent without adding oil up to the desired salinity or higher concentrations. This condition is essential because it allows observing some form of a precipitate, liquid crystal or a second liquid phase that can generate a nonuniform distribution and transport of fluids to be injected owing to phase trapping or different mobilities between phases (SHENG, 2011). When the solution is clean, any mentioned problem will not appear because the solution will be more stable after mixing with the in-situ oil. On the contrary, the chemical must be re-selected.

2.4.3 Solubilization parameters

The solubilization parameters are defined as the ratio of the oil (V_{om}), or water (V_{wm}) solubilized volume to the surfactant volume in the microemulsion phase (V_S). For example, the volume of solubilized oil is the difference between the initial oil volume and the excess oil phase after equilibration (LIU et al., 2008a). Generally, for a Winsor III behavior, when the solubilization ratio for oil and water are equal, the IFT reaches its minimum. The salinity at which the IFT is minimum is known as optimum salinity (C_y). The desired case is when the reservoir brine salinity is very close to the optimum one. The mathematical expressions were presented by HEALY; REED; STENMARK (1976):

$$V_{om} = V_o/V_s \tag{2.9}$$

$$V_{wm} = V_w/V_s \tag{2.10}$$

The above equations assume that *Vs* does not include the cosolvent. HEALY; REED; STENMARK (1976) hold that this assumption is not tenable for the cosolvent, and is expected that it be distributed among microemulsion, excess water, and excess oil phases. Nevertheless, the same authors hold that the IFT values obtained with the solubilization parameters are good.

2.4.4 Phase behavior tests

These type of tests are conducted in pipettes or similar devices. It consists of putting specific volumes of an aqueous solution with different salinity and mixing with the oil solution

in the recipient. Then, the resultant solution is left resting at a temperature of interest, and the volumetric changes are observed. If the properties of the fluid are not significantly dependent on pressure, it can be discarded as critical condition (SHENG, 2011). The primary objective of this test is to find a chemical formula with a high solubilization ratios of oil and water volumes to some surfactant volume, and to determinate the optimal salinity.

Figure 2.9 shows the microemulsion changes from Winsor I to Winsor III and Winsor II, according to the salinity increase.

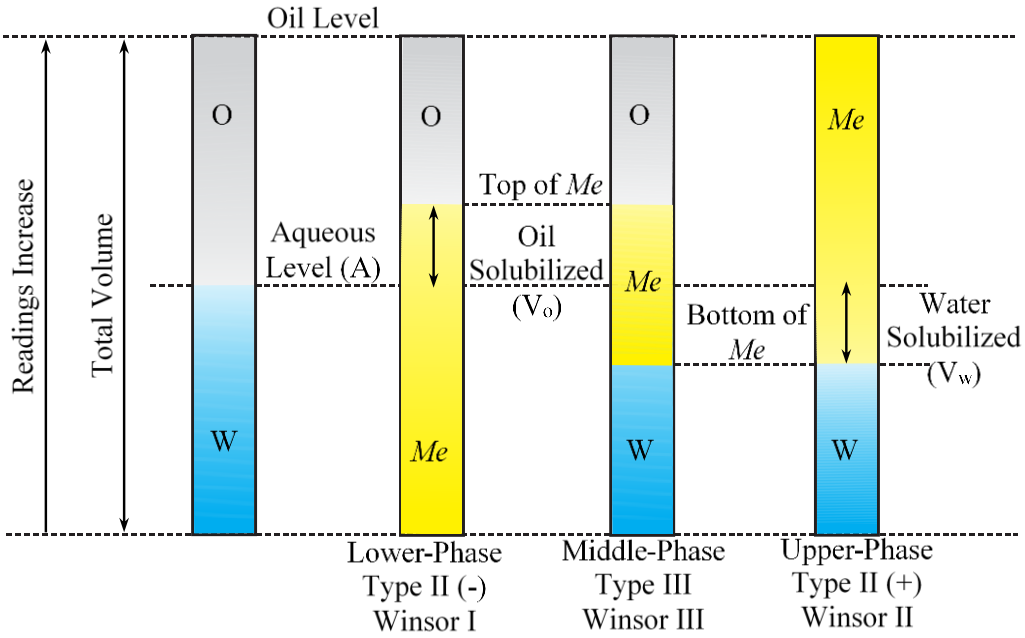

Figure 2.9 Measurements and calculations carried out for phase behavior tests.
Adapted from SHENG (2011).

One way to quantify the solubilization ratio parameters is shown in equations 2.11 and 2.12.

$$V_{om} = \frac{V_o}{A * \%wt\ Surfactant} \tag{2.11}$$

$$V_{om} = \frac{V_w}{A * \%wt\ Surfactant} \tag{2.12}$$

2.4.5 Interfacial tension and critical micellar concentration

IFT value is obtained according to Chun Huh (1979). The author proposed one way to calculate IFT based on the solubilization ratio parameters. As follows:

$$\sigma_{om} = \frac{c}{\left(\frac{V_o}{V_s}\right)^2} = \frac{c}{V_{om}^2} \tag{2.13}$$

$$\sigma_{wm} = \frac{c}{\left(\frac{V_w}{V_s}\right)^2} = \frac{c}{V_{wm}^2} \tag{2.14}$$

For the equations above, HUH (1979) found that in EOR process these expressions are consistent with values of *c* near 0.3 [mN/m]. A reasonable agreement between these equations and measurements carried out with a spinning drop are reported by LIU et al. (2008) and ZHANG et al. (2006).

According to SHENG (2011) and ELMOFTY (2012), to reach an IFT reduction to reduce the oil saturation, the solubilization ratio must be higher than 10.

The IFT behavior as a function of the surfactant concentration and other physical properties are shown in Figure 2.10. The interfacial tension decreases as the surface covered by surfactant increases. At that moment, the aggregation into micelles starts. Upon reaching CMC, any further addition of surfactant will only increase the number of the micelles. In other words, the interfacial tension decreases sharply as the concentration of surfactant increases and, once achieved the CMC, the interfacial tension tends to be more or less constant.

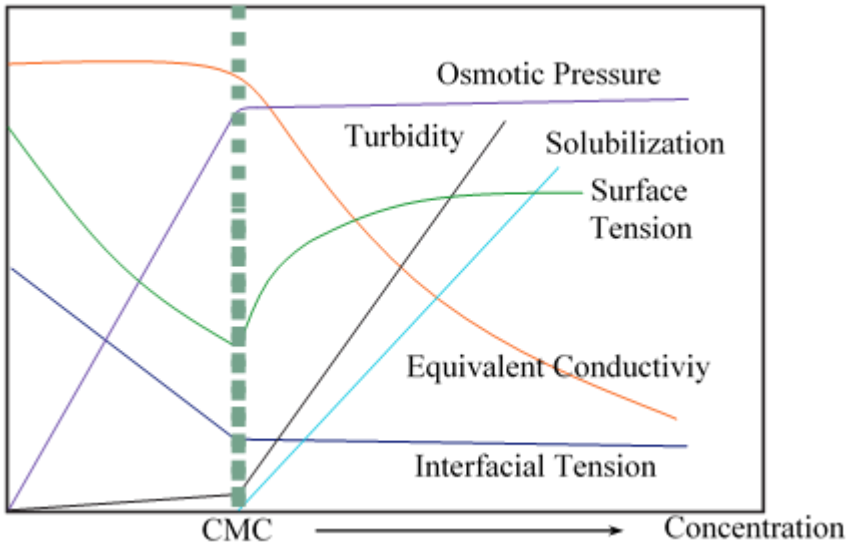

Figure 2.10 Surfactant concentration dependence of some physical properties for solution respect to CMC. Adapted from HOLMBERG; JÖNSIN; KRONBERG (1998) and SCHRAMM (2000).

2.5 Polymer Flooding

This technique is mainly based on the polymer addition to the water of a waterflood to increase its viscosity. Therefore, the mobility ratio of the displacing polymer solution to the displaced fluids ahead and the fingering are reduced (LAKE, 1991). It is important to point out that, when as the viscous fingering is reduced, the sweep efficiency is improved.

On the other hand, some authors such as DEHGHANPOUR; KURU (2009); DODA (2014); URBISSINOVA; TRIVEDI; KURU (2010) and ZHANG; LI; ZHOU (2011) have recently evaluated the relationship between the viscoelastic properties and additional oil mobilization. More viscoelastic fluids exert a more significant pull force on oil droplets or oil residual films, incrementing oil recovery.

2.5.1 Polymers types

Synthetic polymers and biopolymers are the two main types of polymer used in the petroleum industry. The typical synthetic polymer used is the partially hydrolyzed polyacrylamide (HPAM), and a standard biopolymer is Xanthan gum (SHENG; LEONHARDT; AZRI, 2015).

HPAM is used for most field projects due to its lower cost and availability since it can be used for large-scale production (ABIDIN; PUSPASARI; NUGROHO, 2012). Also, HPAM solutions are expected to exhibit significantly greater viscoelasticity than Xanthan gum (SHENG, 2013).

HPAM is obtained by partial hydrolysis of PAM or by copolymerization of sodium acrylate with acrylamide (WEVER; PICCHIONI; BROEKHUIS, 2011). The hydrolysis of PAM consists in converting some of the amide groups ($CONH_2$) into carboxyl groups ($COOH^-$). It reduces the adsorption on mineral surfaces. In commercial products, the hydrolysis usually ranges from 15% to 35%.

The hydrolysis of PAM generates an effect on the rheological properties of polymer solution due to the introduction of negatives charges on the backbones of polymer chains. Therefore, when polyelectrolytes are dissolved in water containing salts, a reduction of viscosity is observed (SORBIE, 2013). Also, there are more factors able to influence the rheological behavior of HPAM solutions as temperature, molecular weight, solvent quality and shear. Some of them will be discussed later.

Usually, the rheological properties are determined through shear viscosity measurements or flow curves which reveal information about the ability of the polymer to flow under different shear rate and target process condition (SAMANTA et al., 2010).

The primary disadvantages of HPAM are the tendency to shear degradation at high flow rates and poor performance in high-salinity water (low viscosity and frequently excessive retention) (NEEDHAM; CO; DOE, 1987).

2.5.2 Polymer solution viscoelasticity

Viscoelasticity is the property of a material that exhibits both viscous and elastic characteristics when it is submitted to deformation. The viscous behavior is represented by the Newton law, while the elastic behavior is modeled by the Hooke's Law (SHENG, 2011).

This study is focused on analyzing the behavior of the storage modulus (G'), also named elastic modulus, which is associated with *"memory"* or elasticity of the polymeric solution. In other words, the material returns to its original configuration when any deforming force is removed. Moreover, the changes caused on the loss modulus (G''), known as viscous modulus (BARNES; HUTTON; WALTERS, 1989), give information about the viscous properties of the solution.

The polymer viscoelastic properties must be measured using oscillatory teste. If G' and G'' exist simultaneously and are horizontally parallel in an amplitude sweep test (AST), we can affirm that the material has a linear viscoelastic region (LVR) (SILVEIRA; LOPES; MORENO, 2016; SORBIE, 2013).

Laboratory results have reported an oil recovery increase when using viscoelastic polymeric solutions (HUIFEN et al., 2004; WANG et al., 2001). This improvement has been attributed to the elastic properties of the polymeric solutions, and their effect on the displacement efficiency increase (JIANG et al., 2008; URBISSINOVA; TRIVEDI; KURU, 2010; WANG et al., 2007).

In the light of the above, in surfactant-polymer flooding, an utterly rheological behavior study of polymer solutions should be performed on target conditions with and without surfactant. Also, the determination of the viscoelastic properties of the polymeric solutions improves the understanding of mechanisms acting in EOR processes.

2.6 Surfactant, surfactant-polymer, and micellar flooding

Several definitions have been proposed to describe and differentiate these processes (GREEN et al., 2011; LAKE, 1991; SAMANTA et al., 2011; SCHRAMM, 2000; SHENG,

2015). All of the three methods are based on the injection of surfactant solution to generate a high reduction in the interfacial tension (IFT) between oil and water. Additionally, these methods involve polymer addition in the surfactants solution or the chase water, resulting in a more favorable mobility ratio. The main difference lies in the surfactant concentration, and the way as the polymer is used during the process. The specific definitions of Surfactant flooding, Surfactant-Polymer flooding, and Micellar flooding are presented below.

2.6.1 Surfactant flooding

Surfactant flooding consists in the addition of a surfactant into the aqueous phase without polymer, which forms an oil bank whose sweep efficiency and pressure gradient are maintained by the injection of chases polymer and water after the surfactant slug (SAMANTA et al., 2011). This process usually presents fingering of the injected fluid due to the IFT reduction and the low viscosity, therefore, generating a high-velocity displacement.

2.6.2 Surfactant-polymer (SP) flooding

The SP is characterized by the addition of low concentrations of a surfactant (0.1% to 2%) into the aqueous phase. Also, the polymer addition increases the solution viscosity to overcome the viscous instability of low interfacial tension. Around 20% to 40% of the pore volume of in SP solution is injected through the oil-bearing target zone, followed by similar amounts of polymer flush (WYATT; PITTS; SURKALO, 2008). This work is focused on this definition.

2.6.3 Micellar flooding

Micellar flooding differs from SP flooding since the surfactant concentration is higher (2% to 12%) and the injected pore volume is lower (5% to 20%). The surfactant at high concentration is incompatible with the polymer (WYATT; PITTS; SURKALO, 2008). Therefore, cosurfactants and/or alcohols are needed because micellar solutions increase the viscosity of the injected fluid as a consequence of the structuring of the micelles. This structure and other properties of micellar solutions are sensitive to changes in salinity, temperature, etc.

2.7 Computed Tomography (CT)

CT is a radiological imaging technique able to generate cross-sectional slices through the object by revolving an X-Ray tube around it, obtaining projections from many different angles. After an image is reconstructed by an algorithm based on these projections.

The reconstructed image is equivalent to a square matrix of 512 values which each unitary square represents a pixel of the slice. The fundamental quantity measured in each pixel of a CT image is the linear attenuation coefficient, τ, which is defined by the Beer's Law:

$$\frac{I}{I_o} = exp(-\tau h) \tag{2.15}$$

where I_o is the incident X-Ray intensity and I is the intensity remaining after the X-Ray passes through a thickness, *h,* of a sample (WELLINGTON; VINEGAR, 1987).

The linear attenuation coefficient depends on both electron density (bulk density - ρ), and the atomic number (Z). Both properties are predominant at different X-Ray energies, i.e., the ρ of the materials is predominant at above 100 kV whereas that *Z* is predominant at below 100 kV.

The CT attenuation data are typically presented on a scale called Hounsfield (H) units, that are defined by air at -1000 [H] and water at 0 [H]. It is also named as CT number.

The CT is a useful tool for petroleum engineering because it allows the generation of dynamic three-dimensional images of phases saturation during displacement process at reservoir pressures and temperatures (VINEGAR; WELLINGTON, 1987). Also, the technique has been useful for petrophysical studies obtaining porosity values, fracture patterns and quantifying complex mineralogies (SHAMEEM; KHAMEES, 2004; THAKUR; BEHBEHANI; DERNAIKA, 2014).

3 LITERATURE REVIEW

This chapter presents a literature review of Surfactant-Polymer process encompassing a screening method and exposing how the concepts and properties defined previously are related to the SP process. Likewise, information related to residual oil mobilization mechanisms are analyzed. Information about effects of salts, temperature and surfactant on the rheological behavior of polymer solutions, phase behavior and the use of CT for EOR process are also included.

3.1 Screening of a Surfactant-Polymer Process

The SP process is classified as a CEOR process. Several authors have presented different criteria for the correct selection of a field candidate to apply this method. Some of these criteria are based on the definitions given in Item 2.6 and are summarized in Table 3.1. The screening criteria can be applied regardless of which of these process is under consideration.

During the review process, it was observed that the API gravity value is not a critical variable in the SP process when compared to the oil viscosity, for instance. Additionally, reservoir depth can be despised as long as the temperature limit is respected and the pore pressure is not considered as a critical variable in the process. On the other hand, oil composition is an essential variable for the process once the phase behavior depends on it. These approaches are later discussed in the text when presenting details of the phase behavior study.

Based on the considerations of Table 3.1, the reservoir conditions, fluids, and rock properties to take into account in this study were selected. Then, a field satisfying these criteria was used as a reference for these features, and it represented a valuable motivation for experimental evaluation of SP process.

The reservoir conditions, petrophysics and fluids properties of the San Francisco (SF) field were selected as references to develop this study. This field was discovered in 1985 and is located 20 km northwest of the city of Neiva (Figure 3.1) in the Upper Magdalena Basin in Colombia.

Table 3.1 Screening criteria for SP process

Reservoir Conditions		**Reservoir Rock Properties**					**Reservoir Fluids Properties**			**Reference**
Temperature. (°C)	**Depth (ft)**	**Permeability (mD)**	**Porosity (%)**	**Lithology**	**Clay**	**Oil Saturation* (Fraction)**	**Water Salinity (ppm)**	**Oil Viscosity (cp)**	**API Gravity (°API)**	
< 90	< 6561	> 50	> 18	Sand and Sandstone	Low	> 0.4	Low	< 30		(CARCOANA, 1982)
< 93.3	< 9000	> 40	>20	Sandstone		> 0.3	< 100000	< 40	> 25	(GOODLETT; HONARPOUR; CHUNG, 1986)
< 93.3	8500	> 20		Sandstone	Low	> 0.25	< 50000	< 20	> 25	(BRASHEAR; V. A. KUUSKRAA, 1995)
< 93.3	9000	> 10		Sandstone		> 0.35		< 35	> 20	(TABER; MARTIN; SERIGHT, 1997)
< 70		>50		Sandstone	Low	> 0.35	< 50000	< 150	< 35	(AL-BAHAR et al., 2004)
< 71.1	< 4600	> 170	> 20	Sandstone		> 0.6	< 150000	< 80	> 14	(EZEKWE, 2011)
< 93.3		> 10		Sandstone	Low	> 0.3	< 50000	< 35		(SHENG, 2015)
< 70	NC^+	> 10	> 18	Sandstone	Low	> 0.25	< 50000	< 35	NC^+	**Proposed in this work**

Oil Saturation*: Before SP, **NC^+:** No Critical Variable.

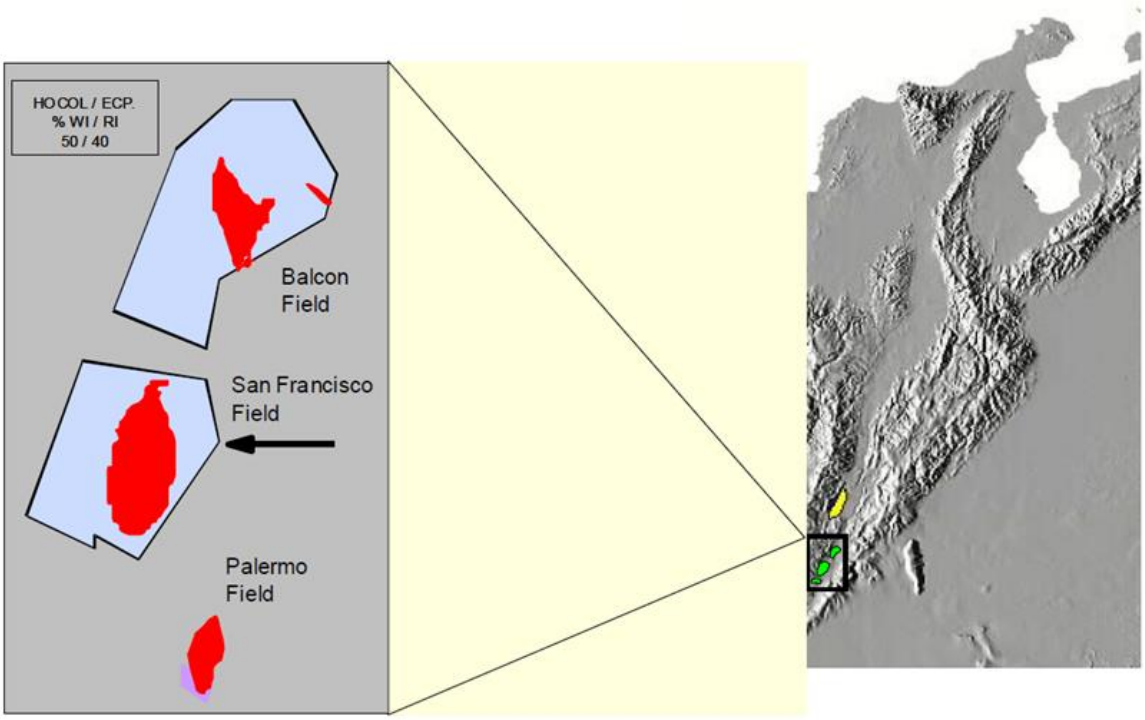

Figure 3.1 Location of San Francisco Field on Colombia.

Source: (SUAREZ et al., 2005)

The Cretaceous Upper Caballos Formation is the main producer unit of SF field. This formation consists of coarse to fine-grained quartz sandstones in an estuarine environment and contains 75% of the stock tank original oil in place (STOOIP). The San Francisco Field is an example of a mature field producing under a mature waterflooding project, at a water cut higher than 90% and an unfavorable mobility ratio (SOTO; SUAREZ, 2011; SUAREZ et al., 2005). The SF field was not submitted to any EOR process, and it is considered a good candidate for CEOR process. A laboratory assessment of an ASP process using SF fluids composition was developed recently (VIDAL PRADA, 2014).

The properties of the field are presented in the Tables 3.2 to 3.5. It is important to highlight that; these field characteristics are only a reference for the features to be used in this work.

Table 3. 2 Reservoir Conditions

Reservoir Temperature (°C)	**Reservoir Pressure (Psia)**	**Depth (ft)**
50	1100	3000

Adapted from SOTO; SUAREZ (2011); SUAREZ et al. (2005) and VIDAL PRADA (2014).

Table 3.3 Reservoir Rock Properties

Permeability (mD)	**Porosity (%)**	**Lithology**	**Oil Saturation* (Fraction)**
20 - 2000	12 - 23	Sandstone	> 0.25

Adapted from SOTO; SUAREZ (2011) and SUAREZ et al. (2005).

Table 3.4 Oil properties Well SF-167

Property	**Measuring Condition**	**Value**
Density (g/ml)	19.9 °C	0.8952
	20.5 °C	0.8951
API Gravity (°API)	19.9 °C	25.8
	20.5 °C	25.7
Viscosity (cp)	40 °C	18.4
	60 °C	9.4
	80 °C	5.8

Source: Universidad Industrial de Santander (UIS) and Ecopetrol S.A.

Table 3.5 Reservoir Brine composition: San Francisco (SF) Field

Salt	**Mw [g/mol]**	**Brine I: SF Brine**	**Brine II: Cations Brine equivalent to SF Brine**
		Concentration [g/L]	**Concentration [g/L]**
NaCl	58.44	5.4932	7.0937
KCl	74.55	0.1496	-
CaCl2.2H2O	147.02	1.6647	-
MgCl2.6H2O	203.3	0.4951	-
TOTAL		7.8026	7.0937

Mw: Molecular Weight

Source: Universidad Industrial de Santander (UIS) and Ecopetrol S.A.

3.2 Oil Mobilization Mechanisms

The knowledge of the oil mobilization mechanisms of the process facilitates and improves the analysis of the core flood results. Below, a brief compilation of what happens during the SP process is presented.

MELROSE (1974) showed a complete analysis of the role of the capillary forces on the displacement efficiency. Despite not reported, the magnitude of the upper critical value of N_c, which corresponds to complete oil recovery, the author holds that increasing the capillary number by a factor of 10 to 100, the residual oil saturation can be reduced by about half of the original value. Moreover, to reach microscopic displacement efficiencies of about 100 %, it is necessary to increase N_c by a factor of 200-300 and, to achieve these values of capillary numbers, interfacial tension values should reach values of the order of 10^{-3} to 10^{-4} dynes/cm.

MOORE; SLOBOD (1955) examined the interplay of the viscous and capillary forces intervene at flood front and determined the efficiency of oil displacement in different wettability conditions. They elucidated that the movement of the oil behind the advance front may occur only if extremely low interfacial tensions (less than 0.1 dynes/cm) are maintained.

DONALDSON; LORENZ; THOMAS (1966) carried out a study about the effects of viscosity and wettability using different crude oil and three different additives: a) one without influence on the interfacial tension, b) an alkali (NaOH) and c) a nonionic surfactant. They concluded that relative permeability curves to oil (K_{ro}) and water (K_{rw}) could be modified individually by these additives that change the wettability. Thus, the additive (a) affected only the K_{ro}, (b) concerned only the K_{rw}, (c) modified both curves.

KREMESEC; TREIBER (1978) discussed the results of seven core flooding tests using three different micellar fluids in a continuous and slug injection schemes. They proposed that two mechanisms act during oil displacement, which are: a) the oil that has been bypassed by micellar displacement front can be solubilized or swelled or b) the wettability can be altered.

SHENG (2011) explained the fact that when IFT is ultra-low, the surfactant solution contacts the residual oil droplets cause them to be emulsified (whether in o/w or w/o emulsions). Therefore, the trapped oil droplets accumulate up to form long oil threads able to pass through interconnect pores. These oil droplets form an oil bank ahead of the surfactant slug. Additionally, the surfactant-rock interaction can change the rock wettability.

The type of microemulsion is related to different phenomena within the reservoir. For a Winsor I microemulsion, the emulsified oil droplets are pulled forward, coalescing and finally, forming an oil bank. The residual oil coalescence is easier for a Winsor II microemulsion, once

the continuous phase is oil. Consequently, the oil droplets aggregate to each other creating an oil bank. A different behavior is observed with Winsor III microemulsion, because it causes the lowest value of IFT, and consequently, oil and water are solubilized in each other, and the oil droplets can flow more easily through pore throats.

3.3 Polymeric Solutions Rheology and Influencing Factors

When a monovalent salt (i.e., NaCl, KCl) is added to a homogenous HPAM solution, the carboxylic group is surrounded by the cations, which shield the charge and reduce the carboxylic group repulsion. The hydrodynamic volume becomes smaller, therefore, the viscosity decreases (SHENG, 2011). When divalent salts are present (i.e., MgCl2.6H2O, $CaCl_2.2H_2O$) in an HPAM solution, their effect is more complex. At high hydrolysis, the solution viscosity decreases sharply until the precipitation of a complex mixture of hydrolyzed products and divalent cations occurs (REICHENBACH-KLINKE et al., 2011; ZHU et al., 2014). Due to their higher positive charges, divalent ions are more effective in shielding negative charges on the polymer chain than the monovalent ions. Consequently, the polymer coils up at lower divalent ions concentration and reduces the hydrodynamic radius of the polymer chain, causing a reduction on the degree of polymer chain entanglement (BATAWEEL; NASR-EL-DIN, 2012; LEVITT; POPE, 2008).

Temperature also influences the rheological behavior of the polymeric solution. Significant changes are reported for 333,15 and 363,15 K (MULLER, 1981). Several authors (GHOSH; MAITI, 1997; MAITI; MAHAPATRO, 1988; ZHOU; WILLETT; CARRIERE, 2000) documented that the relationship between the apparent viscosity of a polymeric solution and the temperature satisfies the Arrhenius equation:

$$\mu = D * exp\left(\frac{\Delta E_\eta}{RT}\right) \tag{3.1}$$

where μ is the apparent viscosity of the polymeric solution, D is a constant characteristic of the polymer solution, T is the absolute temperature, ΔE_η is the viscous activation energy or the activation energy for flow, and R is the universal gas constant.

On the other hand, NASR-EL-DIN et al. (1991) conducted an experimental study to determine the effects of various alkalis, surfactants and brine on the viscosity of dilute aqueous solutions of Alcoflood 1175L and HPAM. They evidenced that the presence of ionic species (NaCl, $CaCl_2$), and anionic surfactants reduced the hydrodynamic size of the polymer molecule

(physical change), inducing a detrimental effect on viscosity. Alternatively, a nonionic species impact on the viscosity behavior is insignificant. The alkalis affect the rheological behavior of the polymer chain physically (Charge shielding) and chemically (hydrolysis).

SAMANTA et al. (2010) reported the anionic surfactant effects on the rheological behavior. They showed a detrimental impact on the viscosity of HPAM solutions using Sodium dodecyl sulfate (SDS). They affirmed that the apparent viscosity of polymer decreases with an increase in the surfactant concentration. Also, SHUPE (1981) presented a reduction of the viscosity of polyacrylamide solutions and attributed this effect to the increased ionic strength of the surfactant solutions, caused by the anionic surfactants themselves and significant amounts of sodium sulfate.

3.4 Phase Behavior

Phase behavior of the fluids is defined as a key factor for the efficiency and the dynamic performance of a core flood process applying surfactants (ALVESTAD et al., 1992). More details about how different factors affect phase behavior are provided below.

HEALY; REED; STENMARK (1976) explored physicochemical properties of multiphase microemulsion systems to understand immiscible aspects of microemulsion flooding and to develop systematic screening procedures useful for optimal design flood. They presented the relationship between interfacial tension and phase behavior. Additionally, they correlated the interfacial tension with the solubilization parameters for various microemulsion phases. Finally, they showed that the addition of polymer to the brine did not affect the interfacial tension behavior in a significant manner.

REED; HEALY (1977) presented a complete and detailed study about the effects of salinity, brine composition, temperature, surfactant structure, cosolvent, and oil aromaticity on complex phase behavior, interfacial tension, and solubilization parameters for ionic surfactants. Table 3. 6 shows the summary of results.

SALAGER (1977) showed a detailed study of the phase behavior, microemulsion formation, and interfacial tension. In addition, he presented detailed experimental procedures to characterize the surfactants and to develop the phase behavior tests. During the phase behavior analysis were the following variables:

a) Surfactant concentration, structure, and composition; b) salinity of the aqueous phase; c) oil structure according to the alkane carbon number (ACN) for alkane series and the effective Alkane Carbon Number (EACN) value for other hydrocarbons or mixtures; d) alcohol type and

concentration; e) water-oil ratio (WOR); and f) temperature. Besides that, the process was not considered as very sensitive to pressure changes. Table 3. 7 shows the phase behavior results for anionic surfactants.

Table 3. 6 Summary of the influence of some variables on phase behavior, interfacial tension and solubilization parameter.

	Results					
Increasing Variable	**Phase Behavior***	V_{om}	V_{wm}	σ_{om}	σ_{wm}	C_y
Salinity	I → III → II	↑	↓	↓	↑	
Alkyl Chain Carbon Number of Surfactant Molecular Weight of Alcohol-(Cosolvent) Oil aromaticity Ca++/NaCl Ratio	I → III → II	↑	↓	↓	↑	↓
Temperature	II → III → I	↓	↑	↑	↓	↑
Biopolymer Concentration	Insignificant Changes					

Phase Behavior*: Expressed by Winsor Classification. ↑**:** Indicates an increase, ↓: Indicates a decrease.

Table 3. 7 Qualitative effects of variables analyzed on the phase behavior of Anionic Surfactants.

Scanned Variable (Increase)	**Ternary Diagram Transition**
Salinity	I → III → II
ACN	II → III → I
Temperature	II → III → I
High Molecular Weight Alcohol	I → III → II
Surfactant Hydrocarbon chain length	I → III → II
WOR	NA
Surfactant Concentration	NA

NA: Not appreciable.

THURSTON; SALAGER; SCHECHTER (1979) showed a Newtonian behavior of the microemulsion viscosity in a transition Winsor I→III→II. They proposed that the maximum viscosity value is reached near to the salinity in which a transition of phase behavior occurs.

POPE et al. (1982) carried out static measurements of phase volumes, interfacial tension, viscosities and phase concentration using mixtures of surfactant (anionic and nonionic), polymer, alcohol, water, oil, and sodium chloride. They observed a phase behavior transition of Winsor I →III→II with and without polymer. Also, they found that anionic surfactants appear to be more compatible with polymers than the nonionic surfactants. Besides that, they reported a little difference in the IFT values with and without polymer and highlighted that polymer increases only the water-rich phase viscosity, with little effect on the microemulsion phase.

ALVESTAD et al. (1992) exhibited the dynamic behavior of surfactant systems for EOR applications regarding phase behavior and core-flood recovery process. The surfactant used was synthesized and optimized for seawater and heptane at 70°C, preventing the use of a cosurfactant. The phase behavior was determined at WOR equal to 20,10,4,2,1,1/2 and 1/3 for surfactant concentrations between 0 to 3 [%wt]. The sample was equilibrated for one week at 70°C. The results showed a transition Winsor II→III→I.

GREEN; WILLHITE (1998) illustrated that the microemulsion transition shown in Figure 2.9 is considered an ideal representation of the phase behavior, i.e., that multi-phase regions are uniquely defined. A real phase behavior is more complex than the transition mentioned above due to several middle-phase compositions are achieved that rather than a single point. This behavior can be caused by fractionation of one or more of the components into a pseudo-component. The presence of a precipitate in equilibrium with an oil-rich microemulsion and several liquid crystalline structures with birefringent properties are some indicators of nonideal phase behavior. Salter (1983) reported a complex experimental behavior.

NISHIMI (2008) explained the phase behavior in water/oil/surfactant systems and the basic principles of low-energy emulsification. Among five different surfactants used by them, only SDS and Disulfosuccionate Sodium Salt (AOT) exhibited two phases with a phase transition Winsor II→I at all salt concentrations. They also noticed that even at the point of balance between hydrophilicity and lipophilicity, a three-phase state, was not observed. The other surfactants presented a transition Winsor II→III→I.

LIU et al. (2008) and ZHANG et al. (2006) presented a laboratory study of an ASP process using crude oils from a West Texas Field, two surfactants and Flopaam 3330S as a polymer. Besides that, the interfacial tension was determined using a spinning drop tensiometer, and the results were compared with the value obtained using Chun-Huh correlation. The phase behavior exhibited a transition I→III→II. Moreover, they concluded that the experimental

tensions were in reasonable agreement with those predicted by Chun-Huh correlation based on the measured solubilization ratios.

LOPEZ SALINAS et al. (2009) performed the microemulsion viscosity measurements using a falling-viscometer with multiple ring-shaped and inductive proximity sensors. The microemulsion viscosity presented a Newtonian behavior. Besides that, the microemulsion viscosity in function of the salinity exhibited two local maxima and a local minimum. The latter is itself near optimal salinity.

WANG et al. (2010) exhibited results of more than 40 core flooding test assessments of a surfactant-polymer process in homogeneous and heterogeneous porous media. A detailed study of IFT between the fluids was carried out. For homogeneous porous media, ultra-low IFT formulations are required to reach very high displacement efficiencies. Whereas for heterogeneous formations, the maximum oil recovery was achieved at IFT critical values above the minimum IFT values, and the optimized viscosity for the process was not the maximum fluid viscosity. The IFT behavior for the different formulations evidenced that it does not exist a tendency associated with the polymer concentration in the solution, and IFT values presented little differences, maintaining the order of magnitude of their values.

SAGI et al. (2013) presented an evaluation of surfactants for CEOR process in a carbonate reservoir at 25°C with a salinity of 11.000 ppm of total dissolved solids (TDS). The phase behavior tests showed a transition of Winsor I→II without observed the Winsor III behavior. For this reason, they proposed some criteria to determine de optimal salinity based on the solubilization parameters and assuming that all the surfactant was in the microemulsion phase.

PACHÓN CONTRERAS et al. (2014) reported the preparation of petroleum sulfonates from selected petroleum distillate fractions from Colombian refineries. They evaluated these fluids as potential candidates for CEOR projects in Colombia. For the phase behavior tests, they used n-heptane and two Colombian crude oil as the organic phase, different petroleum sulfonates concentration, WOR =1, and n-pentanol as cosolvent. All experiments were conducted at 25°C. They reported a direct transition of Winsor I to Winsor II behavior.

3.5 Use of CT for EOR Process

Computed tomography has proved to be a useful tool for studies of the dynamics of fluids during EOR process. The evidence is shown below.

WELLINGTON; VINEGAR (1987) presented several petrophysical applications, including three-dimensional measurement of density and porosity, rock mechanics studies, correlation of core logs with well logs, characterization of mud invasion, fractures and quantification of complex mineralogies. They also included fundamental studies of CO_2 displacement in cores focusing on viscous fingering, gravity segregation, miscibility and mobility control.

VINEGAR; WELLINGTON (1987) showed a review of the principles of CT, explained a method to develop two and three-phase saturation measures based on CT images, described the CT scanner and remote processing software, pressure vessel, and scanner positional system. In addition, they detailed the importance of a correct choice of dopants products (some chemical product with a high atomic number) to be applied on some of the fluids with the purpose of improving the visualization and differentiate fluids during the core flood process. The authors included a review of dopants for brine, oil and gas phases. Finally, they reported independent IFT measurements of iodododecane/Soltrol showing that these systems had the same oil/water IFT as Soltrol alone.

HOVE; NILSEN; LEKNES (1990) showed the visualization of xanthan core-flood using CT. They used sodium iodide (NaI) as aqueous dopant product. Their experiments evaluated the one-phase flow of xanthan solutions and immiscible displacement using light refined oil with a viscosity of 1.4 [cp].

ALVESTAD et al. (1992) reported the use of CT during four core-flood experiments with a surfactant. The use of CT gave valuable information about the flow dynamics and the distribution of the residual oil in the core. They presented a way to calculate the water saturation *(S_w)* based on the CT data as follows:

$$S_w = \frac{CT_x - CT_{oi}}{CT_{wi} - CT_{oi}} \tag{3.2}$$

where:

CT_x = The CT number for image in question;

CT_{oi} = The CT number for 100% oil saturated core;

CT_{wi} = The CT number of 100% water saturated core.

The direct method to obtain the CT number for 100% oil saturated core implies of fully saturate the core sample with oil. Then, it is necessary to do the tomography and, finally, clean

and extract the oil from the core sample. To avoid this procedure, the authors show a way to calculate CT_{oi}.

$$CT_{oi} = CT_{DI} + \frac{CT_o - CT_A}{CT_w - CT_A}(CT_{WI} - CT_{DI}) \tag{3.3}$$

where:

CT_{DI} = The CT number for dry core;

CT_o = The CT number to oil in core holder;

CT_A = The CT number to air in core holder;

CT_w = The CT number to water in core holder.

Thats method is the first one (*CT 1*) used in this research to estimate the saturation profile through CT.

COLES; MUEGGE (1995) focused on the importance of calibrating or have a reference for CT values during the long experimental process. They presented three different methods used to improve the accuracy and reliability of CT results and showed the importance of these procedures for the calculation of saturation profiles. Additionally, they presented the following mathematic expression for the calculation of porosity.

$$\theta = \frac{CT_{ts1} - CT_{ts2}}{CT_{f1} - CT_{f2}} \tag{3.4}$$

where,

CT_f = The CT number of a given fluid;

CT_{ts} = The CT number for 100% saturated core with that fluid.

For water saturation profile calculates, the expression presented is the same as Equation 3.2 without the term for CT_{oi}.

HICKS (1996) presented a summary about of CT utilities in the petroleum engineering and showed the images results of a displacement process using benzyl alcohol, water, and decane to model the oil, water, and gas system. Based on this, gravity segregation of the benzyl alcohol was observed, even though the region was in steady state condition.

SHARMA; BRIHGAM; CASTAINER (1997) introduced the second method (*CT 2*) used in this work to estimate the saturation profile through CT. They presented a complete report on the use of CT techniques for Two-Phase and Three-Phase in-situ saturation measurements. They exposed details about of the experimental procedures, the data acquisition, and data processing computer programs. Also, they showed a mathematic expression to calculate the two-phase saturation as written below:

$$S_o = \frac{(CT_x - CT_{wi})(1 - S_{wc})}{(CT_{swc} - CT_{wi})} \tag{3.5}$$

where:

CT_x = The CT number for image in question;

CT_{wi} = The CT number of 100% water saturated core;

CT_{swc} = The CT number at connate water saturation;

S_{wc} = Connate water saturation obtained from material balance.

The authors eliminated the assumption that X-ray attenuation for a pure component is constant over the complete scanned area, removing the need for pure component CT attenuation values. This approach was verified by waterflood experiments with and without dopant products, exhibiting good agreement when existing sufficient difference between the CT values of the fluids used. The dopant used in these tests was 1-bromo dodecane at 50% concentration. They indicated 1-Iodo dodecane as a possible dopant, once it is more efficient to increase the CT attenuation properties of the oil.

CHAKRAVARTHY et al. (2004) showed CO_2 and WAG flooding experiments in homogenous and fractured rock with in-situ saturation and porosity measurements using CT. They presented the experimental process used to develop the tests. The oleic phase used was Soltrol 130 and Iodohexadecano. They used Berea Sandstones with a diameter of 2.5 cm and a length of about 10 cm. The overall efficiency of the process was analyzed by combining the CT measurements and the measurements of effluent volumes.

LONDON et al. (2014) used the CT to evaluate the performance of three experiments injecting brine and polymer into a sand pack saturated with heavy oil. The authors utilized the following equation to determine the oil saturation in the process.

$$S_o = \frac{CT_w - CT_E}{CT_w - CT_o} * \frac{CT_{wi} - CT_x}{CT_{wi} - CT_{DI}} \quad (3.6)$$

where:

CT_x = The CT number for image in question;

CT_{wi} = The CT number of 100% water saturated core;

CT_{DI} = The CT number for dry core;

CT_o = The CT number to oil in core holder;

CT_w = The CT number of water in core holder;

CT_E = The CT number to the vacuum in core holder;

The equation (3.6) was adjusted once they used a vacuum-saturated endpoint instead of an oil-saturated one. Besides, they showed that the attenuation values for the fluids usually differ from bulk values measured separately. Therefore, these calculations must be calibrated using porosities and saturation obtained from volumetric balances on the injected and produced fluids. That is the third method (*CT 3*) used in this work to estimate the saturation profile through CT.

BATENBURG et al. (2015) described a series of experiments that used CT to visualize the mobilization of remaining oil by ASP flooding after conventional water flooding. The tests were developed in core samples from Gildehauser and Berea Sandstone with diameters of approximately 7.55 cm and lengths of 27.5 and 99 cm. Two light crude oils with viscosities of 1.3 cp and 3.2 cp were used. The tests were conducted at two different temperatures with two different formation brine compositions. Flopaam 3330 S, bromobenzene, and iodobenzene were used as polymer and dopants products, respectively. In addition, phase behavior tests were developed using these dopant products, and they concluded that the systems presented a similar phase behavior with and without dopant products.

4 MATERIALS AND PROCEDURES

Chapter 4 introduces the different materials, devices or equipment and a step by step explanation of the experimental methods used to develop this research.

4.1 Materials

The materials presented below were chosen using as reference the screening and field properties showed in Item 3.1.

4.1.1 Rock samples

Sandstone samples with a diameter of 3.8 centimeters [cm] and length of 27 [cm] of Botucatu Formation, located in Ribeirão Claro at Paraná Sedimentary basin were selected. The Botucatu Formation is mainly constituted by Sandstones of fine to medium granulation, uniform, with a good selection of frosted grains with high sphericity. They are reddish and show medium to large tangential cross stratification, characteristic of walking dunes (MENDONÇA; COCHAR GUTIERRE, 1998).

4.1.2 Brine

Sodium Chloride (NaCl) with purity of 99% obtained from Sigma Aldrich was used as an electrolyte in the distilled water, polymer and SP solutions. The Synthetic Brine selected (Brine II - Table 3.5) contained 0.7093 [%wt] of dissolved NaCl, and its density and viscosity were measured at atmospheric pressure and a temperature of 50° C to be 0.990 [g/cm^3] and 0.6 [cP], respectively.

4.1.3 Oil

A viscosity between 16 – 20 [Cp] was the primary parameter to select the oil phase. Based on this, in this work is used the term “oil I” to describe a mixture of Field dehydrated oil and Kerosene 28.6 [%wt]. This oil mixture was used to develop all laboratory experiments before the core flooding tests. A rheological study determined each fluid proportion. The Oil I density and viscosity were measured to be 0.881 [g/cm^3] and 18.5 ± 1 [cP], respectively, at atmospheric pressure and a temperature of 50° C.

On the other hand, it is important to highlight that iodated oil (*Iododecane* - I_{10}) was selected as dopant product to improve the visualization of the oil phase flow by CT acquisition. Therefore, during core flooding tests, this oil phase is called “Oil II” to describe a mixture of Field dehydrated oil, Kerosene 21 [%wt] and I_{10} 10 [%wt]. The Oil II density and viscosity

were measured to be 0.916 [g/cm^3] and 18 ± 1 [cP], respectively, at atmospheric pressure and a temperature of 50° C.

4.1.4 Polymer and surfactant

The polymer selected was the Synthetic HPAM, Flopaam 3230S from SNF Floerger with a molecular weight (M_w) of 5 x 10^6 [g/mol], 30% degree of hydrolysis, water content less than 1%, thermal stability up to 160 ºC (MELO; LUCAS, 2008). Besides that, the Sodium dodecyl sulfate (SDS) from LabSynth with M_w of 288.373 [g/mol] and a purity of 99.23% was selected as a surfactant.

This polymer was chosen because the molecular weight of HPAM has a direct relationship with the permeability of the porous media through the polymer will be injected (SHENG, 2013). On the other hand, the SDS has already been evaluated as a useful chemical for a CEOR process with a similar oleic phase composition (SANABRIA, 2013).

4.2 Devices and Equipment

Table 4.1 presented the devices and equipment used.

Table 4.1 Devices and equipment

Device / Equipment	**Model**	**Maker**
Reometer	Haake Mars III	Thermo Scientific
Pendant-drop Tensiometer	PAT-1M	Sinterface Tech
Density Meter	DMA - 4100	Anton Paar
Positive Displacement Pump	260D Syringe	Teledyne
Vacuum pump	SK49PN4157	Core Laboratories
Vacuometer	Vacustat	Edwards
Adjustable-Volume Micropipette	I1-V200	Go Pet II
Analytical Scale	XB220A	Precisa
Porosimeter	3020.062	Core Laboratories
Permeameter		Core Laboratories
Core Holder	Série FCH	Core Laboratories
Accumulators	Steel Accumulators	
Pressure Transducer	3051 Coplanar	Rosemount
Pressure Data Acquisition	LabView	
X-Ray Scan	Somaton Emotion 16	Siemens

The devices and equipment are available at the next following laboratories: LEMP (Laboratory of Flow Through Porous Media) and LabMEV (Laboratory of Scanning Electron Microscopy) of Mechanical Engineering School (FEM), LABORE (Reservoir Oil Laboratory), LGE (Flow Assurance Laboratory) and LMMR (Laboratory of Miscible Methods of Recovery) of Center For Petroleum Studies (CEPETRO) at University of Campinas.

4.3 Methodology

This research was developed in three main steps. The first of them involves the design of fluids and the understanding of the interaction between surfactant-polymer. The second step encompasses the activities conducted previously to core flooding tests. The last step includes an assessment of an SP process performance through core flooding tests evaluated by CT. Figure 4.1 summarized the activities realized.

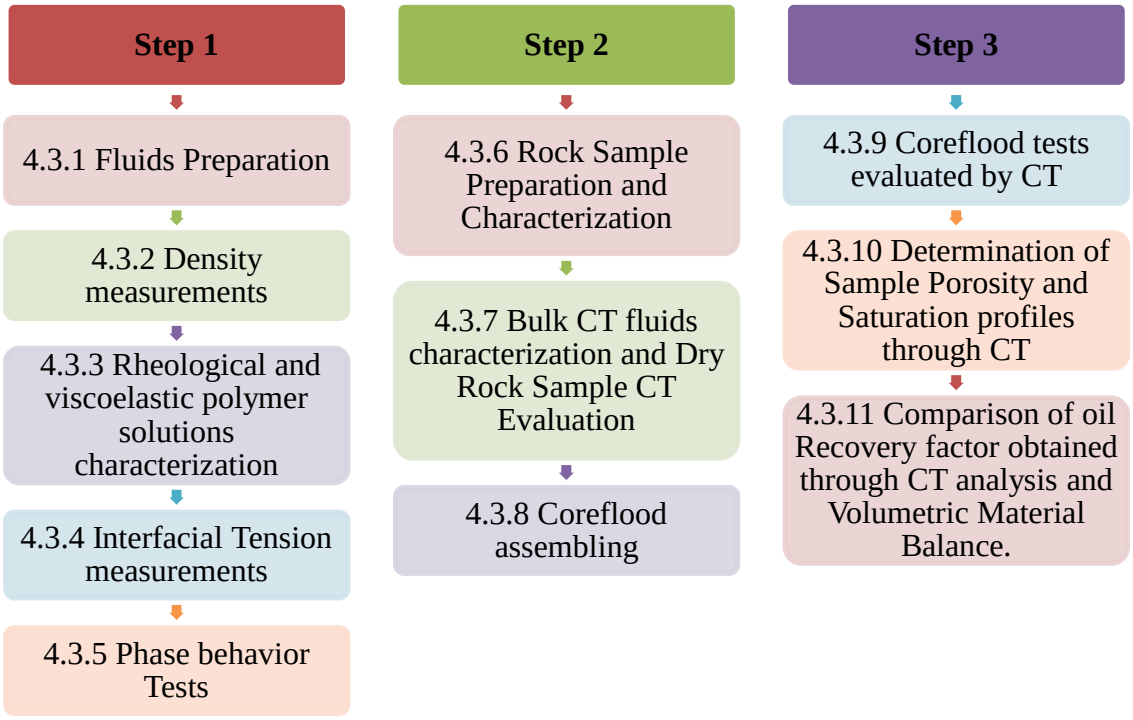

Figure 4.1 Methodology Steps

Below the activities conducted in each step are explained in detail.

4.3.1 Fluids preparation

The procedure used to prepare the fluids followed API RP 63. A stock HPAM solution containing 5000 ppm of the polymer was prepared using the synthetic brines (SB) exhibited in Table 3.5. The SB were deaerated utilizing a vacuum pump. These HPAM solutions were

agitated using a magnetic stirrer during (5 – 7) h to form a consistent solution, i.e., the solution exhibited a homogeneous aspect, and it did not have insoluble particle (fisheye). All of the HPAM solutions were prepared carefully with the minimum agitation to avoid mechanical degradation of the long-chain molecules. The stock solutions were left still overnight to ensure full hydration.

Then, HPAM stock solutions were diluted with SB up to desired concentrations (eleven different concentrations). The new solutions were put into a beaker and homogenized by magnetic stirrer at low speed (120 rpm) for 10 minutes. All HPAM solutions were stored in closed recipients to minimize oxygen uptake.

The preparation of the surfactant-polymer (SP) blend solutions differs from the process exhibit below only in the kind of solution used to prepare the polymer stock solution. In this case, a mixture of brine and surfactant was used. The surfactant (SDS) and polymer (HPAM) concentration analyzed were 0.5, 1, 1.5 and 2 [%wt] and 5000, 2000, 1500 and 1000 ppm, respectively.

4.3.2 Density measurements

Density was measured with an Anton Paar DMA - 4100 density meter, whose measuring principle is the oscillating U-tube method which the fluid sample is introduced into a U-shaped borosilicate glass tube and then, the tube is excited to vibrate at its characteristic frequency. The characteristic frequency changes depending on the density of the sample. Finally, the fluid density value is determined through a precise determination of the characteristic frequency and a mathematical conversion.

Three measurements for oil I, oil II, brine, and each polymer solution with and without surfactant were conducted to guarantee the repeatability of values. The tests were developed at 50° C and atmospheric pressure. HPAM concentrations of 2000, 1500 and 1000 ppm and a SDS concentration of 2 [%wt] were used. The SDS concentration used was the highest surfactant condition for this work.

Figure 4.2 Anton Paar DMA - 4100 Density Meter

4.3.3 Rheological and viscoelastic polymer solution characterization

In this part, the work was divided into two stage. The first was focused on to examine the salts, and temperature effects on the rheological and viscoelastic behavior of polymer solutions prepared with the reference field brines (Table 3.5). Is important spotlight that both synthetics brines are equivalent with the field brine reference, and the more significant difference is the divalent or monovalent cations presence. Therefore, this part aims to select one of those brine compositions to develop the following activities.

The second step was focused only on the investigation of the surfactant effect on the rheological behavior of polymer solutions. This step was conducted using the brine selected previously.

The study was performed in this way aiming to quantify and improve the understanding about of SP interactions based on the external conditions and chemical adding.

4.3.3.1 Rheological and viscoelastic assessments

The rheological and viscoelastic parameters were measured using a HAAKE MARS III rheometer, which is a high precision instrument. The sensor used was a concentric cylindrical (DG41), which is preferable to low viscous fluids. The temperature control system was the THERMO HAAKE C25P refrigerated bath with a Phoenix II Controller. A new sample was applied for each test, and every data were analyzed within the measuring range of the equipment. A mineral pattern oil (IPT-83) was used to verify the accuracy of the viscosity measurements.

Figure 4.3 HAAKE MARS III Rheometer

The flow curves were recorded at shear rates between (10^{-1} and 10^{3}) s^{-1} with 20 measurement points. These data were used for the analysis of viscosity, shear stress, and temperature effect.

The viscoelastic behavior was determined through frequency sweep tests (FST) covering a range of 0.062832 – 628.32 Rad/s with 25 measurements points. For this study, it was necessary to choose a shear stress value within the Linear Viscoelastic Region (LVR) previously determined through amplitude sweep tests (AST) conducted between 0.001 – 100 Pa, with 30 measurements points. These measurements were carried out at least in duplicate at 25 and 50 °C and atmospheric pressure to ensure the repeatability of the results.

4.3.4 Interfacial tension measurements

These measurements address the influence of the polymer concentration and Iododecane content on the interfacial tension behavior between aqueous/polymer and oil phases. For this, a pendant drop tensiometer (PAT-1M, Sinterface Tech) was used (Figure 4.4). This device has a measurement range of 1 up to 1000 [mN/m] and a resolution of ± 0.1 [mN/m]. Its performance is based on the generation of a drop-in front of a high-resolution camera with opposite lighting to generate a drop profile image which is captured in real time. The IFT is determined by fitting the drop shape with the Gauss-Laplace equation, which is shown below.

$$\sigma\left(\frac{1}{R_1}+\frac{1}{R_2}\right)=\Delta P_o+\Delta\rho g z \tag{4.1}$$

Where,

R_1 and R_2 are principal curvature radii of drop shape, σ is the IFT, ΔP_o is the pressure differential at a reference plane, $\Delta\rho$ is the fluids density difference, g is the gravity and z is the vertical height from the reference plane.

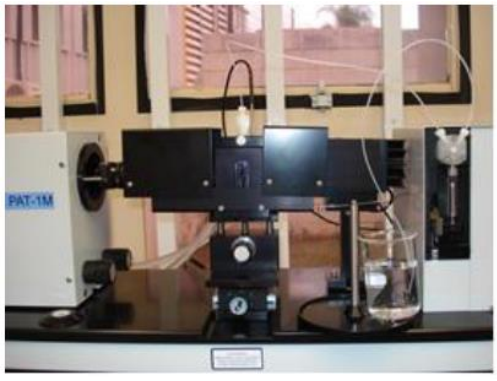

Figure 4.4 Pendant drop (PAT-1M) tensiometer

The measurements were conducted at 50 °C and atmospheric pressure with 20 measurements points during 6 minutes and two times to guarantee the repeatability of the results. The fluids used were an oil phase with and without Iododecane, brine, Polymer solutions with HPAM concentrations of 5000, 2000, 1500 and 1000 ppm without surfactant. The interfacial tension was determined by the buoyant bubble method. A hook-type needle with a diameter of 3 millimeters [mm] was used due to the oil density is lower than the brine and polymer solutions densities.

4.3.5 Phase behavior tests

This kind of analysis was used to determine solubilization parameters, optimal salinity for different surfactant concentration, type of microemulsion and low IFT values through Chun-Huh equations, i.e., IFT values < 1 [mN/m]. The measurements were run at the desired salinity, varying the surfactant concentration. The key assumptions made in this development were:
a) Isothermal conditions at 50 °C, b) Oil phase free of gas, c) Effect of divalent cations and alcohol on surfactant phase behavior is not investigated, d) Polymer and Iododecane have not effect on surfactant phase behavior, e) effect of pressure on surfactant phase behavior is neglected, f) WOR = 1. Similar assumptions have been reported for NAJAFABADI et al. (2012).

4.3.5.1 Development of phase behavior tests

These tests were based on salinity scans at different surfactant concentration Figure 4.5 summarized the applied strategy used for this step.

Solutions were made according to SALAGER (1977). The method is based on the preparation of highly concentrated surfactant and brine solutions; then these are diluted up to desired concentration values.

Different borosilicate pipettes of volumetric capability of 5 [ml] were filled separately up to 2 [ml] with solutions containing SDS at 0.5, 1, 1,5 and 2 [%wt], and varying the NaCl concentration of 0, 0.2, 0.5, 0.7, 0.9, 1.2, 1.5, 2 and 3 [%wt]. Then, the pipettes were heated until the investigation temperature and mixture. Finally, the pipettes were sealed and left still overnight to observe any precipitate appearance. Previously it was defined as an aqueous stability test (Figure 4.6).

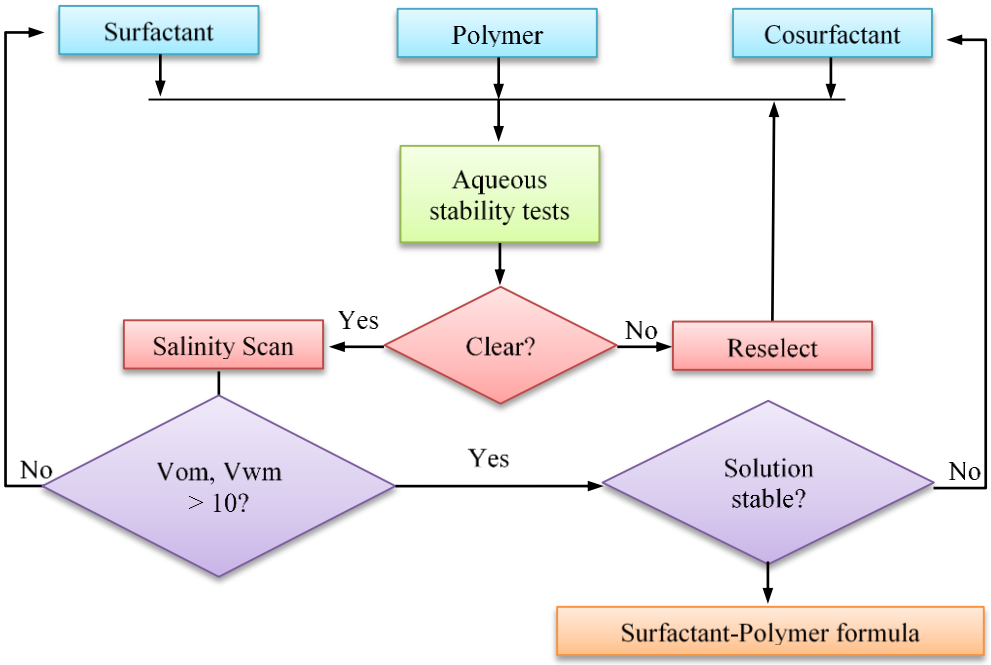

Figure 4.5 Flow chart of phase behavior test

To avoid the precipitation of some compounds during the pipettes filled is recommendable to spill the fluids as follows: 1) Brine, 2) Distilled water, 3) Surfactant Solution.

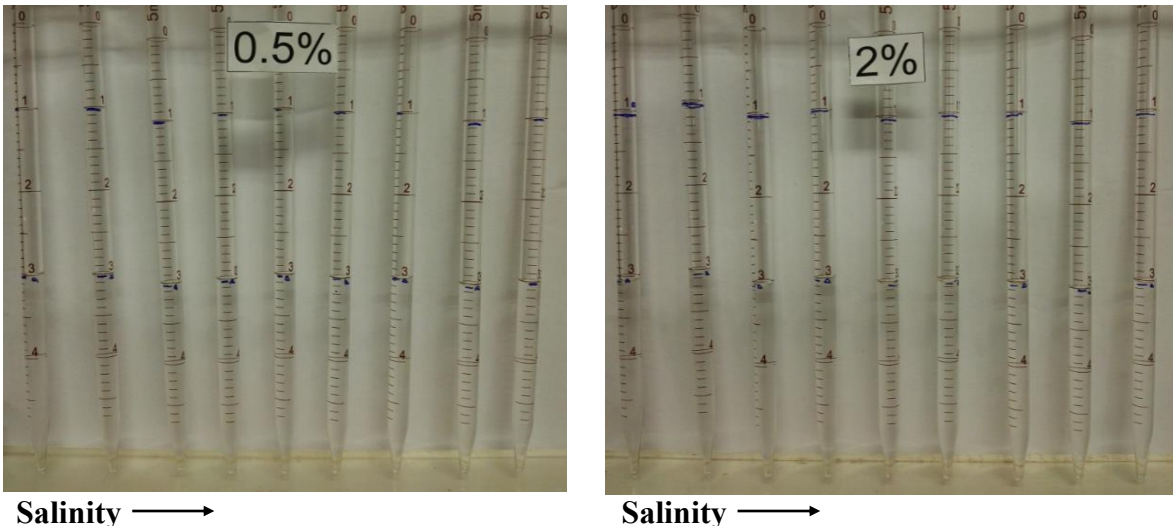

Figure 4.6 Aqueous Stability Tests.
a) SDS 0.5 [%wt], b) SDS 2 [%wt]

Later, 2 [ml] of the oleic phase were put inside the pipettes. These were sealed and equilibrated at constant temperature (Figure 4.7). Then, the pipettes were inverted six times every two hours during 8 hours. The last step was repeated the next day.

The volumetric and properties changes began to register 24 hours after the mixture process finished. The test ended when the system reached the equilibrium. According to HEALY; REED (1974), it occurs when not further macroscopic changes (volumes or number phases, color, transparency, and others) happen in a microemulsion.

Figure 4.7 Finished Pipettes Preparation. Before mixture process

4.3.6 Rock sample preparation and characterization

The rock samples were cut from a block of the Botucatu Formation named 12A using an industrial drill (Figure 4.8). These rock samples were characterized by permeability values below 1000 mD and porosities between 22-24 %, values closer to target conditions exhibited in the Table 3.3.

Then, each rock sample selected was put inside to the core holder exhibited in Figure 4.9. The system overburden was pressurized up to 1000 psi. After it, methanol and toluene were displaced throughout the rock samples aiming to remove the organic and inorganic compounds. A total of six pore volume of each fluid was used. Afterwards, the air was used to dry the rock for 24 hours. Finally, the rock samples were placed in the oven for a minimum of 24 hours. After these activities, the rock samples petrophysics characterization takes place.

Figure 4.8 Rock Samples Preselected

Figure 4.9 Cleaning Core holder Assembling

The porosity was measured using a gas porosimeter based on the nitrogen expansion within the rock to calculate the empty volume of it. This equipment does not give a direct measure of the pore volume (PV) of the rock. In fact, to obtain a real PV is necessary to subtract the dead volume of the system.

The permeability measure was carried out in a gas permeameter. The Equation (4.2) shows the mathematic expression proposed by the equipment maker to obtain the permeability, which is a Darcy Law adaptation.

$$K_g = \frac{CQ_g h_w L}{200A} \tag{4.2}$$

Where,

K_g = Gas Permeability, [Darcy];

Q_g = Gas Rate [**cm^3**/seg];

C = Height of Mercury Column [mm];

h_w = Height of Water Column [mm];

L = Rock Sample Length [cm];

A_{cs} = Rock Sample Cross Section [cm].

The absolute permeability (K_a) obtained value is corrected due to the Klinkenberg effect using the equation (4.3).

$$K_a = 0{,}68\left(K_g\right)^{1{,}06} \tag{4.3}$$

4.3.7 Bulk fluids CT values determination and dry rock sample CT evaluation

To know the bulk fluids CT values is necessary to reduce numerical errors at experimental conditions due to the assumption of the monochromatic X-ray nature during the determination of porosity and saturation profiles using CT images.

For this, an annular cylinder drilled from aluminum rods was used (Figure 4.10). This device was placed inside the core holder, pressurized at 3000 [psi], heated at 50 °C and filled with the fluids at the conditions mentioned previously. Then, CT scans were conducted to determine the attenuation coefficient values for synthetic brine, oil phase, nitrogen and air at 50 °C and atmospheric pressure.

Figure 4.10 Annular Cylinder

The dry rock samples were exposed to the same conditions inside the core holder, and then, were analyzed with the CT scan to determine some internal rock characteristics.

4.3.8 Core flood assembling

Figure 4.11 presents the schematic setup used for core flood tests. The experimental bench includes two accumulators filled with mineral oil to be used as a hydraulic piston for the fluids to be injected. Besides that, the assembling has a thermal bath to heat up the liquids before these come into the core holder up to 50 °C. A resistance heating jacket envelops the core holder to maintain water temperature in the annular space between the rubber that covers the rock and the core holder at 50 °C, approximately. Finally, assuming that the heat loss between the water and the rock is negligible is possible to affirm that the process is carried out under isothermal conditions.

Also, six pressure transmitters were used connected in parallel (three of 9 psi and three of 300 psi). These connections were done because the differential pressure (DP) expected during the imbibition 1 (K_w estimative) is smaller or closer than one psi. While the DP expected for the other stages is closer or higher than nine psi. One of these sensors captures the DP across

the total sample, i.e., between the rock face (inlet) and the end of the rock (output), and the others are responsible for capturing two different differential pressures along the rock (See Figure 4.12 and Figure 4.13). This setup was used to obtain the effective permeability of the injected fluids in three different stretches of the rock.

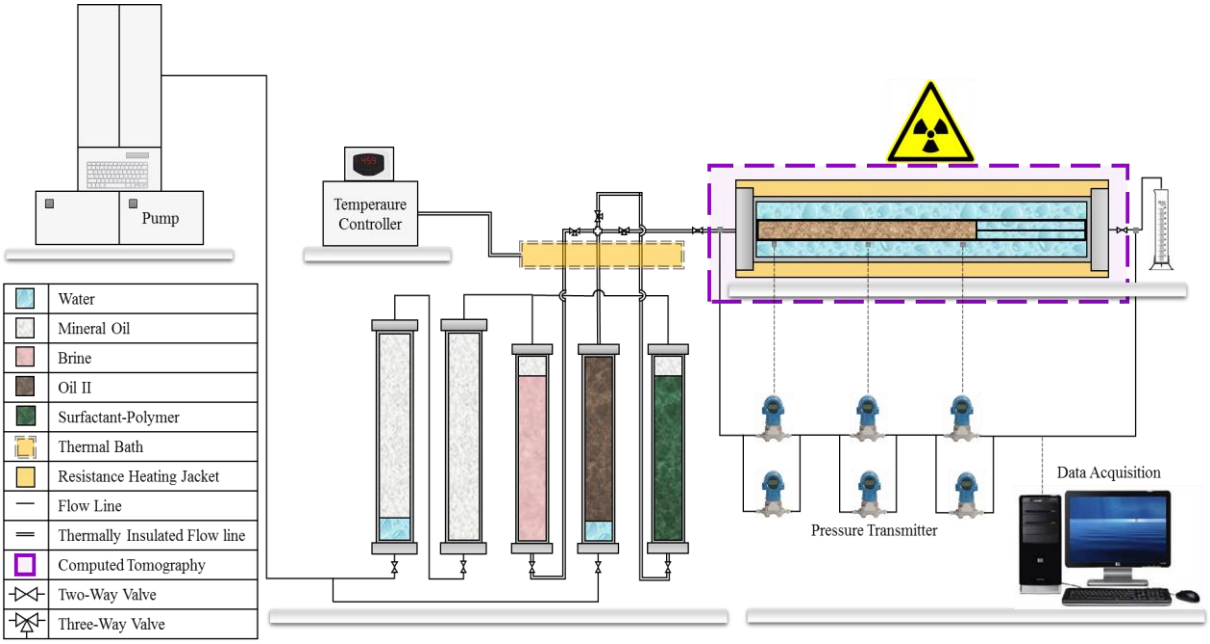

Figure 4.11 Schematic Coreflood Assembling

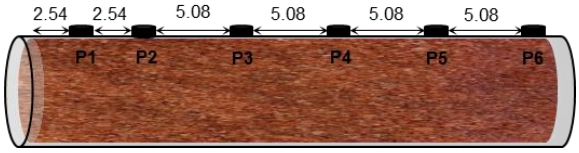

Figure 4.12 Schematic Pressure Taps Distribution

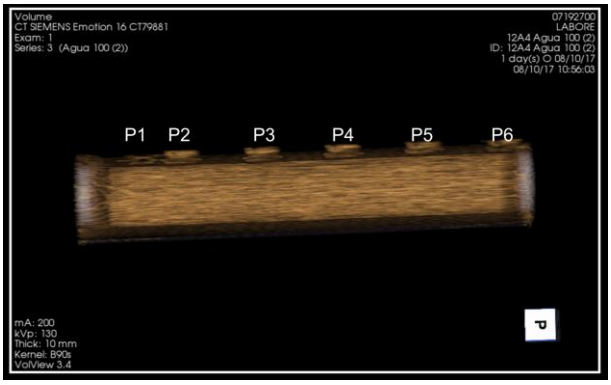

Figure 4.13 Real Pressure Taps Distribution obtained by CT

Figure 4.14 shows the final setup used for the core-flooding tests. Once the core holder with the rock sample is positioned on the tomograph bed, it cannot be moved. This condition is needed because the image treatment is based on mathematical operations using the same position scans, which were acquired at different time instants.

Figure 4.14 Real Core flood Assembling

4.3.9 Core flooding tests

This research encompasses three different core-flooding experiments evaluated by CT. The first test was designed to recreate the oil recovery process by water injection. The second one aims to analyze the oil recovery using a continuous flood of a tailor-made surfactant-polymer (SP) blend through the rock at initial reservoir condition (S_{wi}-Initial Water Saturation and S_o-High Oil Saturation), i.e., in this case, the SP process is studied as a secondary oil recovery method. Finally, the third test aims to assess the performance of the same surfactant-polymer blend solution as a tertiary oil recovery method, i.e., Chemical injection starts when the oil saturation into the rock is close to the residual value (S_{or}). The preliminary planning is shown below (Table 4.2).

The CT scan acquisitions during the core flooding tests were planned as a function of the pore injected volume it being in function of the injected pore volume (PVInj) of fluid. The space interval between slices was of 10 [mm]. Excluding the slices related to the inlet and outlet

diffusers, a total of 26 slices images were registered at each tomography scan. The energy used was 130 kVA and a pitch of 1. The image treatment was done using the software *Image J-Fiji*.

Table 4.2 Experimental Planning to Coreflooding Tests.

		Test 1	**Test 2**	**Test 3**
Kind of Test		Waterflooding	SP as Secondary Method	SP as Enhanced Method
Core Sample **Porosity (%)** **Permeability (mD)** **PV (cm^3)**		12A4 23.82 534.52 72.58	12A4 23.82 534.52 72.58	12A2 23.41 435.32 68.58
Injection Rate (cm^3/min)		0.5	0.5	0.5
Imbibition 1		Brine II	---	Brine II
Drainage 1 **PVInj** **Fluid quantity**		Oil II 7 508.03	---	Oil II 7 480.03
Waterflooding **PVInj** **Fluid quantity**		Brine II 15 1088.65	---	Brine II 7 480.03
Drainage 2 **PVInj** **Fluid quantity**		---	Oil II 7 508.03	---
CEOR 1	**SP Injection 1** **PVInj** **Fluid quantity**	---	Blend HPAM 2000 ppm + 0.5 [%wt] SDS 15 1088.65	Blend HPAM 2000 ppm + 0.5 [%wt] SDS 0.7 48.00
	Drive **PVInj** **Fluid quantity**	---	Brine II 7 508.03	Brine II 4 274.31
CEOR 2	**SP Injection 2** **PVInj** **Fluid quantity**	---	---	Blend HPAM 2000 ppm + 0.5 SDS 0.5 34.29
	Drive 2 **PVInj** **Fluid quantity**	---	---	Brine II 4 274.31

The tests 1 and 2 were conducted in the same rock sample (12A4) as a continuous process. Test 2 was performed after oil re-saturation of rock sample (Drainage 2).

The injection rate was chosen within the stability flood criteria proposed by (DOS SANTOS; BEDRIKOVESTSKY; HOLLEBEM (1997).

The core flood protocol included the steps summarized following:

Initially, the rock sample is exposed to an overburden pressure of 3000 [psi] and 50 °C for a minimum of 24 hours. Then, the vacuum pump is connected up to reach a vacuum value of 0.05 mBar in the vacuometer. This vacuum is maintained for 24 hours. Finally, the brine solution is admitted in aiming to fill up all the pore volume. To guarantee a better water saturation, a positive pressure of 80 psi is applied to the brine accumulator. The imbibition 1 begins after the rock is fully saturated. Then, brine flows at different injection rates with the purpose of estimating the absolute rock permeability (K_w) using the Darcy's Law.

The drainage 1 is the next stage; it consists of the oil injection until no water is produced. i.e., there is no mobile water in porous media. This condition is known as restoration of the rock at initial reservoir conditions (S_{wi} and S_o).

At this condition, the assessment of the oil recovery starts using brine as injection fluid until the no oil is produced. i.e., the rock is at the residual oil saturation (S_{or}) and high-water saturation (S_w). These activities are named waterflooding (WF).

The next step only was conducted using the rock sample 12A4 during Test 2, and it is named Drainage 2. It consists of the oil re-saturate the rock sample with oil, restoring similar initial rock conditions to those of WF, i.e., fluids saturations close to S_{wi} and $S_{o,}$ again.

Then, the chemical injection starts. In test 2 the primary objective was to evaluate the maximum potential of the selected SP blend and compare its performance with the WF. The displacing fluid is injected up to null oil production, similarly to the WF step previously explained.

The test 3 encompasses the chemical injection and starts after a WF have been conducted up to an oil saturation close to the residual oil (S_{or}) condition. The brine quantity to reach the previously mentioned condition was based on the test 1 results, i.e., when the water cut (Wcut) is higher than 90 %, and the oil recovery factor (FR) present smaller changes.

Therefore, the test 2 and test 3 are considered a secondary and tertiary oil recovery methods, respectively.

Finally, each chemical injection was followed by chase brine injection.

5 RESULTS AND DISCUSSIONS

This investigation project was developed in 3 sequential steps. The results obtained at each stage are following presented.

5.1 Results of Step 1 of the Methodology

It covers the density measurements, analysis of rheological and viscoelastic fluids characterization, interfacial tension measurements and phase behavior tests.

5.1.1 Density measurements

The measurement results are summarized in Table 5.1.

Table 5.1 Density Measurement Results at 50 °C

Fluid	**Density [g/cm^3]**
Brine	0.990
Brine + HPAM 2000 ppm	0.991
Brine + HPAM 2000 ppm + SDS 2 %wt	0.996
Brine + HPAM 1500 ppm	0.992
Brine + HPAM 1500 ppm + SDS 2 %wt	0.996
Brine + HPAM 1000 ppm	0.992
Brine + HPAM 1000 ppm + SDS 2 %wt	0.996
Oil I = Marlim Field 71.4% + Kerosene 28.6% in %wt	0.881
Oil II = Marlim Field 69 % + Kerosene 21 % + I_{10} 10 % in %wt	0.912

For polymer solutions, the HPAM and SDS concentrations did not affect the density of the solution significantly. The tendency was to increase the value. Nevertheless, changes were appreciable in the third significant number only. Therefore, both chemical products were considered not influence the density of the brine.

On the other hand, Oil I and Oil II present a notable density difference. That difference is due to the lower kerosene content in the Oil II as compared to Oil I. Iododecane replaced part of the kerosene content in the mixture of the Oil II.

5.1.2 Rheological and viscoelastic polymer solutions assessment

Results obtained for the activities proposed in Items 4.3.1 and 4.3.3 are shown below.

5.1.2.1 Flow Curves

Figure 5.1 shows flow curves for polymer solutions prepared with both brine compositions (Table 3.5) and different HPAM concentrations.

The apparent viscosity of the solutions decreases as polymer concentration diminishes. Besides that, when shear rate increases the solution viscosity decreases, elucidating that the HPAM solutions exhibit a shear thinning behavior. This response is due to uncoiling and alignment of the polymer chains upon exposure to shear flow as observed by other authors (BARNES; HUTTON; WALTERS, 1989; SAMANTA et al., 2010).

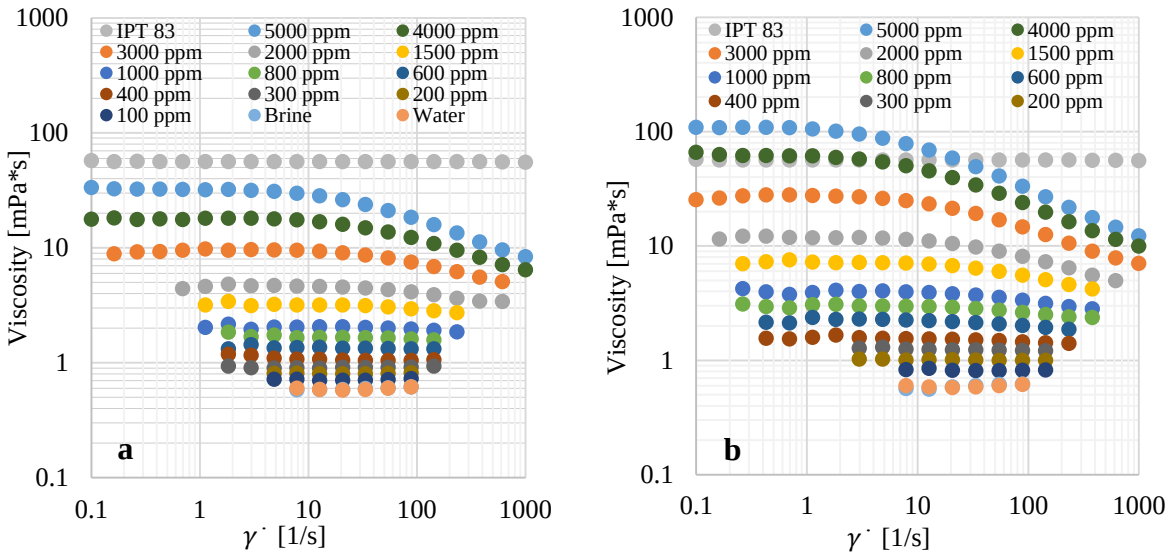

Figure 5.1 Viscosity vs. Shear Rate for polymer solution with different HPAM concentrations at 50 °C. a) Synthetic Brine I b) Synthetic Brine II.

5.1.2.2 Salts and Temperature effects on the rheological behavior of polymeric solutions

Rheological tests were conducted at laboratory temperature (25° C) to isolate temperature effect and to study the salts influence. Figure 5.2 summarized the results and allowed comparing solutions with divalent ions content (SBI) and without them (SB II).

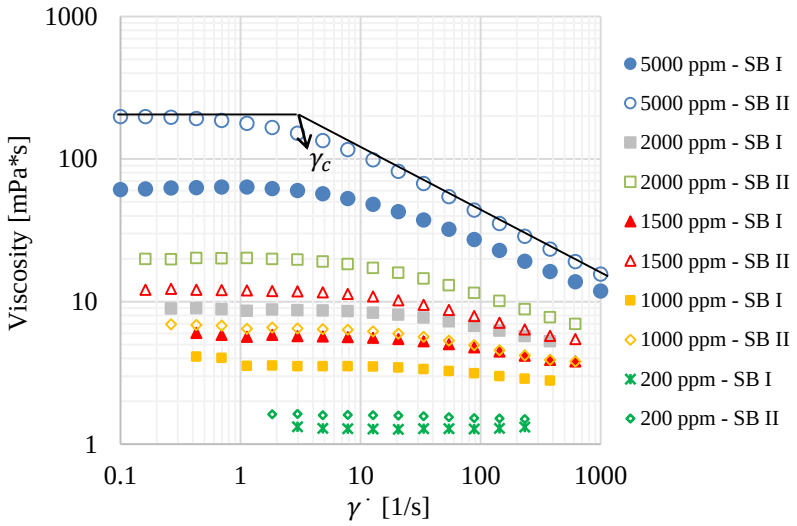

Figure 5.2 Viscosity vs. Shear Rate for HPAM solutions with different Synthetic Brines at 25 °C.
(SB I: Na^+, Cl^-, K^+, Ca^{+2}, Mg^{+2}; SB II: only Na^+, Cl^-)

In Figure 5.2, one can see that the divalent ions influence is more notable for low shear rates and solutions of high HPAM concentration. The divalent ions effect on the polymer chain diminish as the polymer solutions are more diluted, , i.e., for HPAM concentrations below 1000 ppm, the solution viscosity loss is less affected by divalent ion content. Also, the SB I causes a more significant detrimental effect on the polymer solution than SB II.

The presence of Na^+ generates shrinkage on the molecular chains. The effective neutralization of negative charges promotes a compression of the flexible chains. As the Na+ content increases, the ionic strength due to electrostatic repulsion among the anions is shielded raising the flexibility and diminishing the hydrodynamic radius, while the double electrical layers on the polymer molecular chains are compressed (SAMANTA et al., 2010; SHENG, 2011; SORBIE, 2013). On the other hand, the divalent cations (Ca^{+2}, Mg^{+2})interact with the polymer negative loads, neutralizing the effect of the molecular expansion (MELO et al., 2002; MELO; LUCAS, 2008).

Critical shear rate (γ_c) represents the transition between the Newtonian behavior or initial plateau and the beginning of the shear-thinning behavior (Figure 5.2) The reduction in the polymer chain size due to charge shielding according to the increase cations concentration gives a higher critical shear rate. Accordingly, the Newtonian behavior will extend over a wider range of shear rate.

The cations effects explained above also occur at 50 °C. However, SAMANTA et al. (2010) showed that the temperature generates an increment in the average speed of the

molecules within the liquid, thereby, the interaction time with neighboring polymer molecules decreases. As the temperature increases, the average intermolecular forces decrease. Similar behavior was reported (SILVEIRA; LOPES; MORENO, 2016).

The Arrhenius equation (Equation3.1) was used to correlate the temperature effect on the viscosity of HPAM solutions. For this, a shear rate of 7.8 s^{-1} was selected, which is close to the shear rate experienced by the fluid in reservoir conditions (MELO et al., 2005, 2002). Table 5.2 shows the fit parameters for all polymer solutions.

Table 5.2 Fit parameters used for Arrhenius equation on Polymer Solutions

Concentration (ppm)	Synthetic Brine I		Synthetic Brine II	
	ΔE_η(kJ/mol)	A (Pa*s)	ΔE_η(kJ/mol)	A (Pa*s)
5000	18,374	3,196E-05	12,630	7,115E-04
4000	18,846	1,570E-05	12,055	5,646E-04
3000	18,068	1,141E-05	14,645	1,066E-04
2000	19,628	3,110E-06	15,132	4,083E-05
1500	18,474	3,276E-06	14,989	2,672E-05
1000	17,407	3,141E-06	15,097	1,436E-05
800	17,333	2,616E-06	15,065	1,089E-05
600	16,393	3,042E-06	14,873	8,842E-06
400	15,043	3,981E-06	15,266	5,257E-06
300	16,973	1,635E-06	15,645	3,708E-06
200	14,713	3,392E-06	15,073	3,679E-06
100	16,064	1,814E-06	13,019	6,498E-06

The previous data shows that the change in the ΔE_η value is not meaningful regardless HPAM concentration. This result means that the viscous activation energy is almost independent of the polymer concentration, similar to literature reports (GHOSH; MAITI, 1997; MAITI; MAHAPATRO, 1988). Furthermore, the ΔE_η value is related to the influence of temperature on the viscosity of the polymer solutions (SAMANTA et al., 2010). The Arrhenius plot exhibited in Figure 5.3 shows the detrimental temperature effect on the polymer solutions. The temperature is expressed in absolute units.

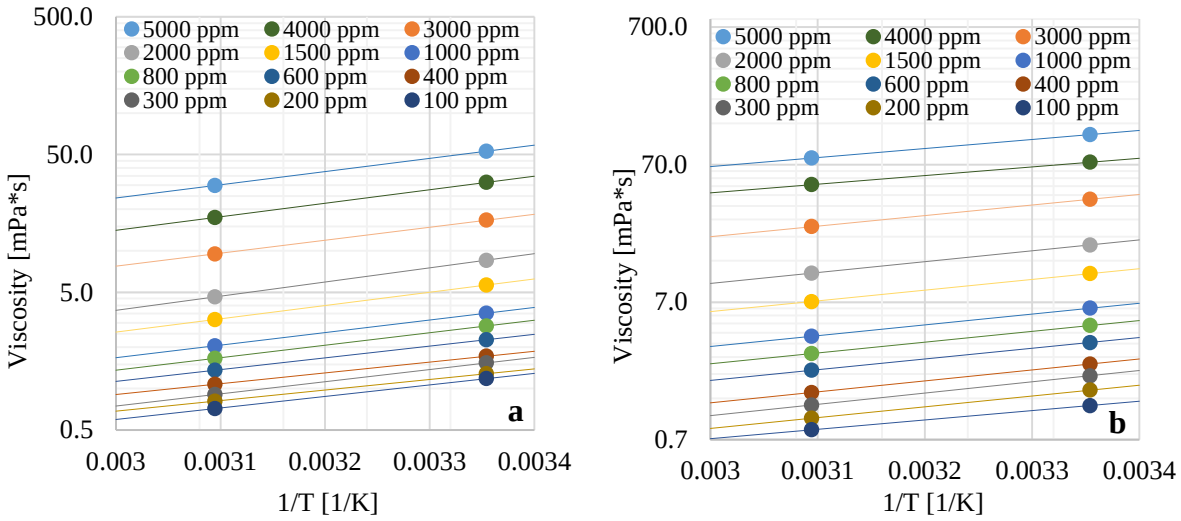

Figure 5.3 Arrhenius plot of viscosity at different HPAM concentration with constant shear rate, γ= 7.8 [s^{-1}]. a) polymer solution with SB I; b) polymer solution with SB II.

In Figure 5.3 one can observe that polymer solutions prepared using SB I and HPAM concentrations below of 400 ppm, the viscosity does not have a significant difference concerning the brine viscosity value at 50 °C.

Nevertheless, the viscosity reduction can influence the displacement flooding efficiency at laboratory and field operations. Even though both temperature and divalent ions generate detrimental effects on the rheological behavior, this work concludes that the most substantial contribution to the viscosity reduction at share rates close to those in the reservoir is due to the presence of divalent ions.

5.1.2.3 Viscoelastic Behavior of Polymer Solutions

Viscoelastic HPAM solutions can reduce the residual oil saturation due to the phenomenon of expansion and contraction of the fluid during the flow through porous media (URBISSINOVA; TRIVEDI; KURU, 2010). This effect modifies the forces (capillary and viscous) that maintain the oil trapped and induces the movement of a part of the residual oil (WANG et al., 2001).

The tests to analyze the effect of the salt on the viscoelastic behavior were conducted at 25ºC, just like the ones presented in Item 5.1.2.2. Initially, we carried out Amplitude Sweep Tests (AST) for all polymer solutions. Figure 5.4 shows a comparison of results of AST for polymer solutions with SB I and SB II at different HPAM concentrations. In Figure 5.4, one can notice the existence of a horizontal and parallel behavior of G’ and G’’; allowing to affirm that in a given range of shear stress exists a Linear Viscoelastic Region (LVR).

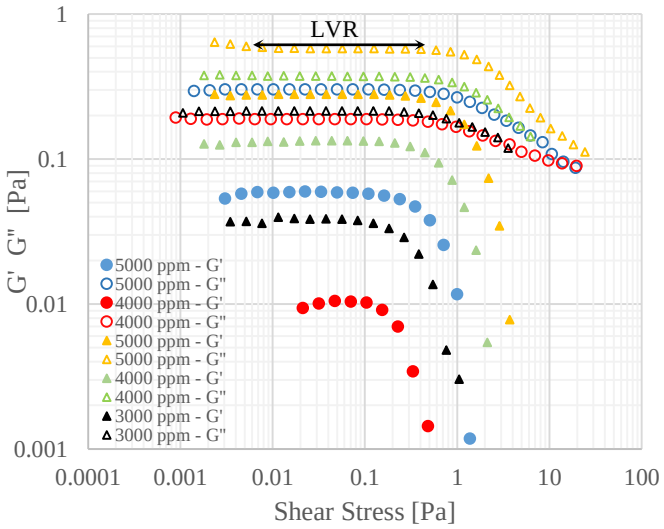

Figure 5.4 AST results. G' G'' vs. Shear stress at 25 °C.

Where the Circle and triangle represent HPAM solutions with SB I and SB II, respectively.

Figure 5.4 reveals smaller LVR when the solution includes divalent ions, due to higher ionic strength, apparently reducing the intermolecular interactions ((PERTTAMO, 2013). Also, the LVR diminishes as the HPAM concentration decreases. Similar behavior has been reported (SILVEIRA; LOPES; MORENO, 2016). For the polymer solution with SB I (the highest divalent ions content) the LVR was present down to 4000 ppm of HPAM. The other polymer solution has LVR down to 3000 ppm of HPAM.

After the AST tests, a shear stress value of 0.1 [Pa] was selected to execute the Frequency Sweep Test (FST). This value was chosen to guarantee that the tests are executed inside the LVR. The results of the FST are shown in Figure 5.5.

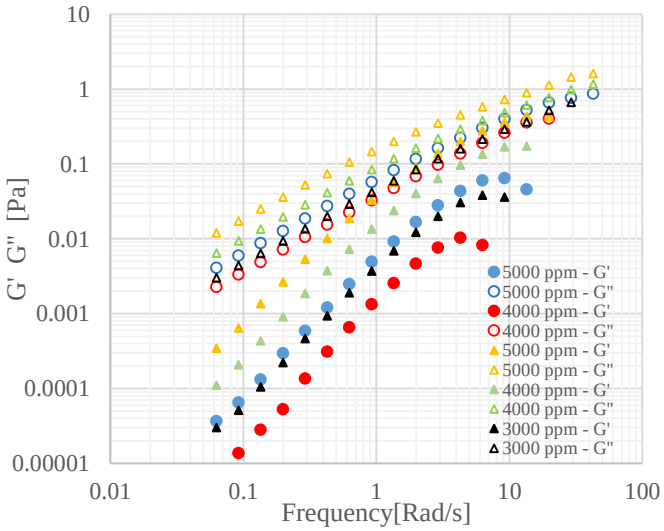

Figure 5.5 G' G'' vs. Frequency at 25 °C.

Circles and triangles represent HPAM solutions with SB I and SB II, respectively.

Figure 5.5 shows that the G' is more affected than the G'' modulus when the solution includes divalent ions. Thus, the measured value of elasticity decreased earlier at lower shear stress value for polymer solutions with SB I as compared to polymer solutions with SB II. similar behavior has been reported (URBISSINOVA; TRIVEDI; KURU, 2010).

Analyzing the temperature effect on viscoelastic behavior, the LVR disappears for polymer solutions with SB I at 50°C at the concentrations tested (See Figure 5.6).

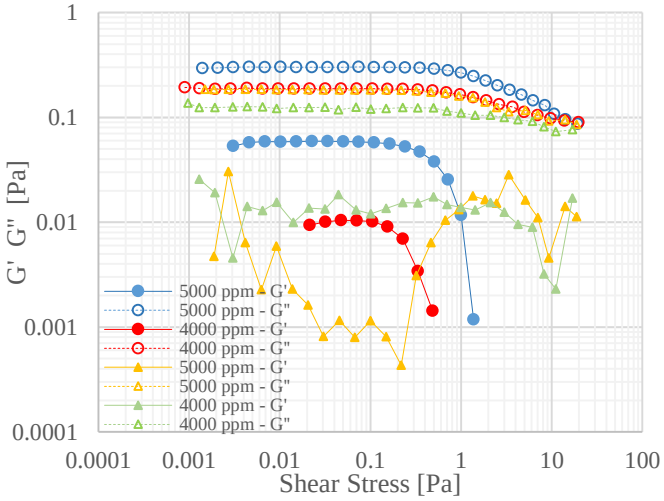

Figure 5.6 AST results. G' G'' vs. Shear Stress of HPAM solution with SB I.
Circles and triangles correspond to a temperature of 25 and 50°C, respectively.

On the other hand, for polymer solutions with SB II, the reduction of LVR is identified when the temperature increases. LVR is present down to 4000 ppm at 50°C. Besides that, G'' was predominant, and G' began to diminish. The above results allow inferring that HPAM concentrations less than 4000 ppm behave as a purely viscous fluid. (See Figure 5.7).

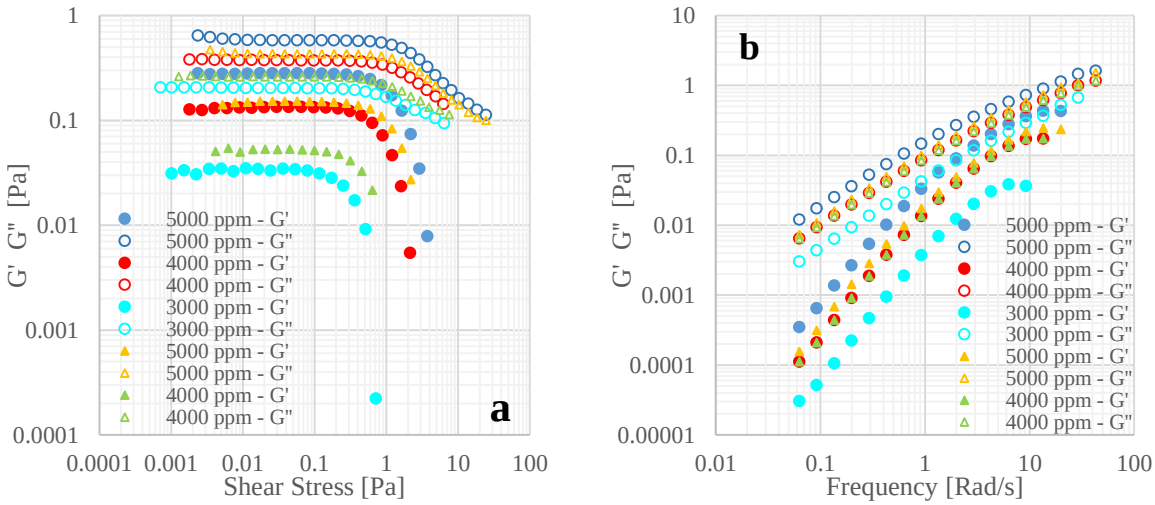

Figure 5.7 Comparisons (a) AST results and (b) FST results for polymer solutions with SB II.
Circles and triangles correspond to a temperature of 25 and 50 °C, respectively.

Analyzing the results presented in Item 5.1.2, one can notice that the polymer solutions with SB II presented the best rheological and viscoelastic behavior for the application proposed in this work. For these reasons, the SB II was selected as the reference brine to developing the next activities in this work.

5.1.2.4 Surfactant effects on rheological behavior of polymer solutions

This investigation aims mainly to evaluate the oil recovery improvement using a continuous and a slug injection scheme of a surfactant-polymer blend monitoring these processes with CT scan. It is expected that the blend can improve the mobility ratio at the same time that reduces the interfacial tension between the fluids in the rock. For this reason, HPAM concentrations of 2000, 1500 and 1000 ppm were selected as possible candidates to be used once their viscosity values at a shear rate of 7.8 s^{-1} are half or less of oil viscosity value.

The surfactant effects on polymer solution viscosity were analyzed for SDS concentrations of 0.5, 1, 1.5 and 2 [%wt]. The results are exposed in Figure 5.8.

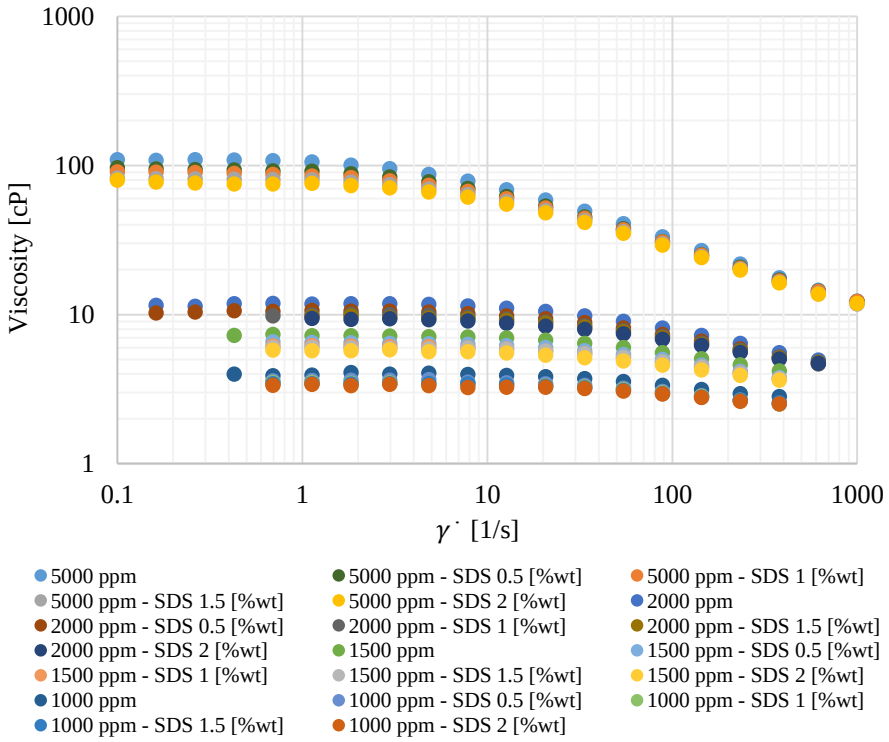

Figure 5.8 Viscosity vs. Shear Rate for polymer Solution with different HPAM and SDS concentrations at 50 °C

The viscosity of polymer solutions decreases as the surfactant concentration increases. Surfactant influence turns insignificant at high shear rates. Also, the surfactant effect is less present in more diluted solutions. The anionic surfactants act to increase the ionic strength and

reduce the hydrodynamic size of the polymer molecule. This mechanism is similar to an increase in the monovalent cations (NASR-EL-DIN et al., 1991; SHUPE, 1981).

5.1.3 Interfacial tension measurements

These measurements were developed using brine, polymer solutions, Oil I and Oil II. The determination of IFT values for fluids containing SDS was not possible because the presence of surfactant generated IFT values lower than 1 [mN/m], which were outside the measurement range of the equipment. Besides, when using HPAM+SDS solutions, it was not possible to generate drops in the needle to run the measurements. Due to the low IFT of the blend, the drop quickly detached from the needle. The results are presented in Figure 5.9.

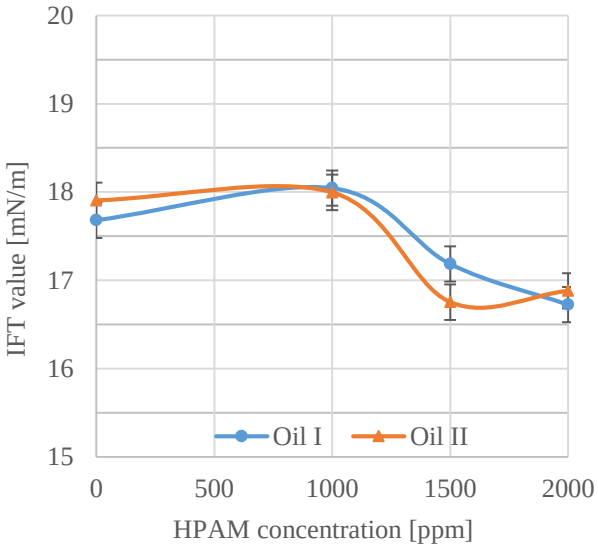

Figure 5.9 IFT behavior between aqueous/polymer solutions and oil phases with different HPAM concentrations at 50°C.

The IFT behavior between aqueous and oil solutions was not strongly affected by the polymer concentrations or iododecane presence. Similar behavior was reported by BATENBURG et al. (2015); HEALY; REED; STENMARK (1976); POPE et al. (1982); VINEGAR; WELLINGTON (1987) AND WANG et al. (2010). Also, in Figure 5. 9, it is possible to observe that a direct relationship between the HPAM concentration or iododecane content on the IFT behavior does not exist.

The highest IFT difference between the analyzed solutions without and with polymer content corresponded to that for 2000 ppm of HPAM and Oil II. The measured IFT differed only of 1.15 [mN/m] to the obtained value for brine (free of polymer) and the same oil. On the other hand, comparing the Oil I (used for the experimental characterization) and Oil II (used

for core flooding tests), it is possible to see that the IFT behavior differs only at the HPAM concentration of 1500 ppm. However, this difference is of 0.44 [mN/m] and is considered negligible.

Based on above observations, it was concluded that the influence of the polymer and iododecane on the interfacial behavior exists but is so small and can be neglected.

5.1.4 Phase behavior tests

The phase behavior observed corresponds to a transition Winsor II→I without finding any Winsor III microemulsion. The Bancroft Rule was used as verification tool of the kind of microemulsion formed, i.e., if it was a Winsor I (o/w) or Winsor II (w/o).

For the optimal salinity selection, some criteria for the salinity scans were proposed in this work. A similar analysis was conducted by SAGI et al. (2013). The criteria proposed are shown below:

- Between 0.2 or 0.3 [%wt] NaCl intervals and after reaching a clear inversion Winsor II to Winsor I, optimal salinity is taken where the maximum value of Vo/Vs is measured.
- For salinity intervals greater than 0.2 or 0.3 [%wt] NaCl, optimal salinity is selected at mid-point of the range defined by the previous criterion.

All surfactant concentrations studied with low salt content exhibited w/o microemulsions. Due to the SDS hydrophilic nature, this behavior was not expected, probably as a result of the presence of natural surfactants in the oil phase able to solubilize some quantity of water into an external oil phase. Besides, as the salt concentration increases the water-solubilized tends to decrease and the oil solubilized starts increase. It is a result of the salts acting as stabilizing emulsions agents because the salt cations are located within the reversed micelles (SALTER, 1983).

SALAGER (1977) pointed out that this behavior corresponds to a reversal status of the surfactant, i.e., a significant change of the partition coefficient value induced for the alteration of some variable exhibit in Table 3. 7. On the other hand, as the surfactant and salt concentration increases, the hydrophilic condition of the surfactant rises. This effect is true because of the diminishing of the range that the Winsor II was present. The Bancroft's rule was a useful tool at this point for recognizing qualitatively changes in the type of microemulsion formed.

The primary objective of this step is to characterize the surfactant solutions according to its ability to reduce the IFT. Therefore, the results after 26 days of equilibration and some details are presented below (Figure 5.10, Figure 5.11, Figure 5.12 and Figure 5.13).

For 0.5 [% wt] of SDS, weak w/o microemulsion are present. At same surfactant concentration and for a 0.7 [%wt] of NaCl one can observe that a solution with high oil content is surrounded by the water without some physically visible change with the time. The term weak is used to express the facility in which the microemulsion spreads into a water phase.

However, when the SDS concentration rises to 1 [%wt], the w/o microemulsion are easier identified. For 0.7 [%wt] of NaCl, a significant quantity of oil has solubilized a relatively low volume of water. This condition is evident because of the w/o microemulsion does not spread easily within the water. Whereas that, when the NaCl content is increased up to 0.9 [%wt] the water-solubilized diminish, elucidating a high dark nature of the microemulsion caused by a higher amount of oil solubilized. Also, it is possible to observe that oil drops are suspended within the water phase. Besides that, at NaCl concentrations above of 1.2 [%wt], the water content into the microemulsion rises, making the microemulsion to spread easier into a water phase than with lower salinity.

Solutions with 1.5 [%wt] of SDS up to NaCl concentration close to 0.7 [% wt] presented similar behavior. Besides that, as according as the surfactant concentration increases, the partition coefficient changes were more pronounced as exhibited in the images obtained from Bancroft's rule applies. In other words, the high hydrophilic nature of the surfactant starts to control the phase behavior as the surfactant concentration increases.

Finally, at 2 [%wt] SDS, the hydrophilic nature of the surfactant is remarkable generating o/w microemulsion for salinities above 0.2 [%wt]. Likewise, the presence of a precipitate with color white to beige in the interface between the fluids at salinities close to the optimal salinity is observed.

SALAGER (1977) showed that for low concentration or in the absence of alcohol, a direct transition Winsor II→I is obtained. Also, the same author affirmed that these systems exhibit some three-phase behavior but often appears as a precipitate or a gel rather than a microemulsion.

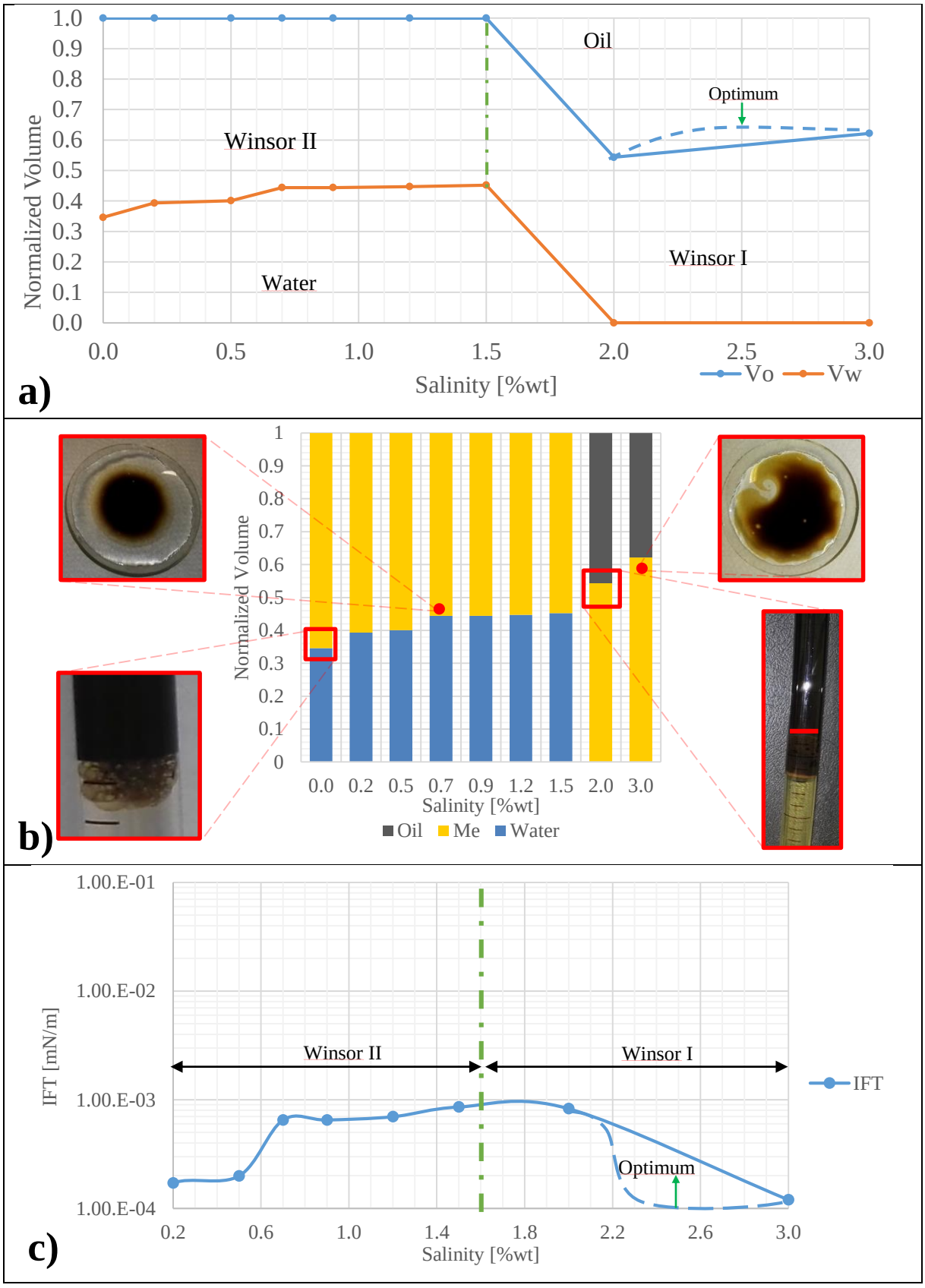

Figure 5.10 Salinity Scan and Phase behavior results for Solutions with 0.5 [%wt] SDS.

a) Volumetric measures. b) Bancroft's Rule and some details. c) IFT behavior in function of salinity.

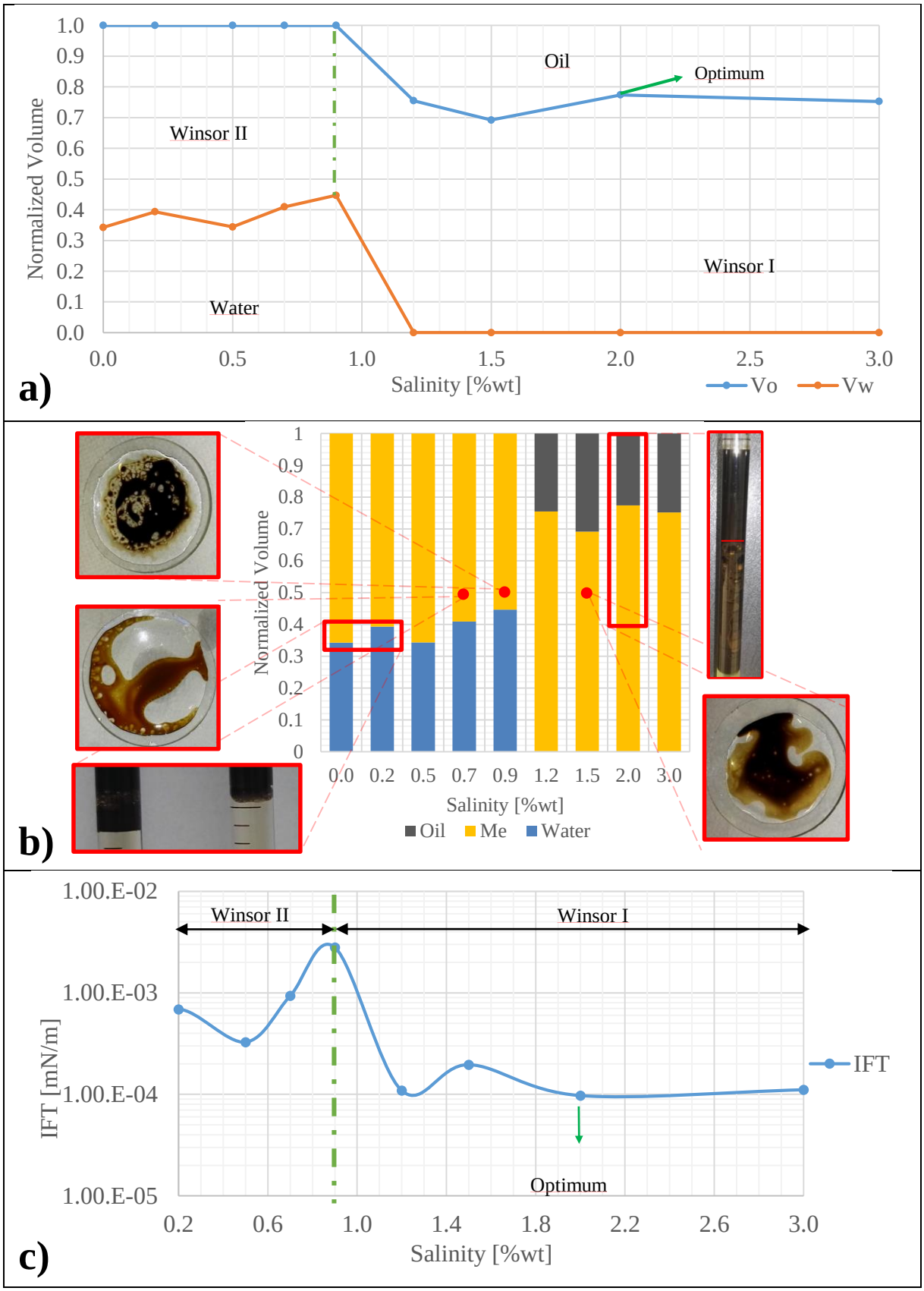

Figure 5.11 Salinity Scan and Phase behavior results for Solutions with 1 [%wt] SDS

a) Volumetric measures. **b)** Bancroft's Rule and some details. **c)** IFT behavior in function of salinity.

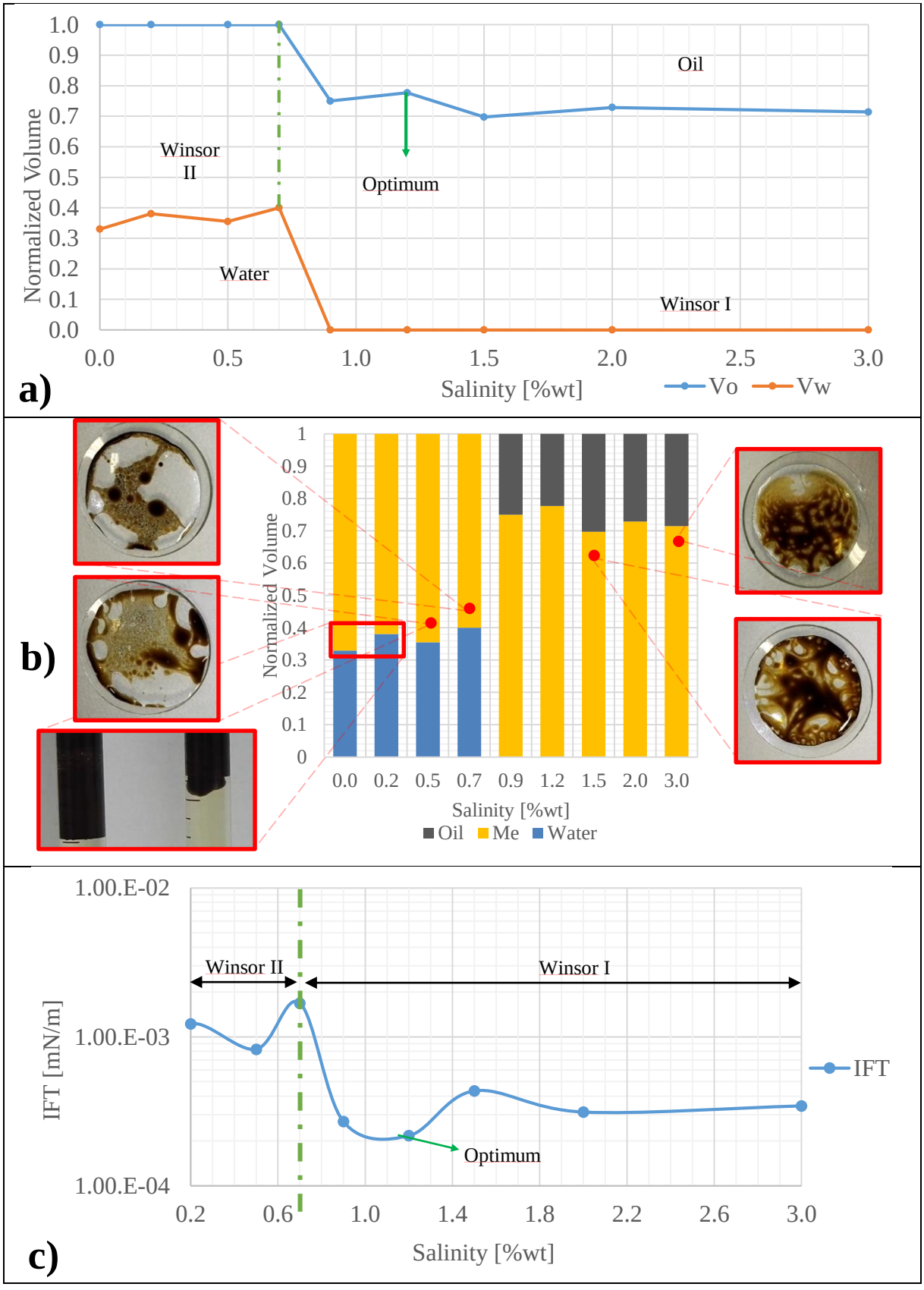

Figure 5.12 Salinity Scan and Phase behavior results for Solutions with 1.5 [%wt] SDS.

a) Volumetric measures. **b)** Bancroft's Rule and some details. **c)** IFT behavior in function of salinity.

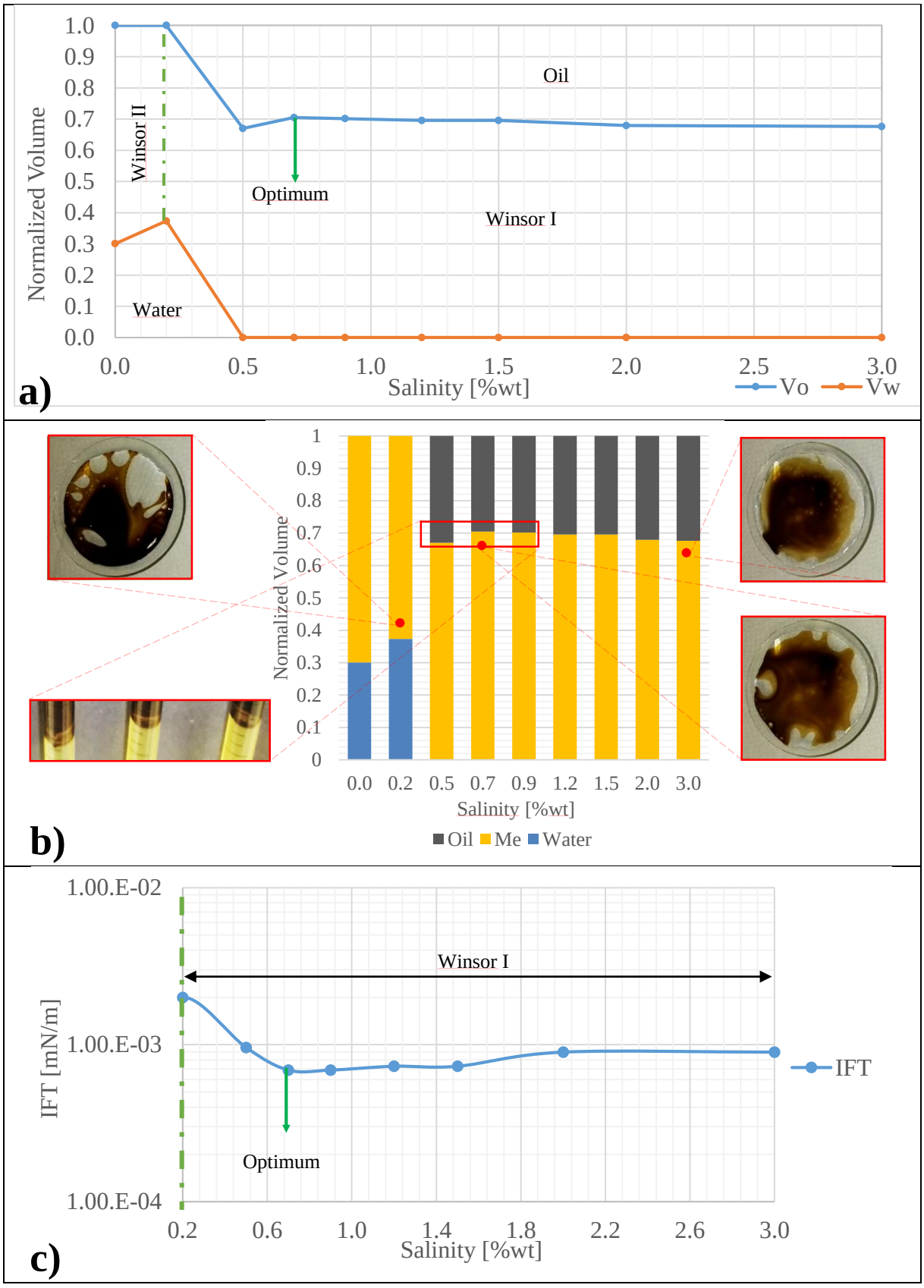

Figure 5.13 Salinity Scan and Phase behavior results for Solutions with 2 [%wt] SDS.

a) Volumetric measures. b) Bancroft Rule's and some details. c) IFT behavior in function of salinity.

Figure 5.14 shows the IFT values with different salinity and surfactant concentrations. These values were obtained through the Chun Huh equations (Equations 2.13 and 2.14). The dashed line is used to represent a possible case of the IFT behavior between 2 to 3 [%wt] of NaCl and 0.5 [%wt] of SDS, after applying the criteria proposed in this work. These intermediate values were not discretized because they are far from the salinity of interest.

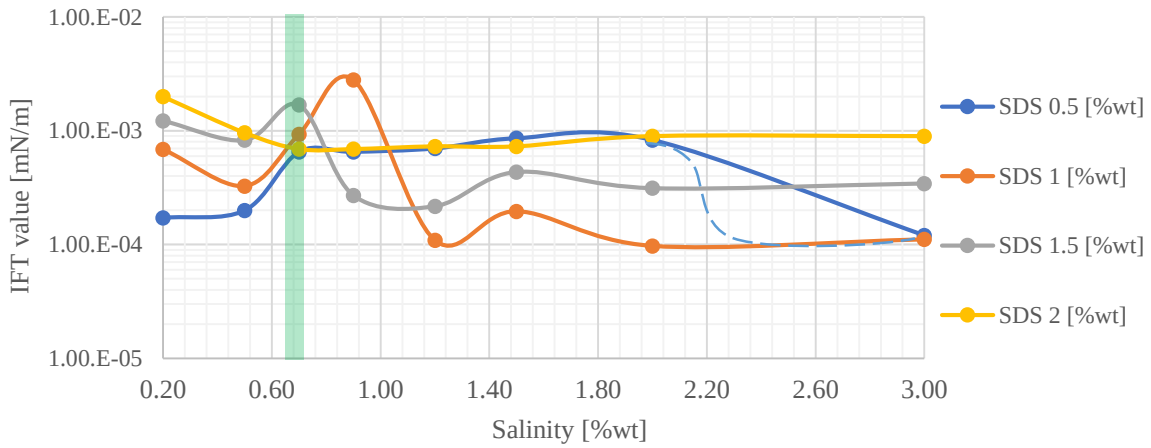

Figure 5.14 IFT behavior in function of Salinity and SDS concentration.

For the desired salinity (0.7 %wt of NaCl), all SDS concentrations generated an IFT reduction to low values, within an order of magnitude between 10^{-3} and 10^{-4}. This values of IFT reduction are adequate to improve the oil recovery factor. Besides that, the optimum salinity reduces as the surfactant concentration increases.

On the other hand, at the salinity of interest, the lowest interfacial reduction was obtained using SDS concentration of 0.5 and 2 [%wt].

Finally, the microemulsion viscosity at 50 °C and 0.7 %wt of NaCl was measured exhibiting a Newtonian behavior for all surfactant concentrations (Figure 5.15.a). Also, the viscosity is maximized near the phase behavior transition, evidencing a drastic change in the formation and aggregation of the micelles (Figure 5.15.b).

Similar behavior was reported by BENNETT et al. (1981) and THURSTON; SALAGER; SCHECHTER (1979) corroborating the usefulness of the proposed criteria above.

Due to the high microemulsion viscosity obtained with 2 [%wt] of SDS, this surfactant concentration was discarded for the core-flooding tests.

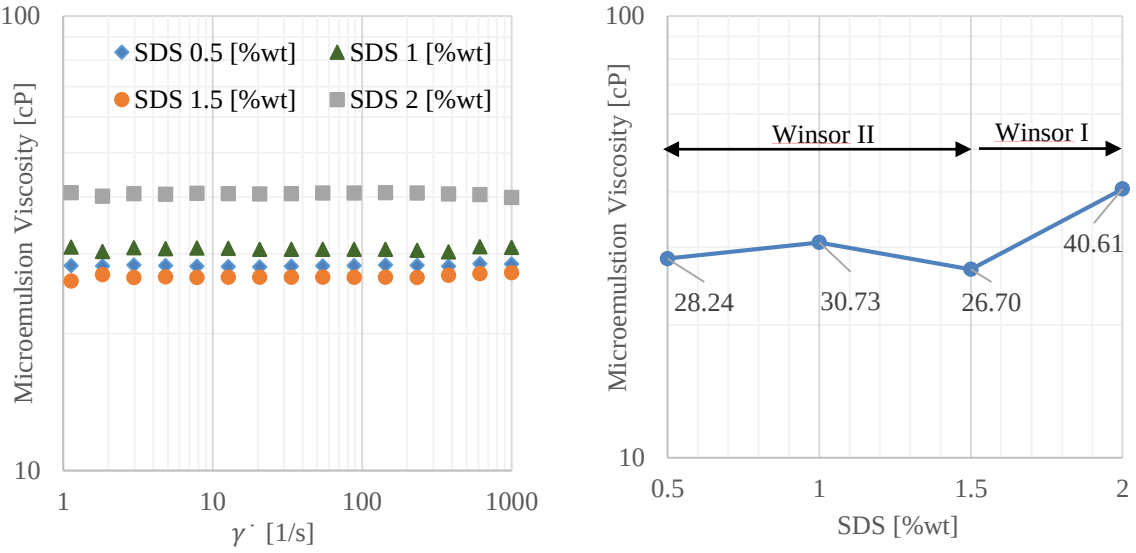

Figure 5.15 Viscosity microemulsion at 0.7 [%wt] NaCl at 50 °C.

a) at shear rate and SDS concentration different. b) At a shear rate of 7.8 S^{-1} varying SDS concentration.

5.2 Results of Step 2 of the Methodology

This section discusses rock sample preparation and characterization, bulk fluids CT values determination, dry rock samples CT analysis and all laboratory activities developed previously to the assessment of the CEOR processes evaluated by CT.

5.2.1 Porosity and permeability measurements

After cleaning and dry the rock samples, the petrophysical properties were measured according to explained in Item 4.3.6. The results are shown in Table 5.3.

Table 5.3 Selected Rock Sample Petrophysics Characterization

Rock Sample	12A4	12A2
Type	Sandstone	Sandstone
Weight (g)	609.03	591.83
Length (cm)	27.01	27.1
Diameter (cm)	3.79	3.71
Area (cm^2)	11.28	10.81
Volume (cm^3)	304.71	292.96
Pore Volume (cm^3)	72.58	68.58
Porosity (%)	23.82	23.41
Permeability (mD)	534.52	435.32

5.2.2 Bulk fluids CT values and dry rock sample CT evaluation

CT values of the fluids were acquired using procedures discussed in Item 4.3.7. The fluids were placed into the core holder, heated up at 50°C and submitted to an overburden pressure of 3000 [psi], which are the same conditions applied to the rock samples during the core flooding tests. Figure 5.16 shows the topogram of the aluminum dispositive within the core holder. The mean CT values of each fluid are presented in Table 5.4.

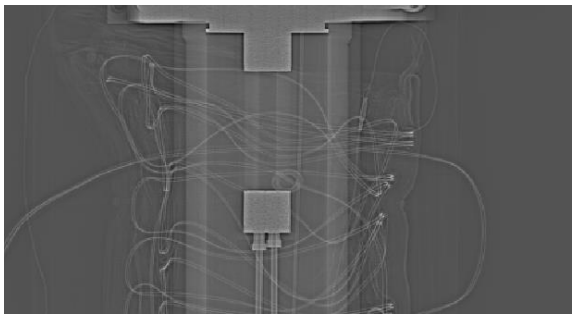

Figure 5.16 Annular Cylinder Topogram

Table 5.4 Bulk CT Fluids Value

Fluids	**CT Number**
Air	- 796.80
N_2	- 802.81
Brine	116.39
Oil II	570.82

Furthermore, the CT scanner was used as a useful tool to visualize inside the core holder and to know the internal structure of 12A2 and 12A4 rock samples.

5.2.2.1 Rock Sample: 12A4

Test 1 and Test 2 were conducted using the same rock sample (12A4). A general and brief geologic analysis of this rock was done aiming to identify some rock characteristic to support discussions and explanations of any phenomena that taking place during the core-flooding tests. The evaluation started with a visual inspection, which allowed to observe a laminar structure in the rock (Figure 5.17.a). Then, the dry rock sample was scanned with CT perceiving a longitudinal lamination in all slices characterized by a higher CT number distribution along it (white lamination in Figure 5.17.b). Higher density materials are associated with this white lamination. A 3D images reconstruction confirmed the presence of this structure throughout the entire rock sample length. (red color in Figure 5.17.c).

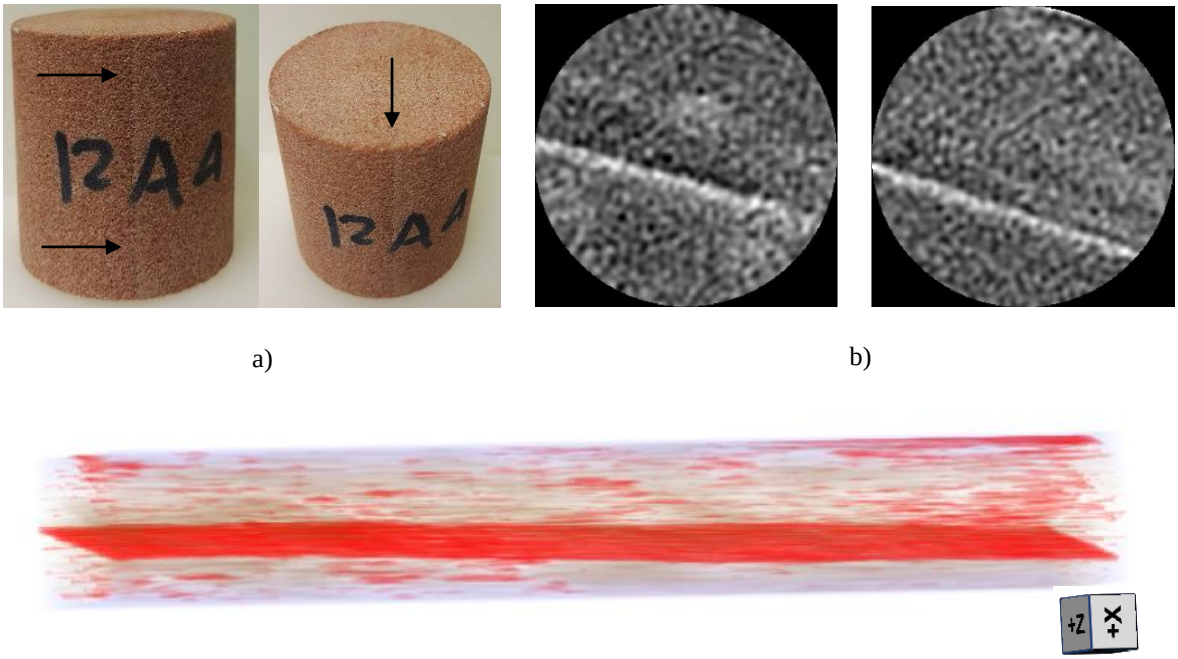

a) b)

c)

Figure 5.17 Initial CT analysis dry rock sample 12A4.

a) Dry Rock Sample segment photography, b), c) Slices 6 and 20 along the rock, respectively, d) 3D Reconstruction of the entire rock sample, where the red color represents the laminations and intrusions of high-density materials.

Besides that, Figure 5.18 a,b exhibit three different zones, at the inlet of the dry rock sample, that which were analyzed using Scanning Electron Microscope (SEM). Comparing the three images of the zones at a zoom of 180 X (Figure 5.18. c, e, and g), it is possible to see a different kind of cementation in the zone 2 (Figure 5.18.e) corresponding to lamination region. After that, a section with better resolution of each image was analyzed at 300 X (Figure 5.18. d, f, and h) elucidating the presence of an important quantity of fines adhered on grains.

Region 3 covers the major portion of the sample. Therefore, this area was used to obtain a mapping of chemical elements such as Carbon, Aluminum, Silicon and Iron (Figure 5.18, i, j, k, and l). Based on this map, different specific locations in this region were selected to develop an accurate spectral analysis (Table 5.5). These activities aim to sustain a general idea of the mineralogical rock composition.

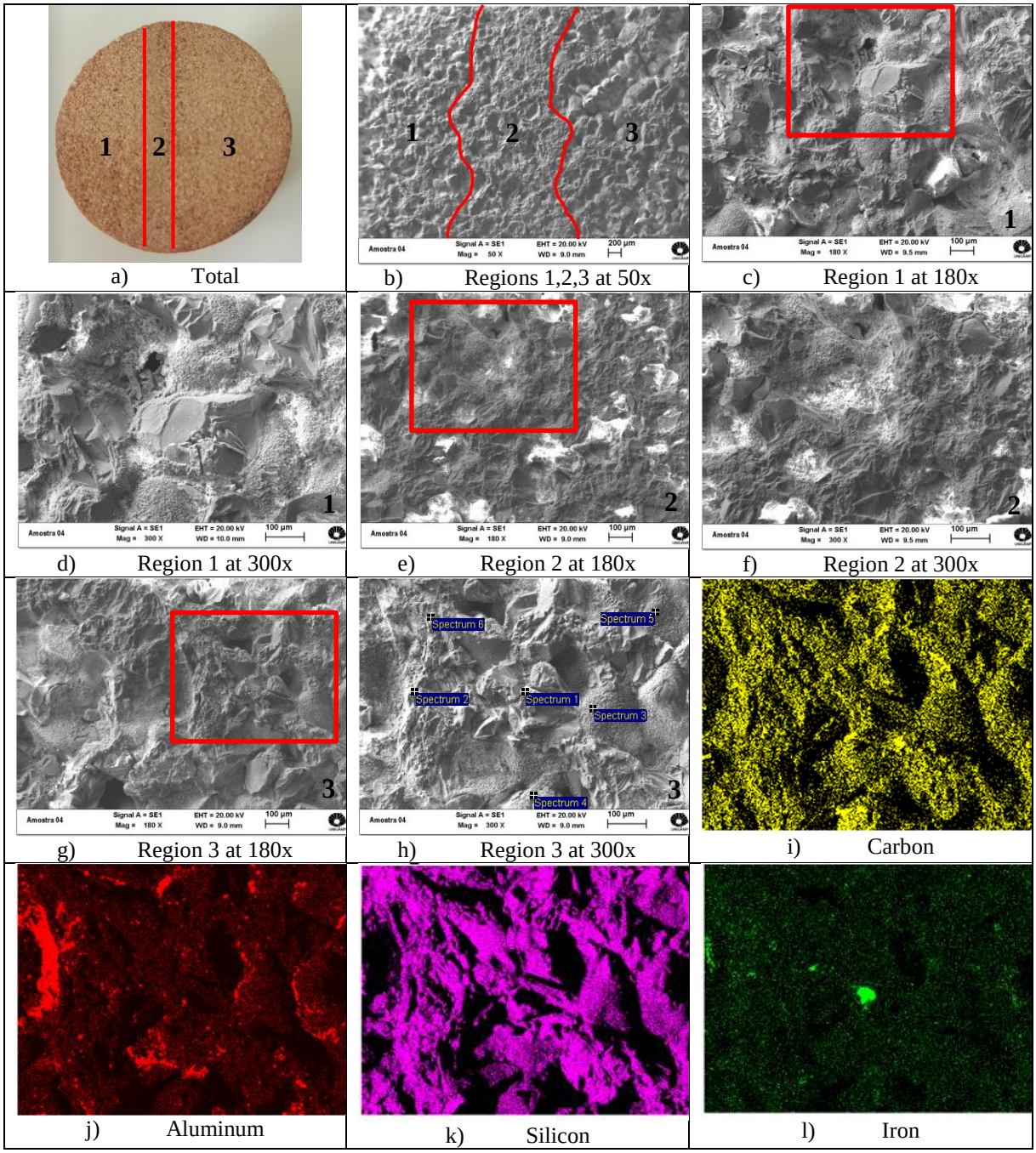

a) Total b) Regions 1,2,3 at 50x c) Region 1 at 180x

d) Region 1 at 300x e) Region 2 at 180x f) Region 2 at 300x

g) Region 3 at 180x h) Region 3 at 300x i) Carbon

j) Aluminum k) Silicon l) Iron

Figure 5.18 SEM Results.

a) and b) Three different zones at the inlet of dry rock sample, c) Region 1 at 180 X, d) Region 1 at 300 X, e) Region 2 at 180 X, f) Region 2 at 300 X and points for a punctual spectral analysis, g) Region,3 at 180 X, h,) Region 3 at 300 X, i) Carbon mapping, j) Aluminum mapping, k) silicon mapping and l) iron mapping.

As result of the element mapping and punctual analyze, it is possible to affirm that the main element present in the Botucatu formation is the Silicon, usually associated with Quartz. Besides that, there are aluminum and Iron in low quantities, which are commonly associated with clays. Probably, region 2 includes a high clay content, once cement that generates high CT number response.

Table 5.5 Punctual Analyzes on rock sample region 3.

Spectrum	Element				
	Sodium	Aluminum	Silicon	Chlorine	Calcium
Spectrum 1	0.0	0.0	100	0.0	0.0
Spectrum 2	0.0	0.49	99.51	0.0	0.0
Spectrum 3	0.0	1.12	98.41	0.0	0.47
Spectrum 4	0.0	0.0	100	0.0	0.0
Spectrum 5	0.0	0.63	99.37	0.0	0.0
Spectrum 6	0.0	0.0	99.48	0.0	0.52

WU; CAETANO-CHANG (1992) presented that the Botucatu formation is composed of higher than 93% of quartz. The remaining part is distributed among feldspar and cement, which are present in the form of traces of iron oxide-hydroxide and few autigene clays on the surface of the grains.

Finally, the relative permeability curves of it rock sample is presented in Figure 5.19. These curves were determined by the JBN method (ABBAS, 2016; MAMUDU; TAIWO; OLAFUYI, 2016, 2017). The highly water-wet nature of the Botucatu Sandstone is evidenced, as also reported by other authors (HERNANDES DE LEON, 2015; RIOS, 2014; SANABRIA, 2013).

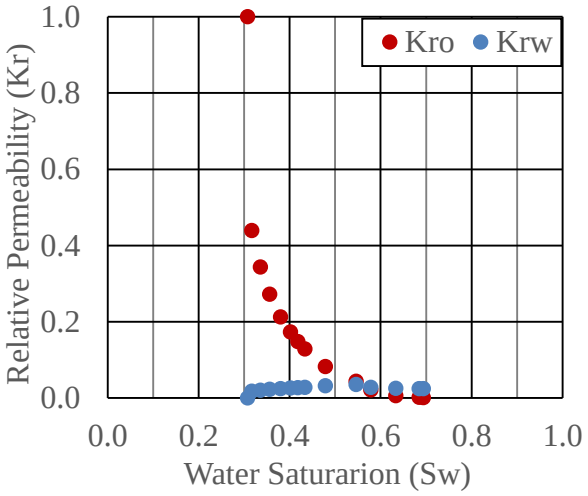

Figure 5.19 WF Relative Permeability Curves

5.2.2.2 Rock Sample: 12A2

The same CT scanning analysis was applied to the dry rock sample used in test 3. The results allowed visualizing that the 12A2 rock sample presents intrusions of some discontinuous laminations that are not visibly appreciable. Figure 5.20 shows the result.

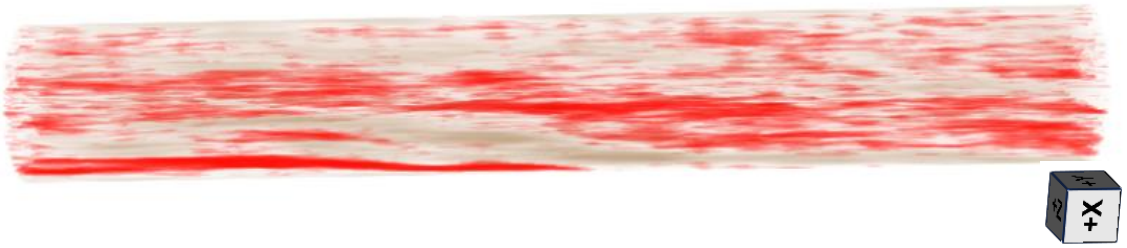

Figure 5.20 Initial CT analysis dry rock sample 12A2.

5.3 Results of Step 3 of the Methodology

This section encompasses the results obtained for the core flooding proposed in Item 4.3.9 (Test 1-WF, Test 2- SP as a secondary recovery method and Test 3- SP as a tertiary oil recovery method). The CT was used as a tool to estimate the porosity profiles of the rock samples and to calculate the saturation profiles of the injected fluid. The CT was a useful tool to improve the understanding of the dynamic of the fluids within the rock as a function of the injected pore volumes.

5.3.1 Test 1 - Imbibition 1

In this step, the absolute permeability of the rock sample 12A4 was determined by water injection (Figure 5.21) and corresponded to 260.9 mD. This value was smaller than the value obtained during petrophysical characterization (gas permeameter) probably due to the swelling of clays present in the rock when they were exposed to a low salinity brine, the fines migration (Figure 5.22), or the Klinkenberg effect.

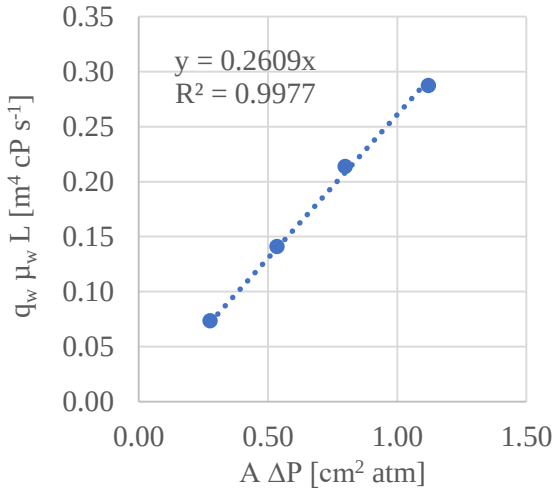

Figure 5.21 Absolute Permeability 12A4

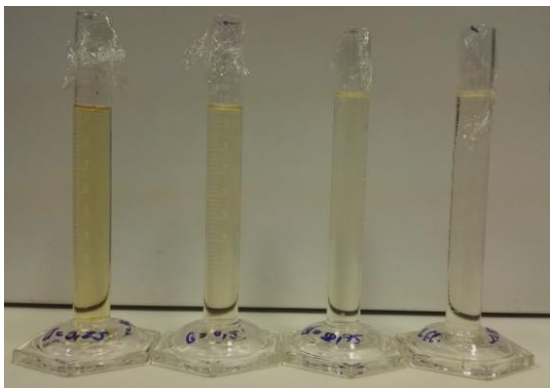

Figure 5.22 Imbibition 1 Effluent

Another useful application of the CT acquisition was the determination of the porosity profile throughout the rock sample before and after the Imbibition 1. These results were compared with the value determined using a gas porosimeter. Figure 5.23 and Table 5.6 summarize the results.

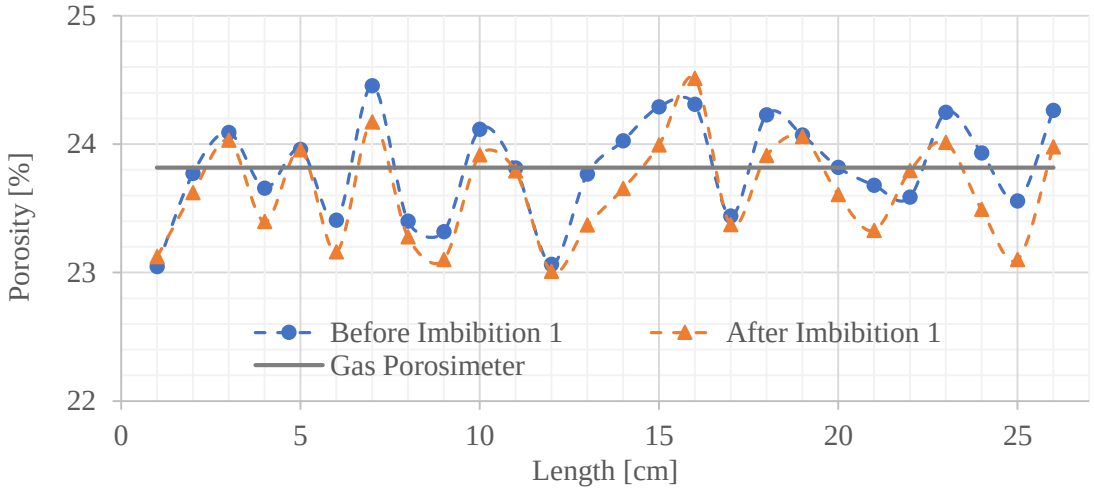

Figure 5.23 Comparison between CT porosity profiles before imbibition 1, after imbibition 1 and gas porosimeter of 12A4 rock sample.

Table 5.6 Average porosity Values obtained using CT respect to gas porosimeter of 12A4 rock sample

Porosity Measurement Method		**Mean Value (%)**
Gas Porosimeter		23.82
CT	**Before Imbibition 1**	23.82
CT	**After Imbibition 1**	23.64

The behavior of the porosity profile exhibits little changes throughout the rock maybe because of the fines migration. Small particles can be removed and then either deposited in other parts or drained out the rock sample. These changes are minor and can be disregarded because the tendency of the profile is maintained.

The porosity results obtained with CT data can be used to create a porosity map of the rock sample to improve the simulation of these core flooding tests.

5.3.2 Test 1 - Drainage 1

After Imbibition 1, the oil injection starts, attempting to mobilize all of the existent mobile water inside the rock and establish the initial reservoir conditions (S_{wi} and S_o). A total of 7.08 pore volume (PV) of oil was injected. The breakthrough (BT) of oil occurred when 0.56 PV has been injected, and it took approximately 88 minutes. At the BT instant, about 81.58% of the total mobile water had been produced. Figure 5.24 presents the produced volumes (*oil*

produced-N_p and water produced-W_p) calculated by the material balance, showing that after oil BT there was a progressive production of water until zero mobile water remained.

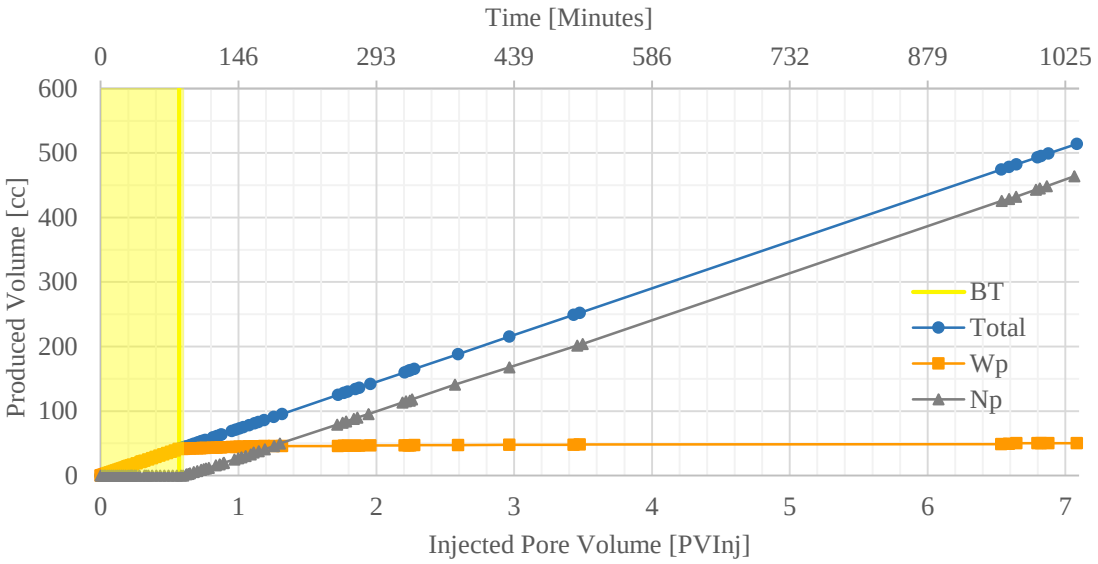

Figure 5.24 Drainage 1 – Produced Volumes calculated by Material Balance

The water displacement up to the oil BT was developed with a homogenous advance front due to the favorable mobility ratio between the fluids ($\mu_o > \mu_w$). This behavior can be observed with the water saturation profile obtained by CT scan (Figure 5.25) which were determined through Equation (3.5).

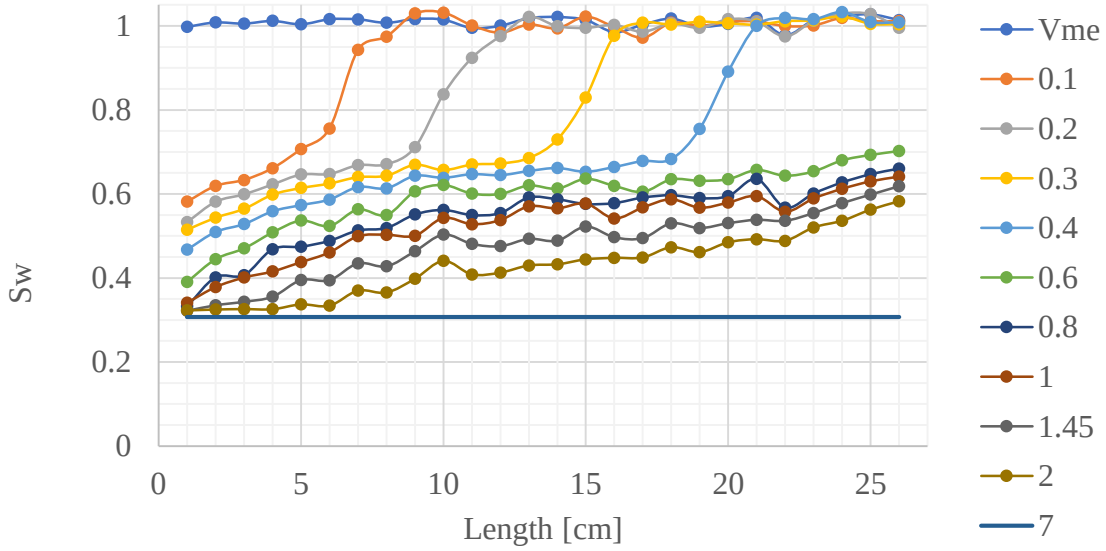

Figure 5.25 Drainage 1 - Water Saturation Profiles in function of Injected Pore Volume (PVInj) through of rock sample 12A4.

From Figure 5.25, it was noticed the necessity to carry out another CT scan closer to the final injection of each stage. The mathematic expression used to obtain the saturation profile (Equation 3.5) is based on a tomography at the residual condition of the displaced fluid. Therefore, in this condition $CT_x = CT_{swc}$ and the last saturation distribution is equivalent to the value obtained through material balance (constant value). Thus, the fluids distribution associated to PVInj = 7 is not the real distribution of the fluids along the rock.

After the oil BT, the water saturation profiles exhibited smaller values close to the inlet and higher values near to the outlet which means even though before the BT the displacement front was more like a piston, some oil has flowed for preferential channels. Finally, after 6 PV of oil injected, the system was considered under steady-state flow, i.e., there was no water production, and the differential pressure tends to be constant (Figure 5.27).

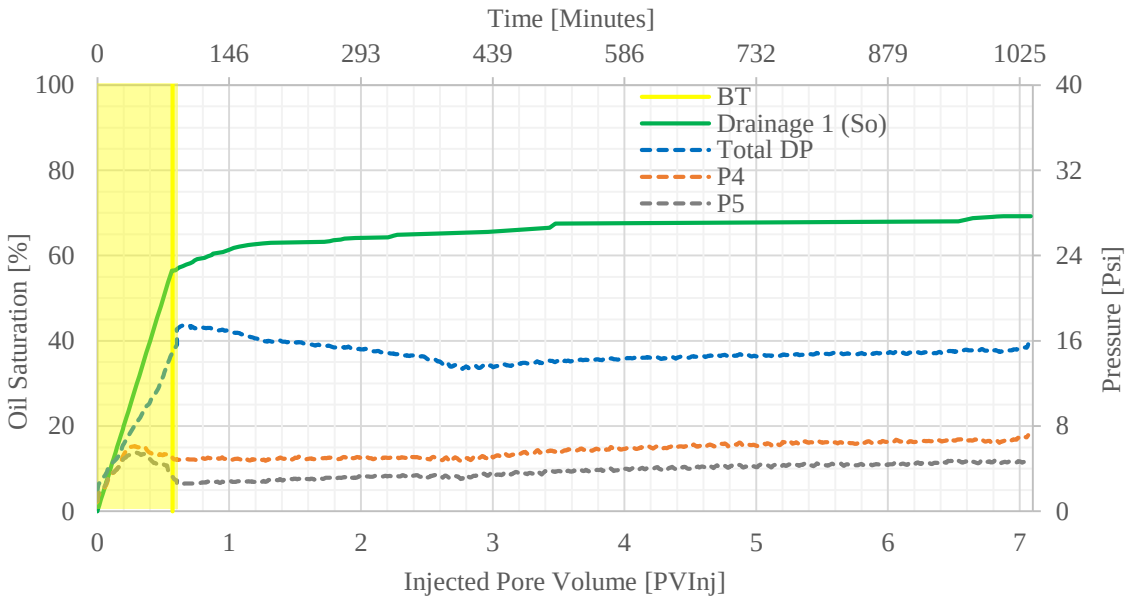

Figure 5.26 Drainage 1 – Oil Saturation and Historical Pressure

The 3D reconstruction of the CT images up to 1 PVInj is presented in Figure 5.27, in which the green color represents the spatial distribution of the high CT number associated with the doped oil, blue color represents the water, and the red color is the rock lamination shown in Item 5.2.2.1. These images confirmed that before of BT, some preferable flow channels have been developed for the oil, and it accumulated close to the outlet rock face, i.e., some oil droplets have been transported and settled down with more frequency closer than the end of the rock sample. However, the oil located there need to reach a critic saturation necessary to flow.

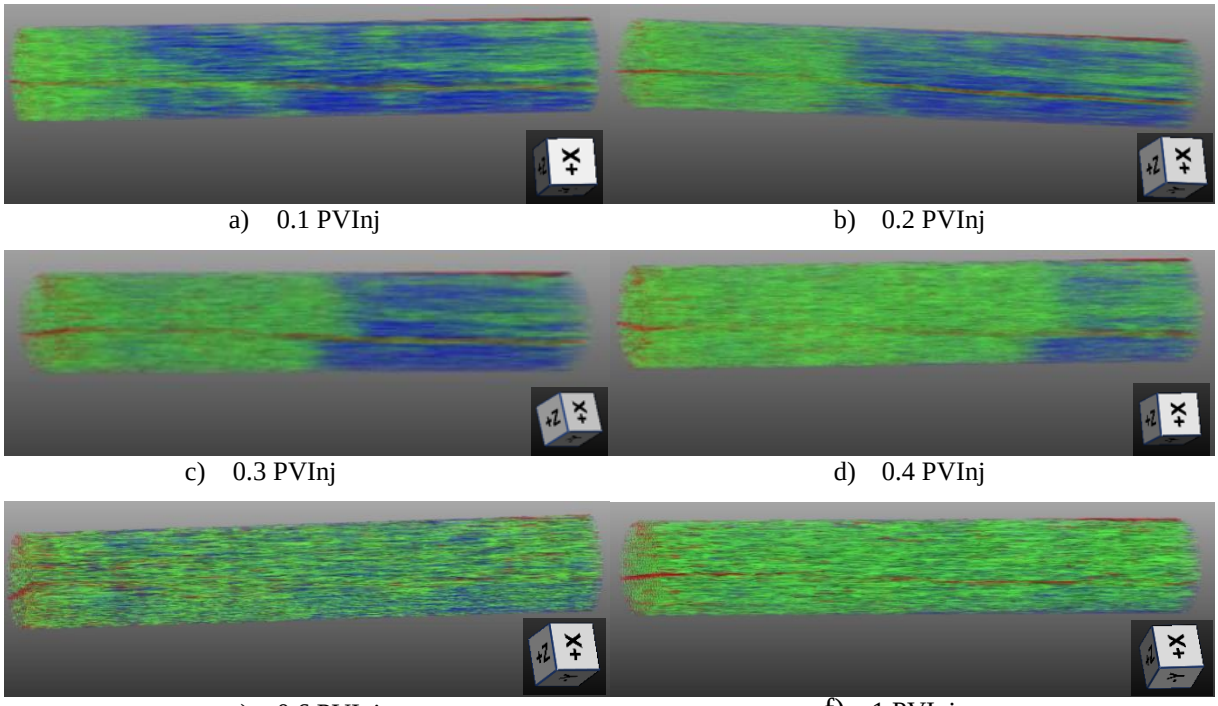

a) 0.1 PVInj b) 0.2 PVInj

c) 0.3 PVInj d) 0.4 PVInj

e) 0.6 PVInj f) 1 PVInj

Figure 5.27 Drainage 1 - 3D Images in Function of PVInj of oil.

The color green, blue and red correspond to oil, water location, and rock lamination, respectively.

Then, the effective permeability to oil (K_o) was calculated using the final differential pressure value of each pressure tap (P4, P5 and total). For this, K_o for each segment was calculated assuming a series system and applying the following mathematic expression:

$$\overline{K} = \frac{\Sigma_{i=1}^{n} L_i}{\Sigma_{i=1}^{n} \left(\frac{L_i}{k_i}\right)} \qquad (5.\ 1)$$

Table 5.7 presents the results and exhibits that exists a flow heterogeneity through the rock sample.

Table 5.7 Drainage 1 - Effective Oil Permeability by stretch

	ΔP (psi)	Permeability (mD)
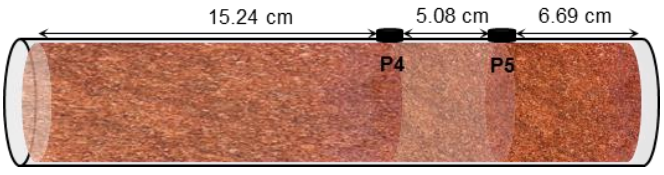	Inlet-P_4 = 8.51	$K_{inlet-P4}$ = 369.15
	P_4-P_5 = 2.25	K_{P4-P5} = 464.74
	P_5-Outlet = 4.90	$K_{P5-outlet}$ = 281.64
	ΔP Total = 15.66	$\overline{K}$ = 355.54

This average K_o value is used as the reference absolute permeability value for the porous media for test 1 and test 2. The main parameters determined in this stage show in Table 5.8.

Table 5.8 Consolidated of parameters determined during Drainage 1.

Parameter	Value	Unit
Water Volume inside the rock	22.31	cm^3
Oil Volume inside the rock	50.26	cm^3
Initial Water Saturation	0.31	-
Oil Saturation	0.69	-
Time Breakthrough (BT)	87.8	min
Water Produced at BT	41	cm^3
Total Water Produced	50.26	cm^3
Flow Rate Stage	0.50	cm^3/min
Oil Effective Permeability	355.54	mD

5.3.3 Test 1 - Waterflooding (WF)

Once the rock was saturated according to initial reservoir conditions (S_{wi} and S_o), we started the assessment of the water injection as a secondary recovery method. A total of 15 pore volume (PV) of water were injected. The BT of water occurred when 0.07 PV has been injected and it took approximately 9.61 minutes. At the BT of water, about 17.43 % of the initial mobile oil had been produced. Figure 5.28 presents the produced volumes calculated by the material balance, showing that after BT there was a significant oil production up to about 7 injected pore volume (PVInj) of water. An increasing Wcut characterized this production. After BT, the injection continues to guarantee a residual oil saturation evidenced by null oil production and the differential pressure stabilization.

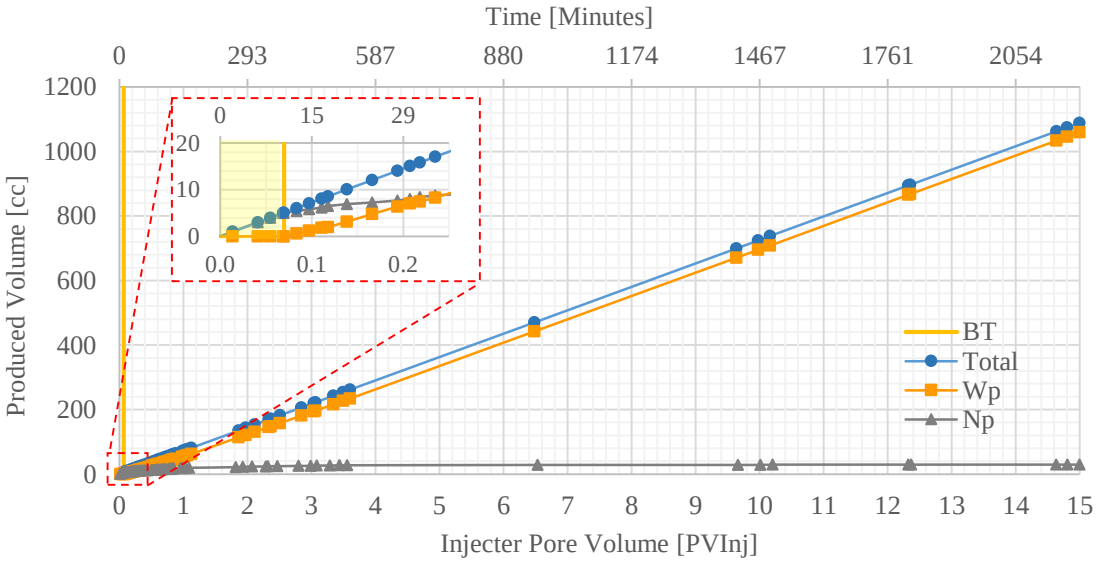

Figure 5.28 Waterflooding - Produced Volumes calculated by Material Balance

The fact that a significant oil production occurred after the BT shows the existence of viscous fingering. The analysis of water saturation profiles in function of the PVInj of fluid (Figure 5.29) determined by CT (Equation 3.5), confirmed the viscous fingering. These profiles exhibit a higher water saturation at the begging and at the end of the rock sample while for a length between 10 cm to 20 cm the water saturation is lower and even in some sections continue being near to initial water saturation, i.e., at the time BT happens, significative amounts of oil have not been mobilized of these zones, yet.

Then, an increment on water saturation along the sample becomes more noticeable at one PVInj. The oil trapped close to the outlet face was produced and, at 3 PVInj of water, the saturation distribution becomes more homogenous. However, the water saturation remained higher at the injection face. Finally, after injection of 10 PV, some local differences on oil saturation remained along the core sample, which were removed by the water injection up to 15 PV.

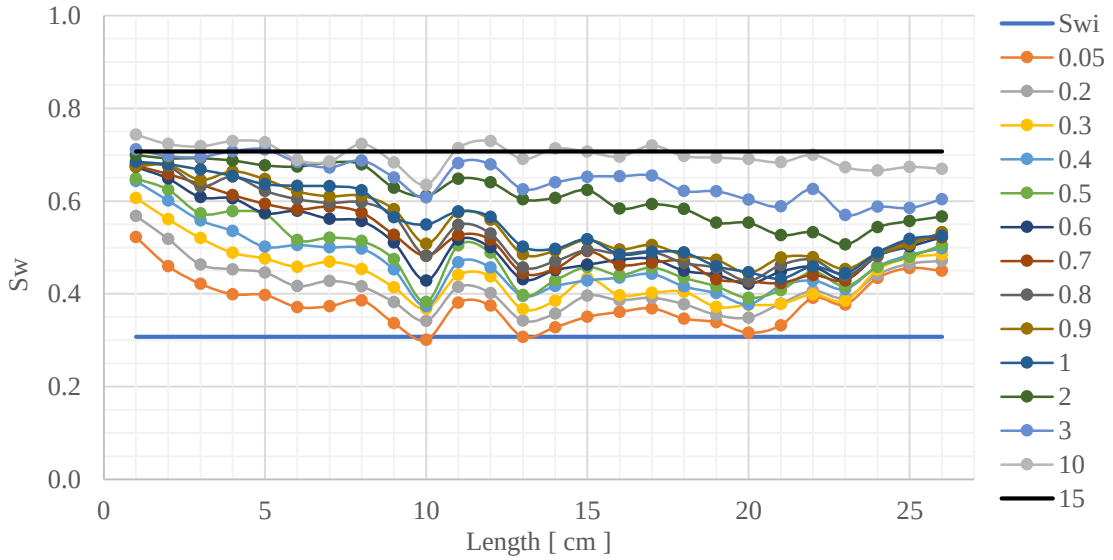

Figure 5.29 Waterflooding - Water Saturation Profiles in function of Injected Pore Volume (PVInj) through of rock sample 12A4.

Figure 5.30 show a 3D reconstruction of the images mentioned above. In these only the location of the water (blue color) and the lamination (red color) are presented.

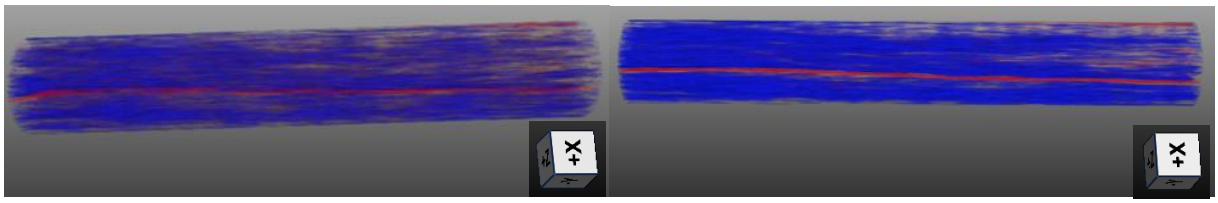

a) 0.1 PVInj b) 0.5 PVInj

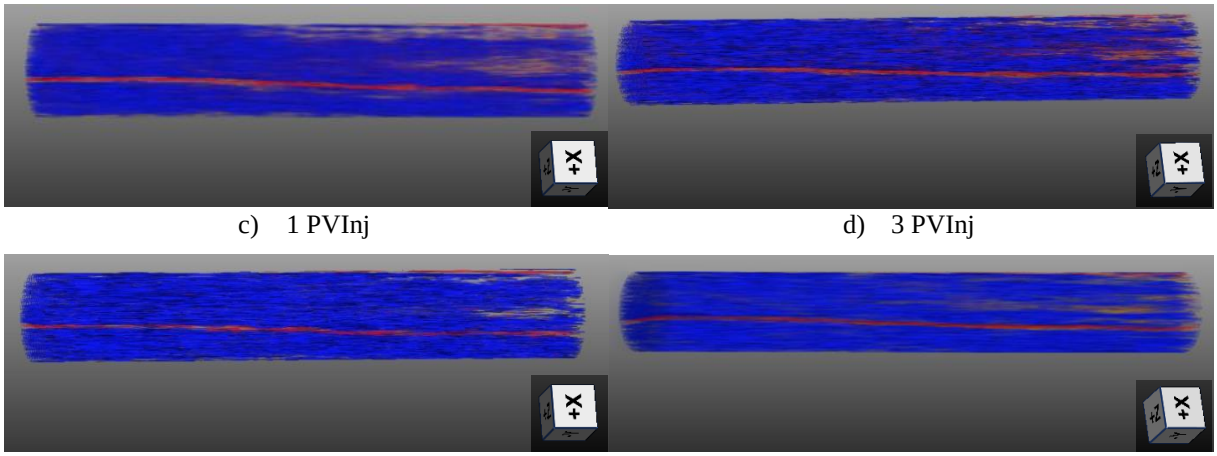

c) 1 PVInj d) 3 PVInj

e) 10 PVInj f) 15 PVInj

Figure 5.30 Waterflooding - 3D Images in Function of PVInj of water.
Blue color represents the water location and red color the rock lamination.

Figure 5.31 shows that the final oil recovery factor of the WF was 57.57 %. This figure also exhibits the pressure behavior. The pressure drops until BT, as it is expected. After that, the pressure increases due to water challenging to displace the high quantity of mobile oil remaining in the rock occasioned by the viscous fingering.

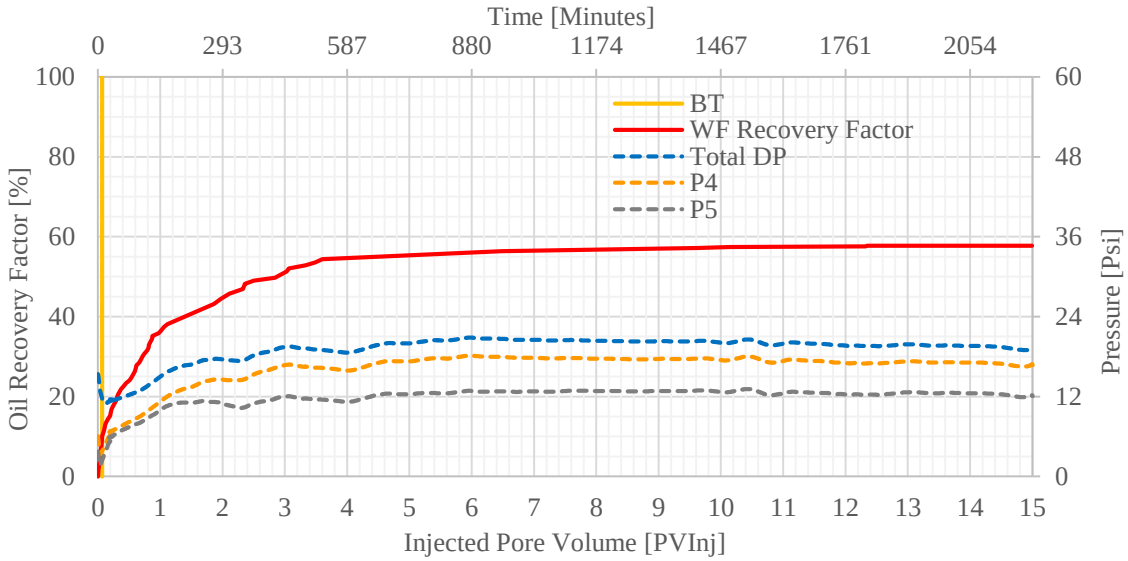

Figure 5.31 Waterflooding – Oil Recovery Factor and Historical Pressure in function of the PVInj and time.

Under steady state conditions, the effective water permeability (K_w) for each section of the rock sample was calculated in the same way mentioned in the previous step (Imbibition 1). Table 5.9 shows the results.

Table 5.9 Waterflooding - Water Effective Permeability by stretch

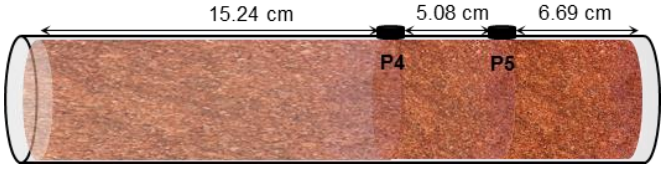	ΔP (psi)	Permeability (mD)
	Inlet-P4 = 2.40	$K_{inlet-P4}$ = 41.32
	P4-P5 = 4.68	K_{P4-P5} = 7.06
	P5-Outlet = 12.04	$K_{P5-outlet}$ = 3.62
	ΔP Total = 19.12	$\overline{K}$ = 9.20

Based on the previous analysis, the average water effective permeability is reduced. Finally, the main parameters determined at this stage are shown in Table 5.10.

Table 5.10 Consolidated of parameters determined during Waterflooding.

Parameter	**Value**	**Unit**
Water Volume inside rock	51.35	cm^3
Oil Volume inside rock	21.23	cm^3
Water Saturation	0.71	-
Residual Oil Saturation	0.29	-
Time Breakthrough (BT)	9.61	min
Oil Produced at BT	5.06	cm^3
Total Oil Produced	29.03	cm^3
Flow Rate Stage	0.5	cm^3/min
Oil Recovery Factor	57.75	%
Water Effective Permeability at Sor	9.20	mD
Water Relative Permeability at Sor	0.025	mD

5.3.4 Test 2 - Drainage 2

This stage was performed to restore the rock sample to a similar condition of the initial oil reservoir conditions (S_{wi} and S_o). A total of 7.39 pore volumes (PV) of oil were injected. The BT of oil occurred when 0.08 PV of fluid had been injected, which took approximately 16.6 minutes. At the BT instant, about 12% of the mobile water had been produced. Figure 5.32 presents produced volumes calculated by the material balance, showing that after BT the water production continues until approximately 5.6 PVInj.

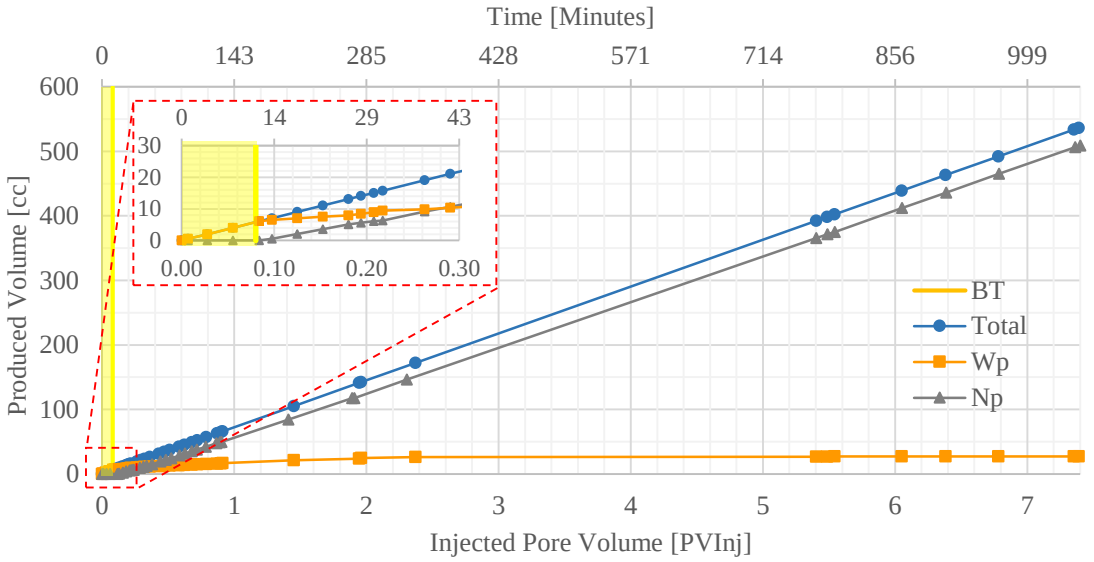

Figure 5.32 Drainage 2 – Produced Volumes calculated by Material Balance

The water saturation profiles obtained by CT through the rock sample during the second drainage are presented in Figure 5.33. After the injection of 0.1 PV, all sections of the sample presented a water saturation below the connate value, confirming the fast BT of oil. The initial saturation profiles have a notable difference in the first 5 cm of the rock sample by the proximity to input diffuser as is expected.

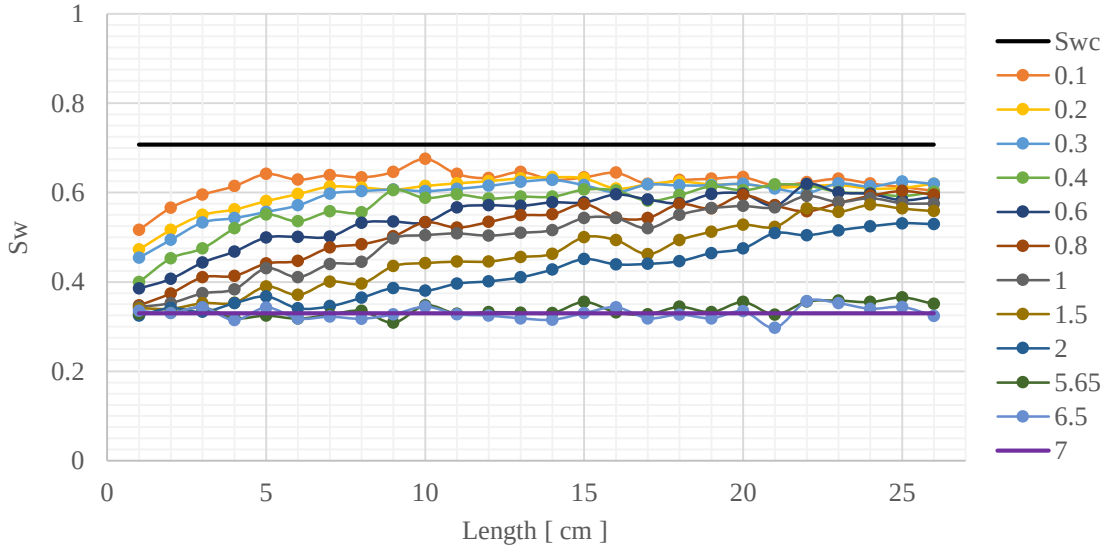

Figure 5.33 Drainage 2 - Water Saturation Profiles in function of PVInj of water through of rock sample 12A4.

As proposed before, additional CT scans were run at the end of the second drainage test. This way, the connate water distribution along the sample was successful determined. The last three CT acquisitions showed a homogenous water distribution above 5.65 PVInj of oil,

allowing affirming that the residual water in the porous media was immobile. Figure 5.34 show the evolution of the oil saturation as a function of PVInj of oil in a cross-section or the rock sample (2D). Because the CT scans were conducted at high energy, the density of the fluids or denser materials dominates the CT numbers response. The golden color relates to high CT numbers allowing visualizing the doped oil and some rock denser mineral, such as the lamination. The blue color is associated with water distribution.

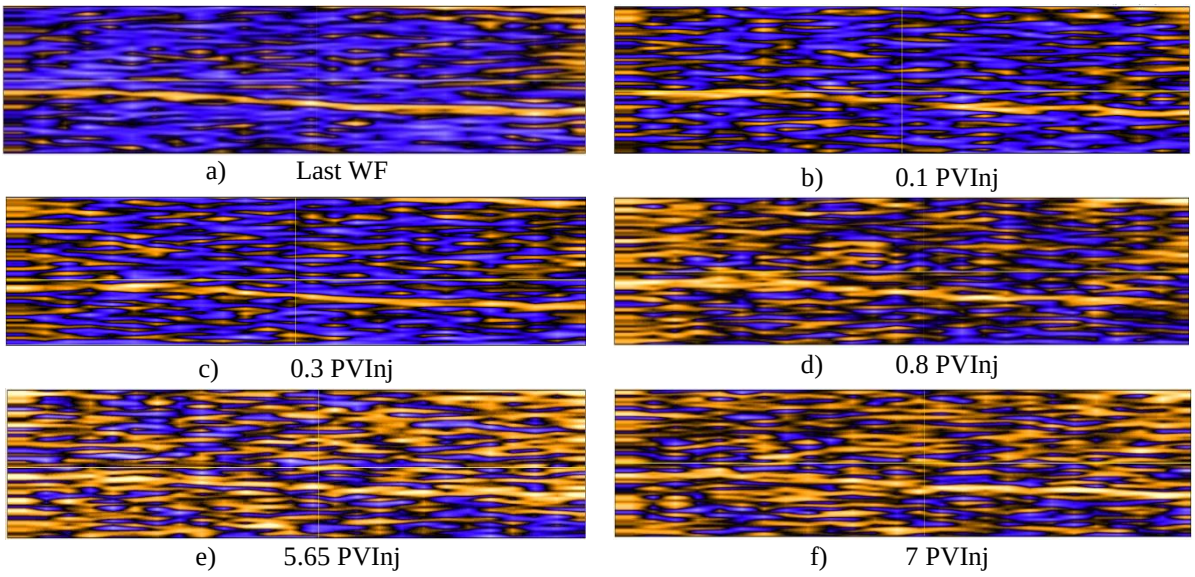

Figure 5.34 Drainage 2 – 2D Oil Saturation in function of PVInj.

Golden color represents higher CT numbers related to the oil location and rock lamination. Whereas, the blue represents the qualitative water location.

Figure 5.35 shows the oil saturation and pressure behavior during the drainage 2. This step exhibits a different behavior from that observed in the drainage 1. Once the oil injection starts entering the porous medium, the pressure within the rock raises until the oil BT. This behavior was attributed to the high initial resistance of the oil to flow. After that, the pressure begins to fall until stabilization.

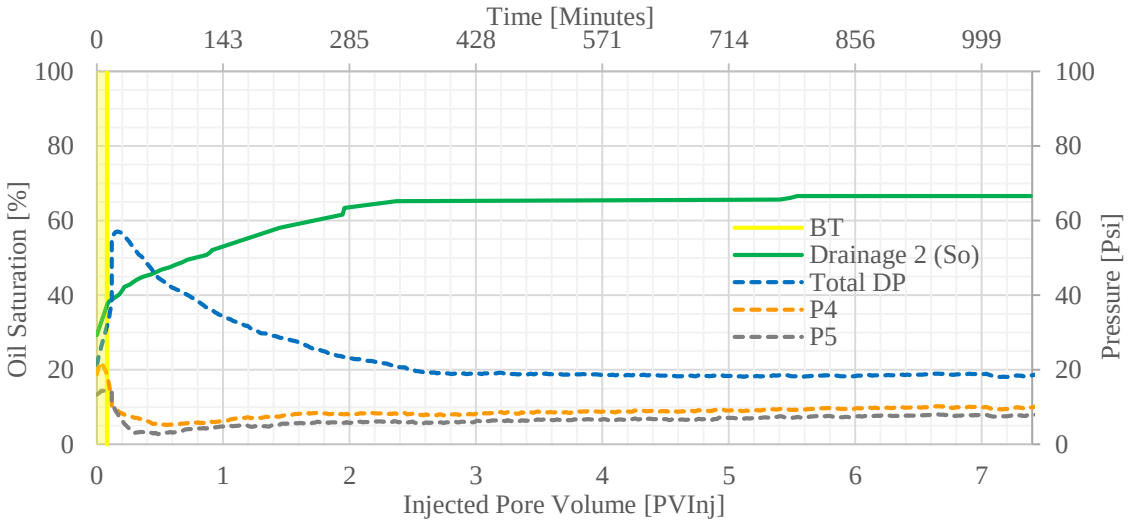

Figure 5.35 Drainage 1 – Oil Saturation and Historical Pressure

Analyzing the behavior of the oil effective permeability (K_{o2}) just as in the previous stages, it is possible to observe a reduction in the total oil effective permeability of the porous media respected to drainage 1. Table 5.11 presents a K_{o2} reduction in the first and last segments of the rock.

Table 5.11 Drainage 2 - Effective Oil Permeability by stretch

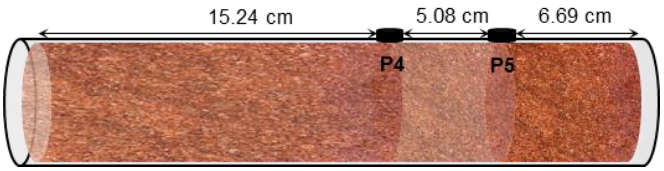

ΔP (psi)	Permeability (mD)
Inlet-P4 = 8.63	$K_{inlet-P4}$ = 303.49
P4-P5 = 2.12	K_{P4-P5} = 494.59
P5-Outlet = 7.95	$K_{P5-outlet}$ = 239.45
ΔP Total = 15.66	$\bar{K}$ = 297.912

A summary of the parameters determined in this step is presented in Table 5.12.

Table 5.12 Consolidated of parameters determined during Drainage 2.

Parameter	**Value**	**Unit**
Water Volume inside the rock	24.28	cm^3
Oil Volume inside the rock	48.30	cm^3
Initial Water Saturation	0.33	-
Oil Saturation	0.67	-
Time Breakthrough (BT)	16.6	min
Water Produced at BT	6.07	cm^3
Total Water Produced	27.07	cm^3
Flow Rate Stage	0.5	cm^3/min
Oil Effective Permeability	297.91	mD

5.3.5 Test 2 - Surfactant/Polymer injection as a secondary oil recovery method.

After the drainage 2, the rock sample is under similar initial conditions of WF (Item 5.3.3). For this reason, the chemical injection performance can be compared with the waterflooding.

A total of 10 PV of the chemical solution was injected. In this case, the stop criterion was a null oil production and a stabilization of the differential pressure to guarantee a residual oil saturation within the rock. The BT of chemical blend occurred when 0.26 PV had been injected, which took approximately 38 minutes. At the BT, about 51.26% of the initial mobile oil was produced. Figure 5.36 presents the produced volumes calculated by the material balance, showing that after BT there was a continuous two-phase production until about 3.84 PVInj of chemical blend. This production period was characterized by a high water volume production (Wcut > 90%).

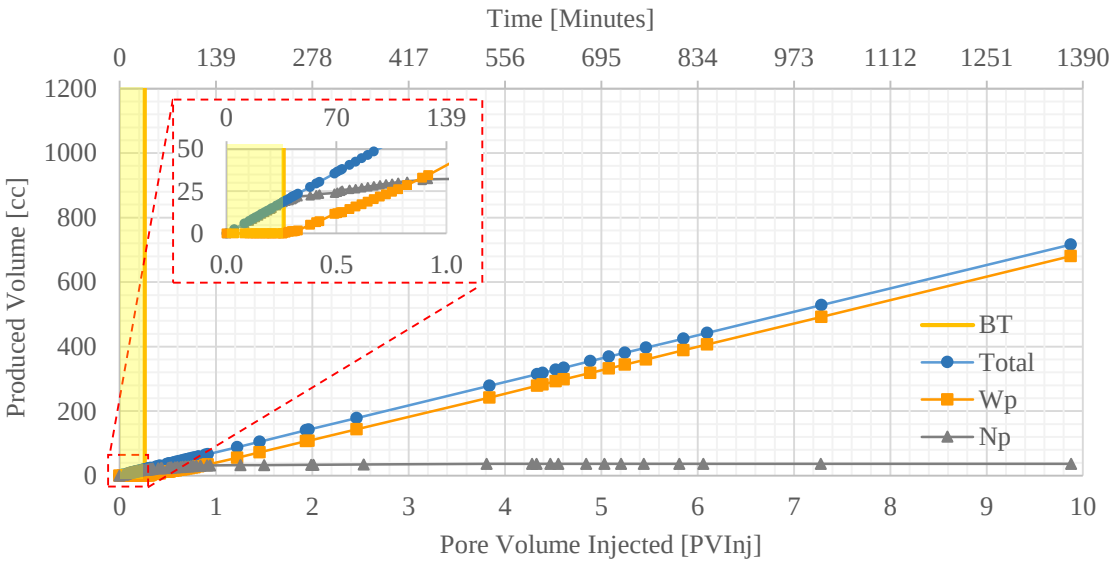

Figure 5.36 Chemical Injection – Produced volumes calculated by material balance

Figure 5.37 shows the chemical saturation profiles where one can notices two relevant facts. The first of them (*red arrow number 1*) occurs around 0.1 and 0.2 PV of the chemical injection. That occurrence can be explained by a significant amount of oil removed from the initial rock region and driving by a microemulsion phase, which is not flowing easily, probably because it has a high viscosity as showed in Figure 5.15.

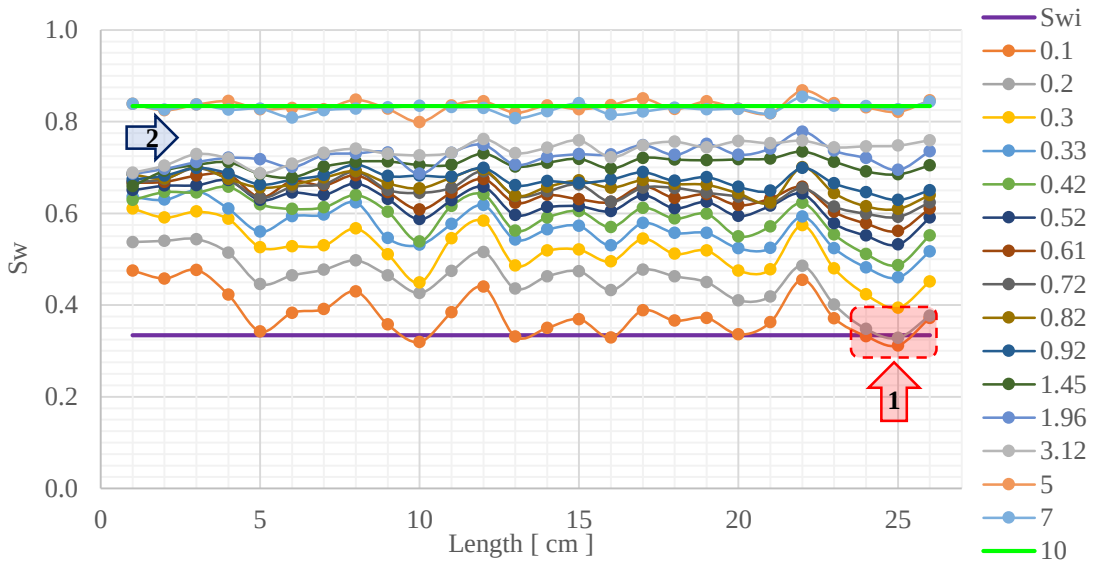

Figure 5.37 CEOR process – Water Saturation Profiles in function of Injected Pore Volume (PVInj) through of rock sample 12A4.

Furthermore, this phenomenon is evidenced by the history of pressure (Figure 5.38) due to the total differential pressure having a progressive increment accompanied by a continuous oil production until the chemical BT. After it, the pressure begins to fall to stabilize as was expected. However, only the P5 presented a similar response to it. Probably, the P4 transducer record failed during this phenomenon.

Despite the above, the use of a blend of surfactant-polymer allowed achieving a final oil recovery factor of 75% (Figure 5.38).

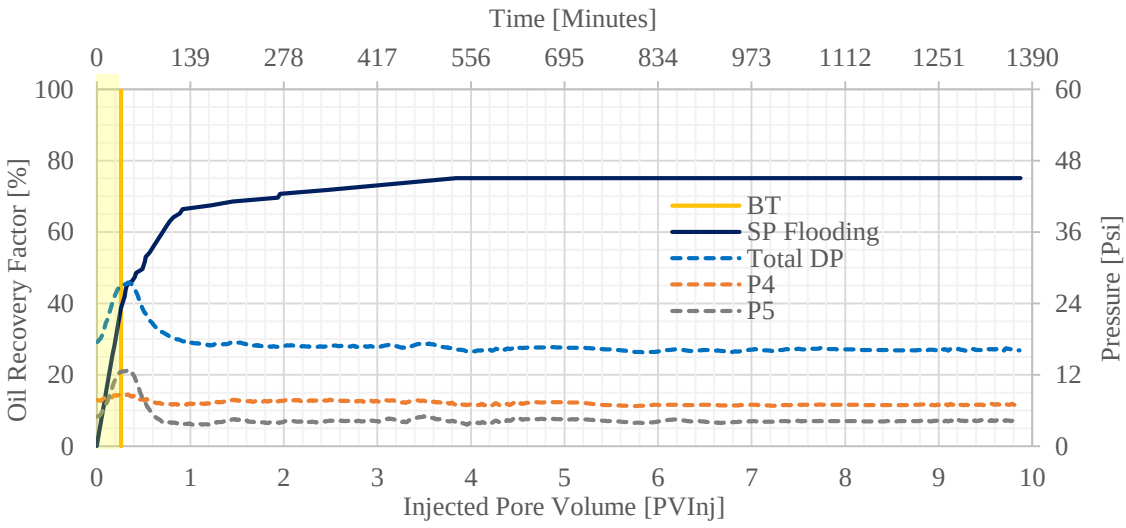

Figure 5.38 CEOR process – Oil recovery factor and Historical pressure in function of PVInj and time.

Once the chemical reached the BT, it was produced a mixture of fluids with some different visual characteristics (Figure 5.39).

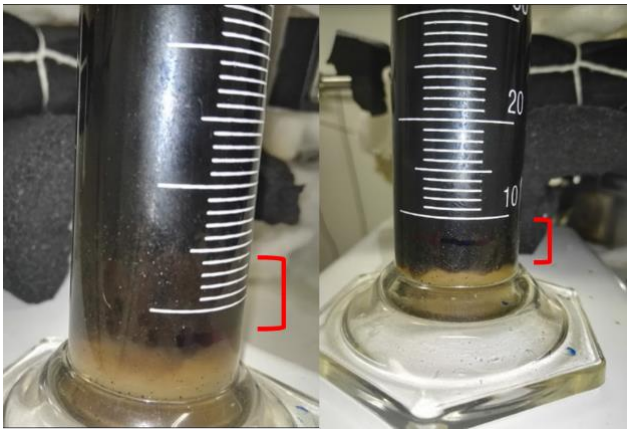

Figure 5.39 Fluids produced right away the BT happened

The second fact detected in Figure 5.37 (*blue arrow number 2*) occurred during the higher microemulsion production. This fact is confirmed by the loss of accuracy on the saturation profiles calculated by the CT scans. It was considered a limitation of the mathematic expressions (Equations 3.2, 3.5 and 3.6) used to process the CT data acquired due to these were developed to two-phase flow. Even though the SP process is considered an immiscible process, three different displacement phases (Oil phase, Microemulsion (*Me*) phase, and aqueous phase) coexists in significant quantities within the porous media. Therefore, a variable representing *Me* phase is not included in the mentioned equations, and additionally, a bulk CT value of *Me* is difficult to quantify experimentally.

Based on the above, for this case, the CT is a reliable and accurate tool in a condition which the displacement performance really corresponds to two-phase flow, i.e., when a minimum quantity of microemulsion is present inside the rock. For our case, it occurs at low and high amounts of the chemical fluid injected.

Analyzing the applicability of the Equations 3.2, 3.5 and 3.6 inside a pixel of the CT images, the following can be noticed:

a) These mathematical expressions are applicable where the volumetric quantity of water (S_t^w), oil (S_t^o) and microemulsion (S_t^{me}) meets the cases expressed by the Figure 5.40.

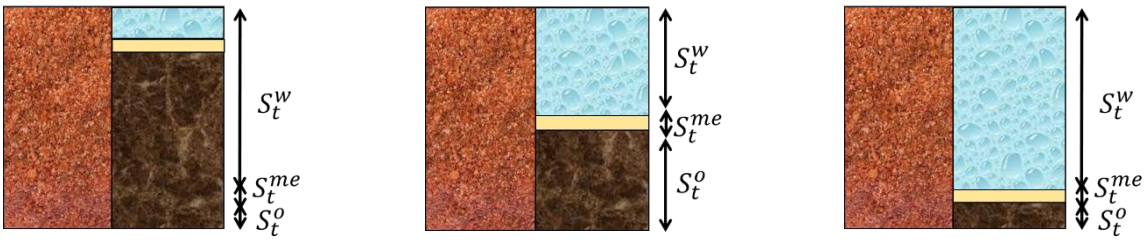

(a) (b) (c)

$$S_t^{me} << S_t^w \text{ and } S_t^{me} << S_t^o$$

Figure 5.40 Schematic representation of the fluids distribution analysis inside a pixel.

a), **b)** PVInj of chemical ≤ 0.8. **c)** 5 ≤ PVInj of chemical ≤ 10.

b) These mathematical expressions lost accuracy in the cases shown in Figure 5.41:

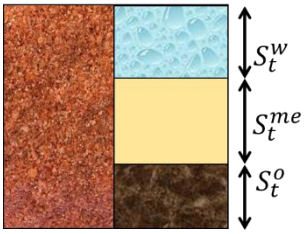

$$S_t^{me} \geq S_t^w \text{ and } S_t^{me} \geq S_t^o$$

Figure 5.41 Schematic representation of the fluids distribution analysis inside in a pixel between 0.8 < PVInj of chemical < 5.

Figure 5.42(a) shows an example of the emulsion produced by the rock with unknown water/oil proportions up to 1.2 PVInj. Figure 5.42(b) presents the same fluids after one week of gravity separation elucidating changes in oil and water collected volumes.

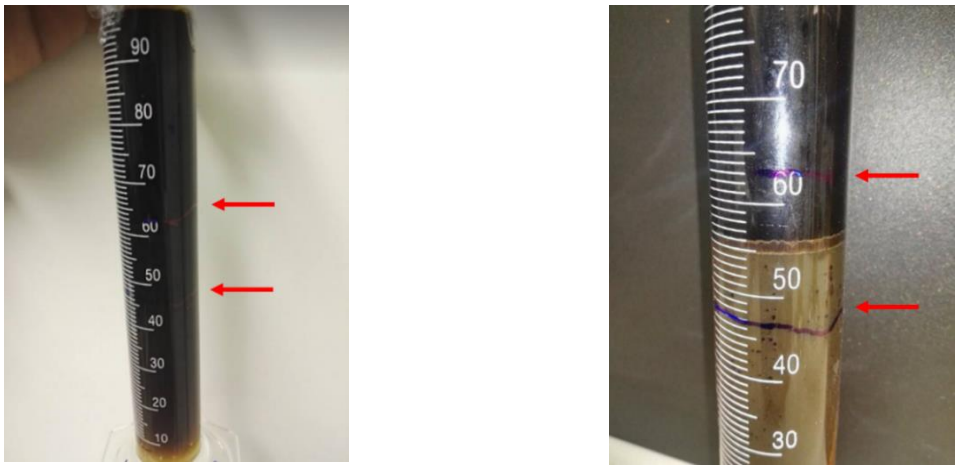

(a) (b)

Figure 5.42 Produced fluids after 1.2 PVInj.

a) at the moment of 1.2 PV have been injected, b) after one week

Figure 5.43 shows the evolution of the oil saturation in function of the PVInj of the chemical in a cross-section along the rock sample. The golden color represents higher CT numbers related to the doped oil location and rock lamination. The blue color is associated with a qualitative position of the aqueous solutions.

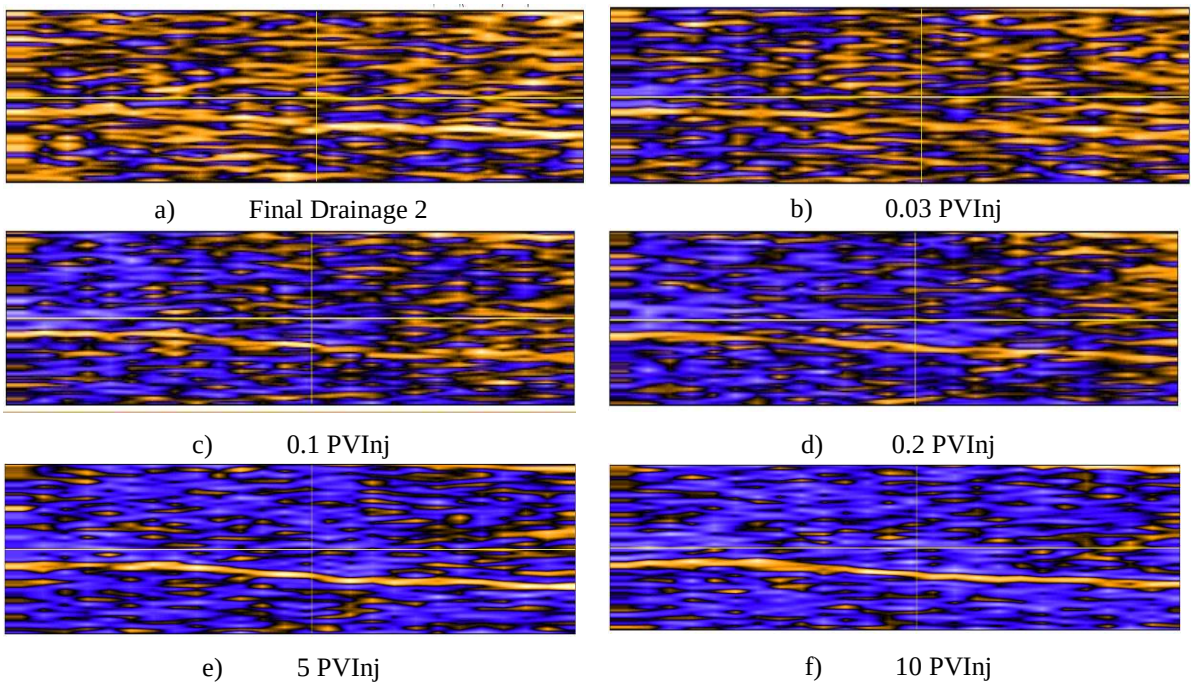

a) Final Drainage 2 b) 0.03 PVInj

c) 0.1 PVInj d) 0.2 PVInj

e) 5 PVInj f) 10 PVInj

Figure 5.43 Chemical Injection – 2D Oil Saturation in function of PVInj

Finally, the main parameters determined at this stage are shown below:

Table 5.13 Consolidated of parameters determined during Surfactant/Polymer Injection.

Parameter	**Value**	**Unit**
Chemical Volume inside the rock	60.55	cm^3
Oil Volume inside the rock	12.06	cm^3
Chemical Saturation	0.83	-
Residual Oil Saturation	0.17	-
Time Breakthrough (BT)	37.45	min
Oil Produced at BT	18.59	cm^3
Total Oil Produced	36.27	cm^3
Flow Rate Stage	0.51	cm^3/min
Oil Recovery Factor	75	%
Chemical Effective Permeability at Sor	185.84	mD
Chemical Relative Permeability at Sor	0.034	mD

5.3.6 Test 1 and Test 2 - Comparative oil recovery performance evaluated by CT and volumetric material balance

Initially, the oil recovery factor (FR) results calculated through the produced volumes are compared with the CT data results analyzed using the three procedures presented in Item 3.5 (*CT 1*, *CT 2* and *CT 3*). Figure 5.44 shows these results.

Figure 5.44 shows the useful application of the CT scan to determine the fluids saturations inside the rock during the WF process. In this case, the three methods used for CT analysis matched with the volumetric material balance (MB). However, in the SP injection, the *red square* emphasizes the limitation exposed previously in Item 5.3.5.

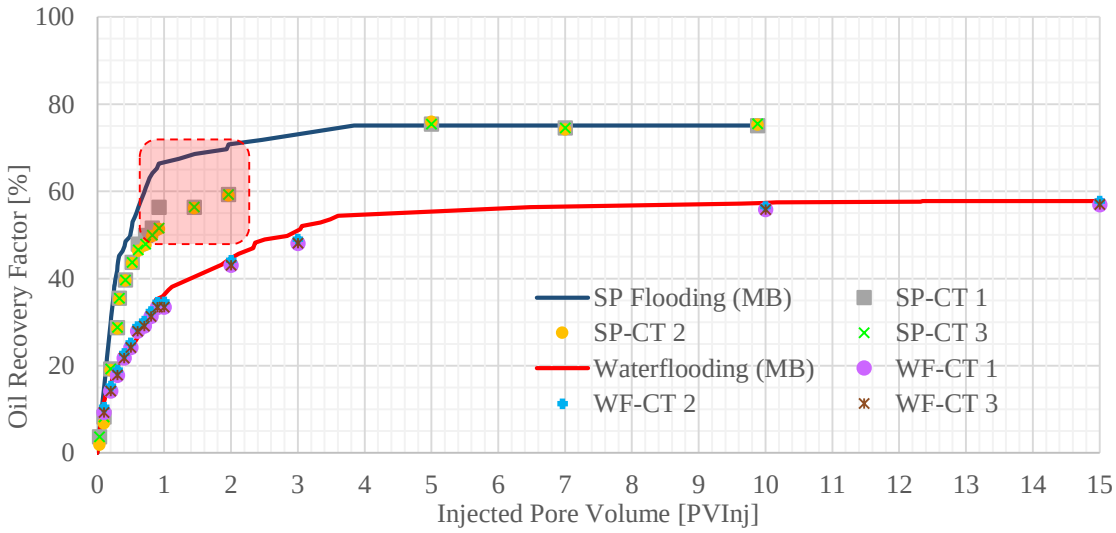

Figure 5.44 Comparison of Oil Recovery Factor obtained using Material Balance and CT for WF and SP process.

Figure 5.45 shows the oil recovery factor difference between both secondary oil recovery process (WF and SP). The highest efficiency of the SP process occurs at approximately 0.7 PVInj obtaining 30% of incremental oil related to same water volume used by WF method. After 0.7 PVInj, the process efficiency starts to decrease and finally stabilize around to 17%.

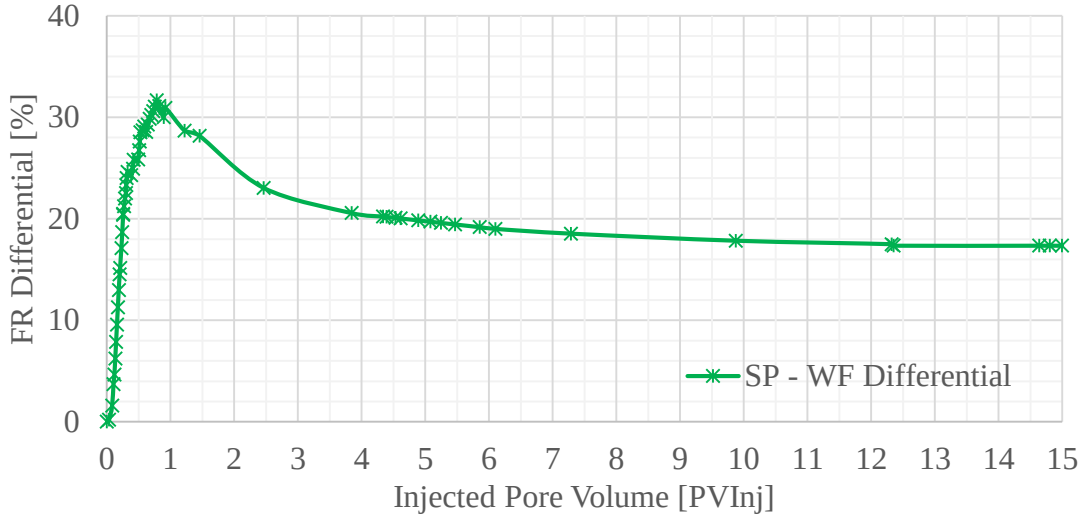

Figure 5.45 Oil Recovery Factor Differential between SP and WF.

The discussion above does not imply that a continuous SP injection is required to improve oil recovery significantly. If a small quantity of chemical (0.7 PV) was used alternating with the water injection, an improvement lower than 17% on the final WF oil recovery factor could be obtained.

This thesis motivated the assessment of tertiary flooding (Test 3) following presented.

5.3.7 Test 3 - Imbibition

Figure 5.46 shows the absolute permeability of the rock sample 12A2, used for Test 3. The permeability corresponded to 287.7 mD. This value is smaller than the value obtained during petrophysical characterization, similarly to test 1.

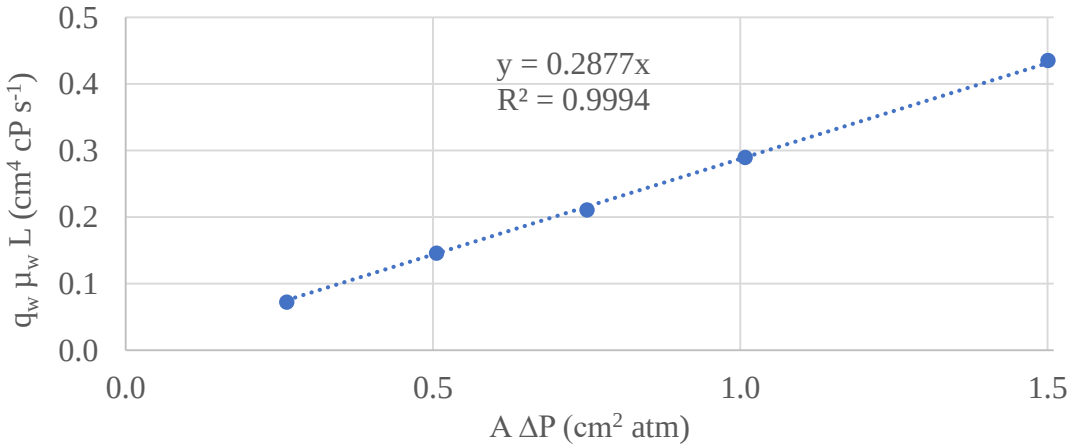

Figure 5.46 Absolute Permeability 12A2.

Also, porosity profile of the 12A2 rock sample was determined by the CT demonstrating, once again, the CT accuracy for this application. Comparing the porosimeter value and tomographic results (Figure 5.47), one can observe that the behavior before and after K_w determination maintains the profile trend and does not present significant numerical changes (Table 5.14).

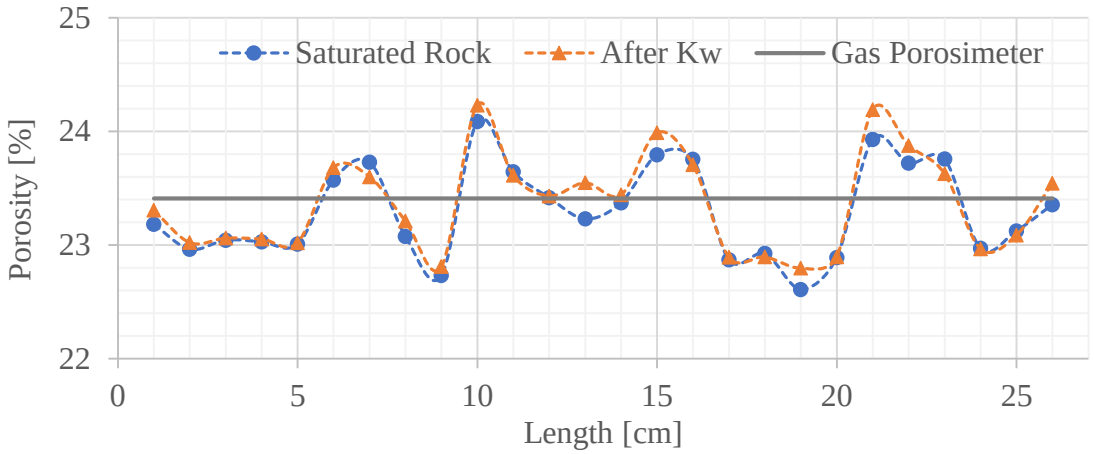

Figure 5.47 Comparison between CT porosity profiles of before imbibition, after imbibition and gas porosimeter value of 12A2 rock sample

Table 5.14 Porosity values obtained using CT respect to gas porosimeter value of 12A2 rock sample.

Porosity Measurement Method		**Mean Value (%)**
Gas Porosimeter		23.41
CT	**Before Imbibition**	23.30
CT	**After Imbibition**	23.37

5.3.8 Test 3 - Drainage

After the Imbibition, the oil injection starts to displace all the existent mobile water inside the rock and restore the initial rock reservoir conditions. Figure 5.48 presents the produced volumes calculated by the material balance, showing that after BT there was a continuous production of water until reaching the steady state.

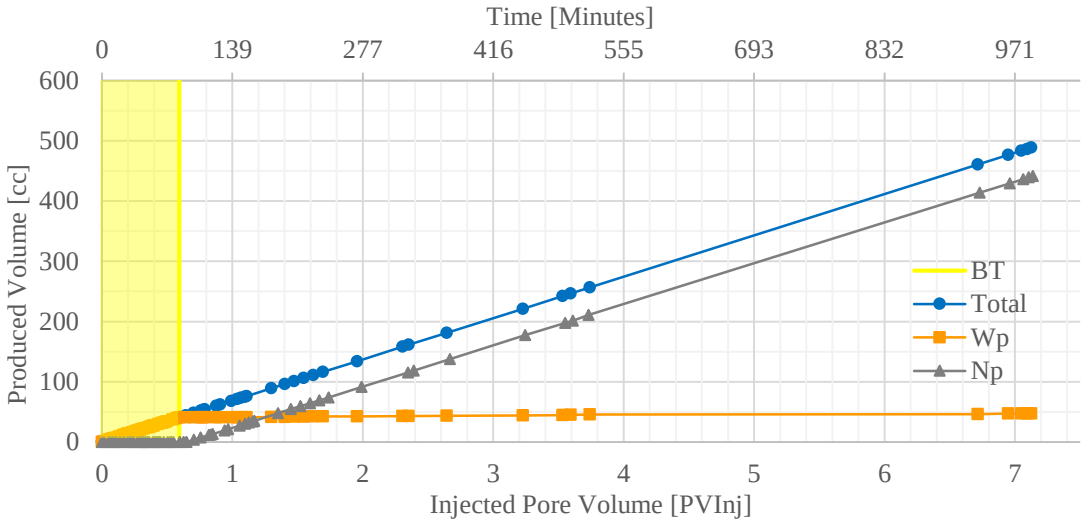

Figure 5.48 Drainage - Produced Volumes calculated by Material Balance

A total of 7.13 pore volumes of oil were injected. The BT of oil occurred at 0.59 PVInj, which took approximately 89.94 minutes. At the BT instant, about 86% of the mobile water had been produced.

The displacement of fluids until BT was performed with a homogenous advance front. This is confirmed by the water saturation profile obtained through CT technique (Figure 5.49) using the Equation (3.5).

When 3.6 PV of oil had been injected, the water saturation profile started to stabilize and finally, it presented homogeneous distribution through the rock sample when 6.5 PV of oil or more were injected.

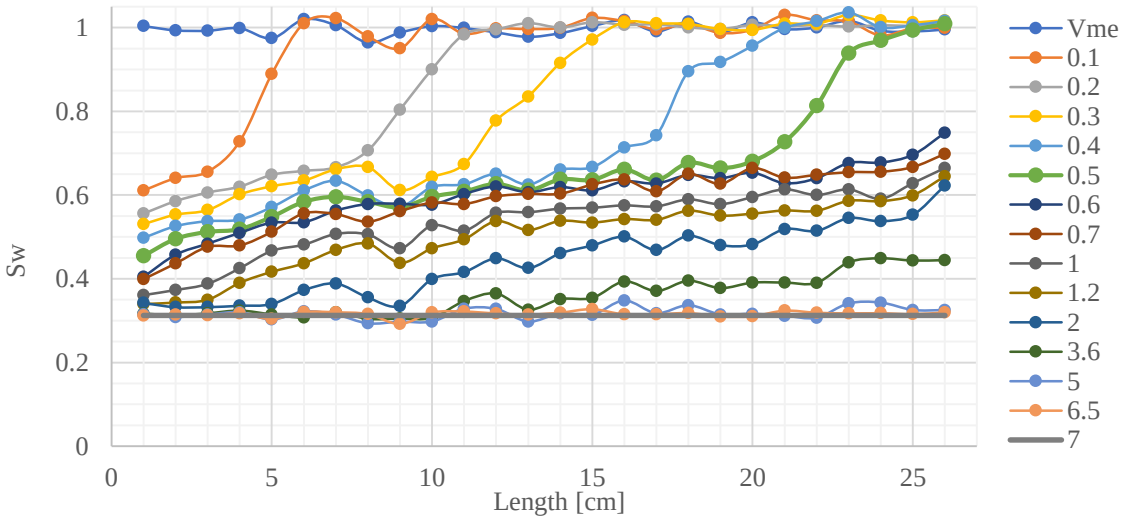

Figure 5.49 Drainage 1 - Water Saturation Profiles in function of Injected Pore Volume (PVInj) through the rock sample 12A2.

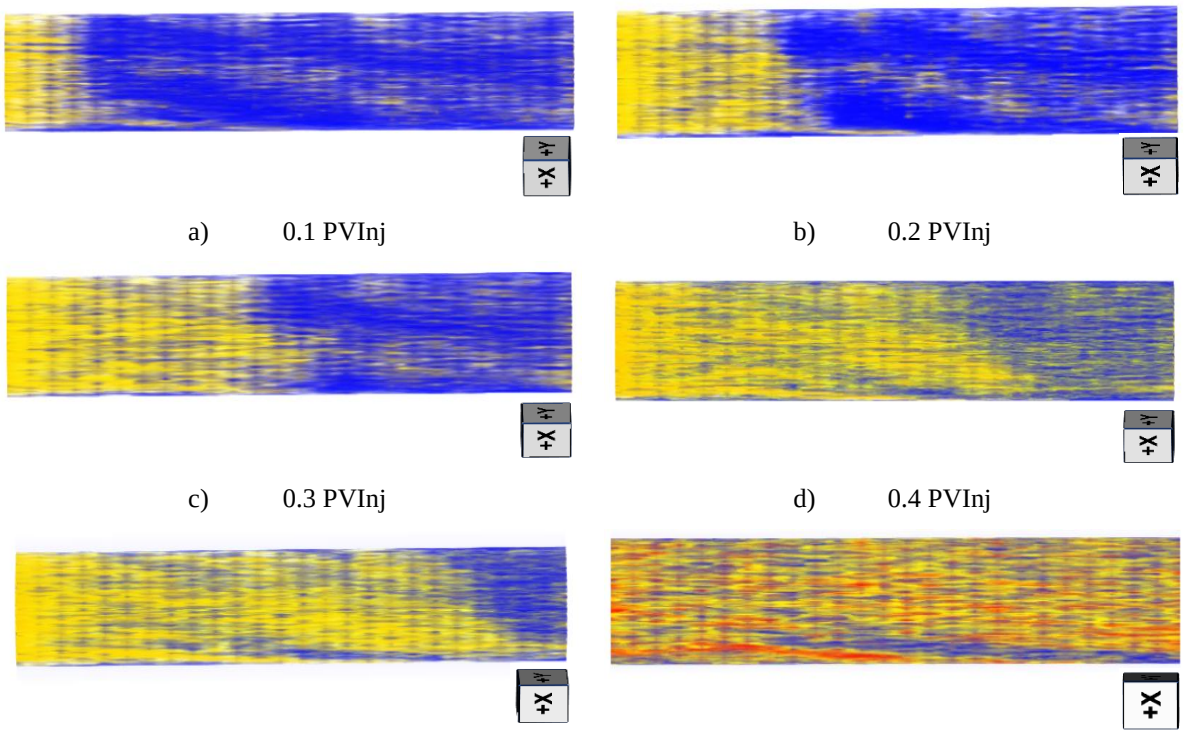

a) 0.1 PVInj b) 0.2 PVInj

c) 0.3 PVInj d) 0.4 PVInj

e) 0.5 PVInj f) 7 PVInj

Figure 5.50 Drainage - 3D Images in Function of PVInj.

The yellow, blue and red colors correspond to oil, water location, and discontinuous rock laminations, respectively.

The pressure history (Figure 5.51) exhibits an initial rise due to replace water with oil. After the oil BT, the differential pressure tends to stabilize.

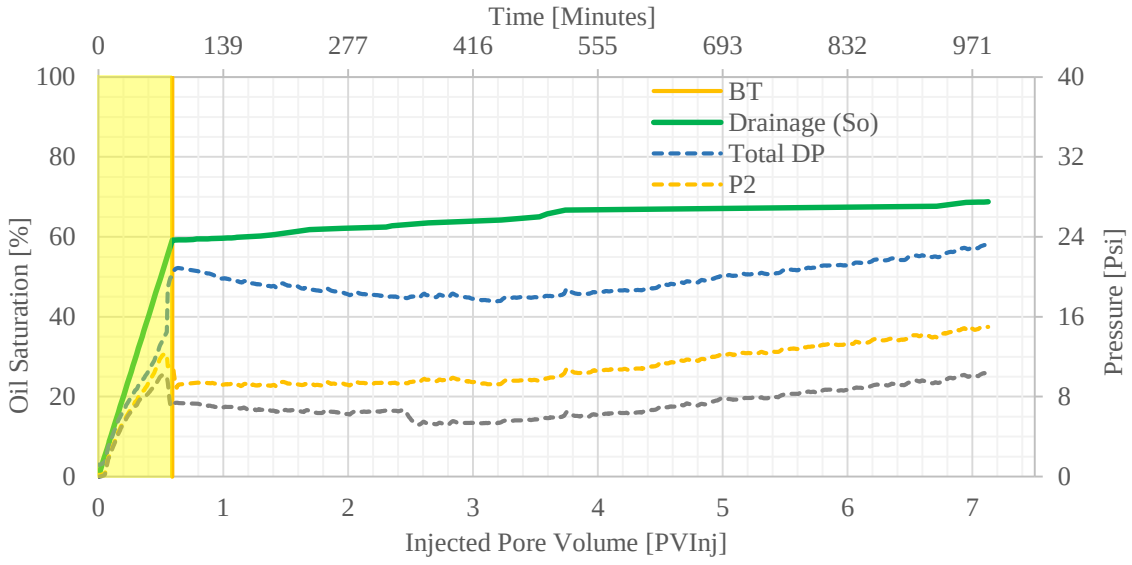

Figure 5.51 Drainage 1 – Oil Saturation and Historical Pressure in function of PVInj and time

Then, the oil effective permeability (K_o) was calculated using the final total differential pressure value of each tap pressure (P_2, P_4 and total).

Table 5.15 presents the results and shows that exists heterogeneity to flow in the rock sample.

Table 5.15 Drainage - Effective Oil Permeability by stretch

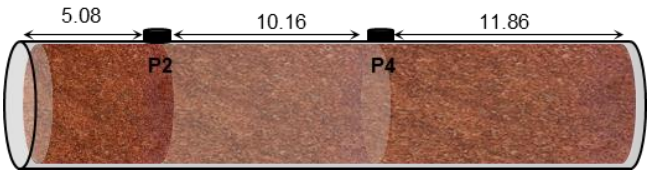	ΔP (psi)	Permeability (mD)
	Inlet-P_2 = 8.10	$K_{inlet-P2}$ = 123.85
	P_2-P_4 = 4.73	K_{P2-P4} = 424.25
	P_4-Outlet = 10.25	$K_{P4-outlet}$ = 228.56
	ΔP Total = 23.08	$\bar{K}$ = 231.91

The main parameters determined in this stage show in Table 5.16.

Table 5.16 Consolidated of parameters determined during Drainage 1.

Parameter	**Value**	**Unit**
Water Volume inside the rock	21.42	cm^3
Oil Volume inside the rock	47.16	cm^3
Initial Water Saturation	0.31	-
Oil Saturation	0.69	-
Time Breakthrough (BT)	89.95	min
Water Produced at BT	40.56	cm^3
Total Water Produced	47.16	cm^3
Flow Rate Stage	0.46	cm^3/min
Oil Effective Permeability	231.91	mD

5.3.9 Test 3 – Surfactant/Polymer injection as a tertiary oil recovery method.

Once the rock has been reestablished to initial reservoir conditions (S_{wi} and high S_o), the assessment of the Surfactant/polymer injection as a tertiary method supported by CT, started. First, a total of 6.71 pore volumes of brine were injected. This amount was determined based on the results reported for WF (Item 5.3.3), which the oil recovery performance and differential pressure not exhibited significant changes 7 PVInj of water, and the Wcut was higher than 90%. Therefore, the rock would be close to S_{or}. The BT of brine occurred when 1.1 PV of fluid had been injected, which took approximately 14.36 minutes. At the brine BT, about 16% of the initial oil had been produced. The oil recovery factor due to waterflooding stabilized in 49.95% with a Wcut of 94.88% by the end of the brine injection.

After the brine injection, CEOR process is applied and evaluated by CT. It consisted of two slugs of surfactant-polymer blend kept separated by a brine drive fluid. In the first chemical slug, a total 0.69 PV of SP blend was injected during approximately 82.47 minutes. This slug broke through after 0.26 PVInj, after 20.47 minutes of injection. The amount of the first chemical slug was chosen as the instant which the SP process presented the highest efficiency during the test 2, corresponding to 0.7 PV of chemical blend (Figure 5.45). This stage was named CEOR1 (Figure 5.52).

After having injected 3.88 PV of drive brine, the second chemical slug started, and a total of 0.53 PV of SP blend was used. This slug reached the outlet face after 0.33 PVInj, then 45.35 minutes of injection. Finally, a total of 4.27 PV of brine was used as the second drive fluid. This stage was named CEOR 2 (Figure 5.52).

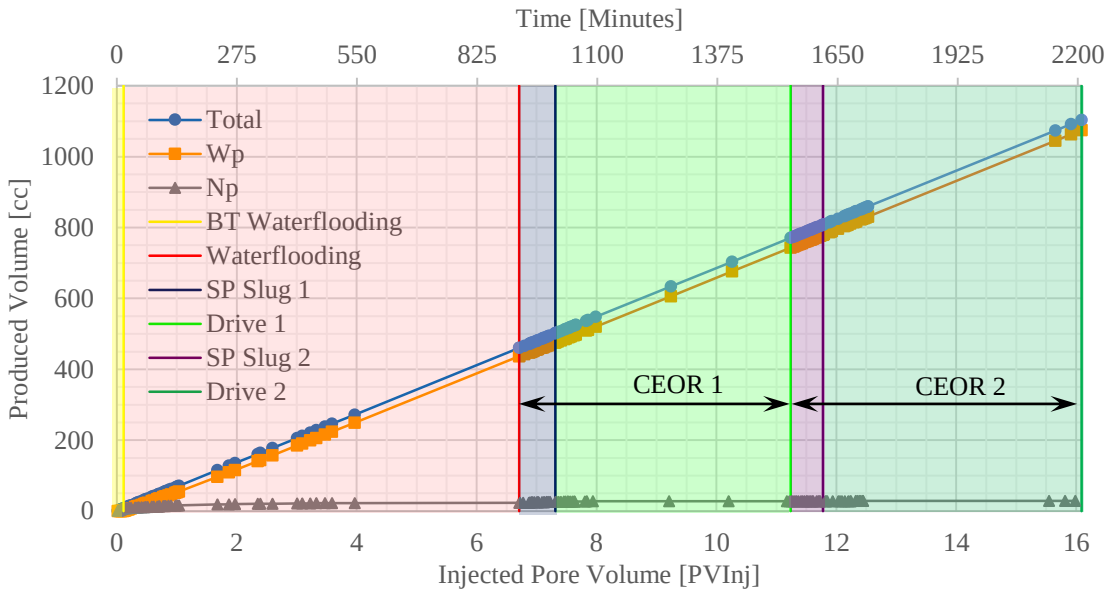

Figure 5.52 SP as CEOR process – produced volumes calculated by material balance.

Figure 5.52 presents the produced volumes calculated by the material balance of each stage in this oil recovery scheme. During the WF an significative amount of oil was produced after the BT, evidencing the existence of viscous fingering. The water saturation profiles confirmed it (Figure 5.53).

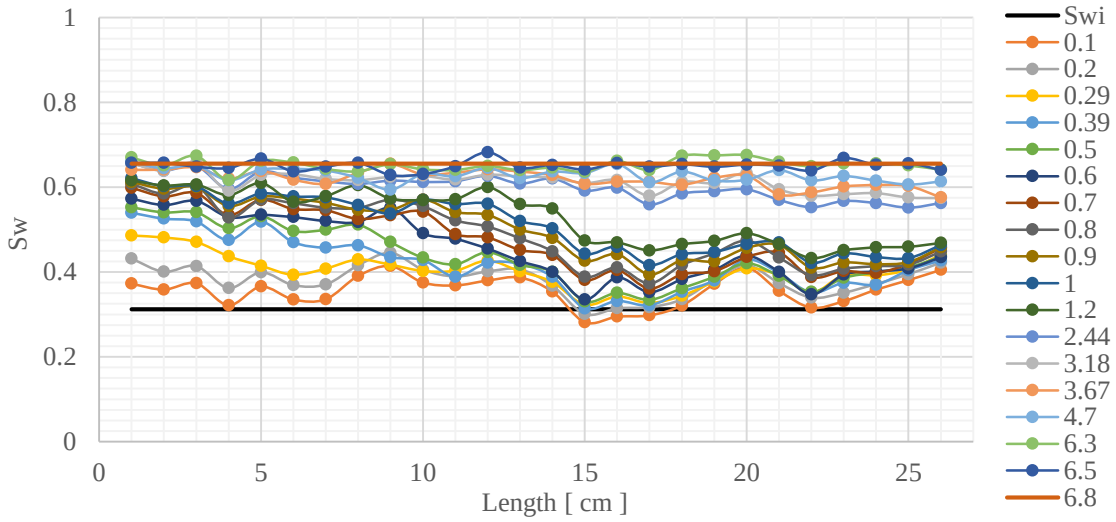

Figure 5.53 Waterflooding – Water saturation profiles in function of PVInj through rock sample 12A2.

As the water injection progresses, there is a continuous increase of the water saturation at the region close to the inlet face of the rock sample. After the middle of the rock, the water saturation does not present significant changes until 1.2 PVInj due to the generation of water fingering. This fingering creates a gap in the saturation profiles which was filled at 2.44 PVInj of water, i.e., before this instant, the water was heterogeneously distributed inside the rock sample. However, after 6 PVInj, the water tends to be homogeneously distributed within the rock.

Figure 5.54 shows 3D images reconstructions. In these images, there is water (blue color), and discontinuous laminations (red color) only.

a) Dry core sample CT

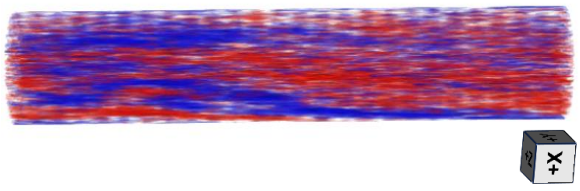

b) 0.1 PVInj

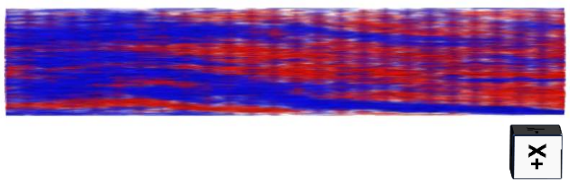

c) 0.5 PVInj

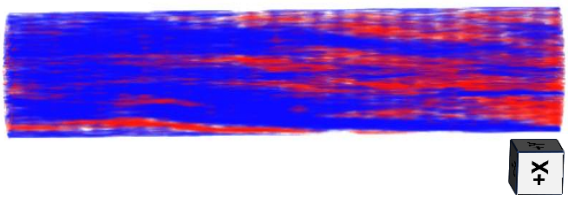

d) 1.2 PVInj

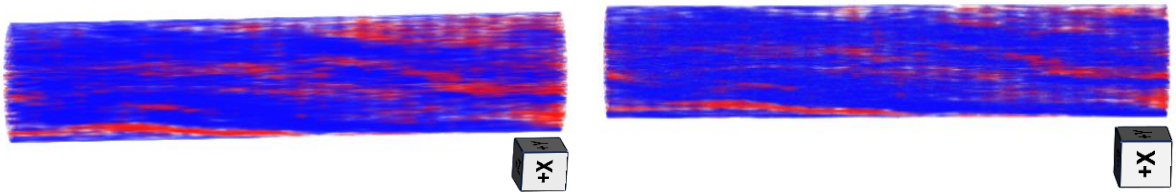

e) 2.44 PVInj f) 7 PVInj

Figure 5.54 Waterflooding - 3D Images in Function of PVInj of water.
Blue color represents the water location and red color the discontinuous laminations of the rock.

The results of the water effective permeability (K_w) are presented in Table 5.17 which shows that exists heterogeneity to the flow fluids through the rock sample.

Table 5.17 Waterflooding - Effective water permeability by stretch

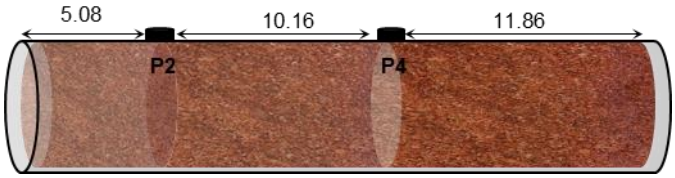

ΔP (psi)	Permeability (mD)
Inlet-P2 = 4.29	$K_{inlet-P2}$ = 8.08
P2-P4 = 10.01	K_{P2-P4} = 6.92
P4-Outlet= 19.03	$K_{P4-outlet}$ = 4.25
ΔP Total = 33.33	$\bar{K}$ = 5.55

It is possible to observe a gradual reduction in the water effective permeability of the porous media, and it is interesting to note that K_w behavior coincides with the discontinuous lamination distribution inside the rock.

Despite the similar petrophysical and initial drainage performance between 12A2 and 12A4 rock samples, the usage of CT scanner as a tool to evaluate these core flooding test allows affirming that, the performance and displacement efficiencies during the waterflooding were different due to the internal rock heterogeneities. These heterogeneities dominated the fluids dynamics through preferable flow paths across the 12A2 rock sample.

The main parameters determined in this stage show in Table 5.18:

Table 5.18 Consolidated of parameters determined during waterflooding.

Parameter	**Value**	**Unit**
Water Volume inside the rock	44.97	cm^3
Oil Volume inside the rock	23.60	cm^3
Water Saturation	0.66	-
Residual Oil Saturation	0.34	-
Time Breakthrough (BT)	14.36	min

Parameter	Value	Unit
Flow Rate at BT	0.52	cm^3/min
Oil Produced at BT	7.56	cm^3
Total Oil Produced	23.56	cm^3
Flow Rate Stage	0.5	cm^3/min
Oil Recovery Factor	49.95	%
Water Effective Permeability at S_{or}	5.55	mD

Figure 5.55 shows the water saturation profiles during CEOR 1 process. The fact that the profiles between 0.1 to 0.5 PVInj got out the lower limit established by the volumetric MB is not a numerical mistake or a limitation of the CT. This behavior is characterized by the increases in the average value of S_w and therefore, a decrease of the average value of S_{or} through the rock (Table 5.19). In fact, it is a response to the mobilization of the residual close to the inlet face of the rock and their displacement throughout the sample.

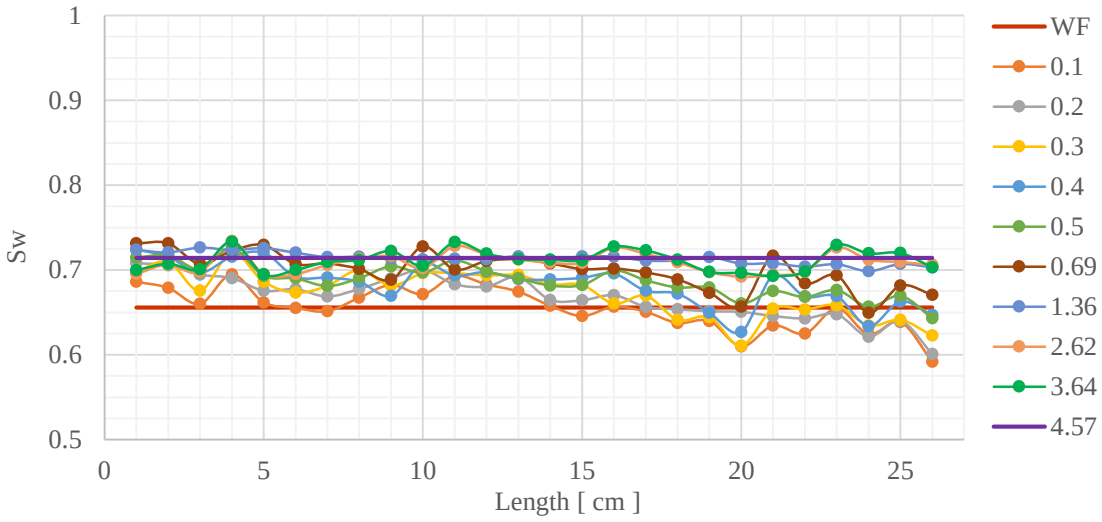

Figure 5.55 CEOR 1 - Water Saturation Profiles in function of PVInj through rock sample 12A2

Table 5.19 Average saturation values in function of PVInj of CEOR 1 determined by CT.

PVInj	0.1	0.2	0.3	0.4	0.5
Average S_w	0.655	0.667	0.672	0.684	0.687
Average S_o	0.345	0.333	0.328	0.316	0.313

Figure 5.56 show the 3D reconstruction of some images during CEOR 1 process. The yellow, blue and red color are the oil, water, and discontinuous rock lamination distributions, respectively.

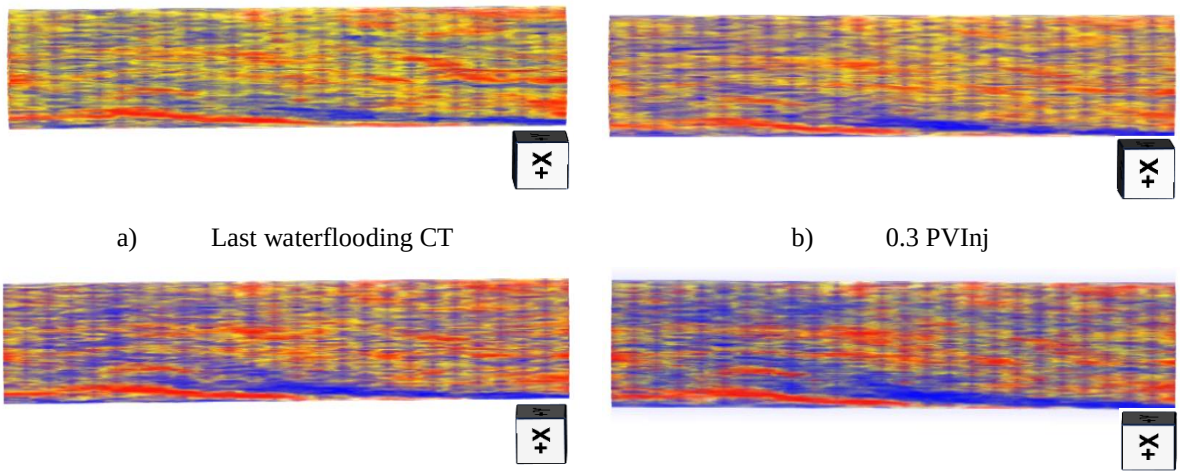

a) Last waterflooding CT b) 0.3 PVInj

c) 0.69 PVInj d) 4.57 PVInj

Figure 5.56 CEOR 1 - 3D Images in Function of PVInj of the chemical.

Yellow, blue and red color are the location of oil, water, and discontinuous rock lamination, respectively.

Table 5.20 shows the main parameters determined in this stage::

Table 5.20 Consolidated of parameters determined during CEOR 1.

Parameter	Value	Unit
Water Volume inside the rock	48.97	cm^3
Oil Volume inside the rock	19.60	cm^3
Water Saturation	0.71	-
Residual Oil Saturation	0.29	-
Cumulative Time Chemical BT	943.33	min
Cumulative Oil Produced at BT	24.51	cm^3
Cumulative Total Oil Produced	27.56	cm^3
Flow Rate Stage	0.5	cm^3/min
Cumulative Oil Recovery Factor	58.43	%
FR incremental respect to WF	8.48	%

During CEOR 2 stage, the water saturation distributions got out the upper limit established by the volumetric MB due to once additional oil is mobilized by the second SP slug injected (Figure 5.57). Part of this incremental oil is then moved, and part remains inside the pores close to the outlet face. The average values of fluids saturation calculated by CT confirm this behavior (Table 5.21).

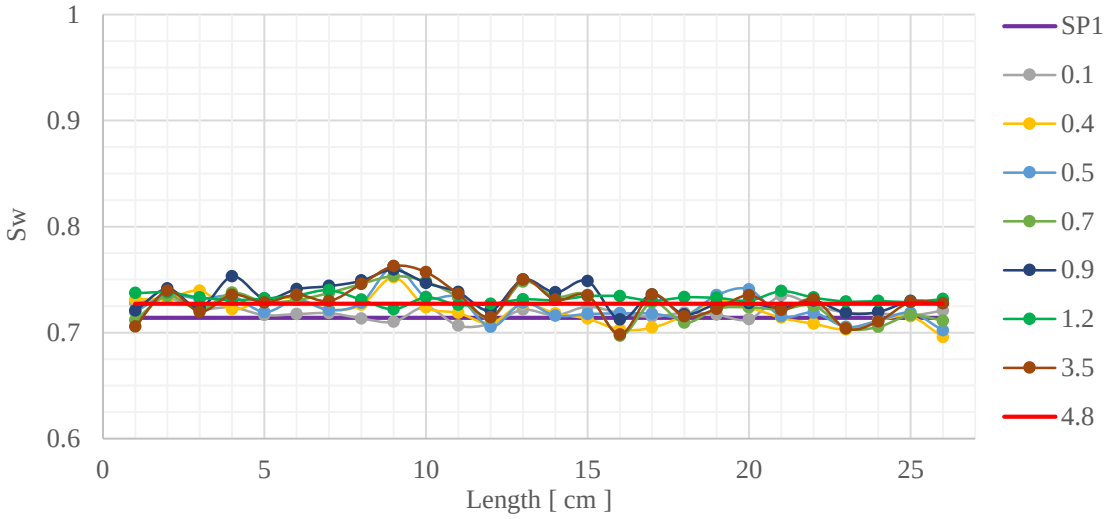

Figure 5.57 CEOR 2 - Water Saturation Profiles in function of PVInj through rock sample 12A2

Table 5.21 Average saturation values in function of PVInj of CEOR 2 determined by CT

PVInj	0.1	0.4	0.5	3.5
Average Sw	0.719	0.720	0.724	0.729
Average So	0.281	0.280	0.276	0.271

The main parameters determined in this stage are shown in Table 5.22.

Table 5.22 Consolidated of parameters determined during CEOR 2.

Parameter	**Value**	**Unit**
Water Volume inside rock	49.87	cm^3
Oil Volume inside rock	18.70	cm^3
Water Saturation	0.73	-
Residual Oil Saturation	0.27	-
Cumulative Time Chemical BT	1579	min
Cumulative Oil Produced at BT	27.79	cm^3
Cumulative Total Oil Produced	28.46	cm^3
Flow Rate Stage	0.5	cm^3/min
Cumulative Oil Recovery Factor	60.34	%
FR incremental respect to CEOR 1	1.91	%
FR incremental respect to WF	10.39	%

Figure 5.58 presents the histories for oil recovery and differential pressure of test 3. Based on those results, it is possible concluded that each recovery method achieved a S_{or} and there, any incremental oil was obtained a reduction of the previous residual saturation ($FR_{WF} < FR_{CEOR\ 1} < FR_{CEOR2}$). The above statement is confirmed by the stabilized plateau of the pressure history before the next stage starting.

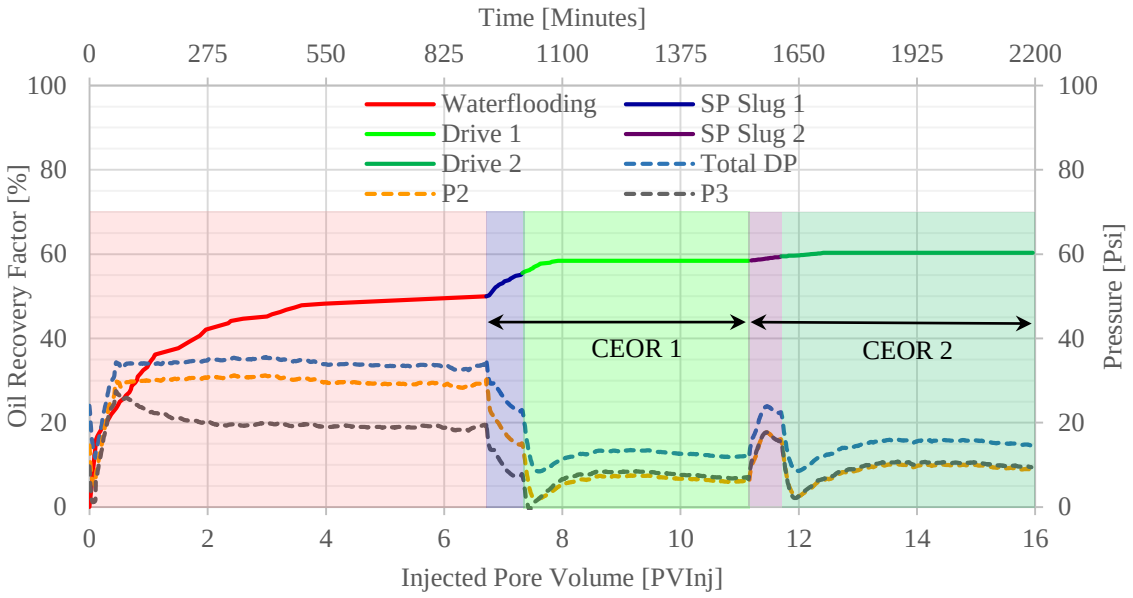

Figure 5.58 Test 3 – Oil recovery factor performance and Historical pressure in function of PVInj and time.

5.3.10 Test 3 - Oil recovery performance evaluated by CT and volumetric material balance

Oil recovery factor (FR) calculated through the volumetric MB are compared with the CT data analyzed by the three different procedures presented in Item 3.5 (*CT 1*, *CT 2* and *CT 3*). The comparison is presented in Figure 5.59.

The three methods used to analyze the CT results provide a good agreement for both process (WF and SP) concerning the results obtained by the volumetric material balance. This matching demonstrates the utility of the CT tool to improve the understanding of the dynamics of fluids in porous media when the microemulsion within the rock does not reach a significant quantity, and therefore, the water and oil volumes in each pixel of the image is accuracy quantified through the CT.

An oil recovery incremental of 10.39 percentage points compared to WF could be obtained using the surfactant/polymer blend proposed as a tertiary oil recovery method under the tested conditions. Nevertheless, a CEOR process is more efficient when is used in early stages during the field development.

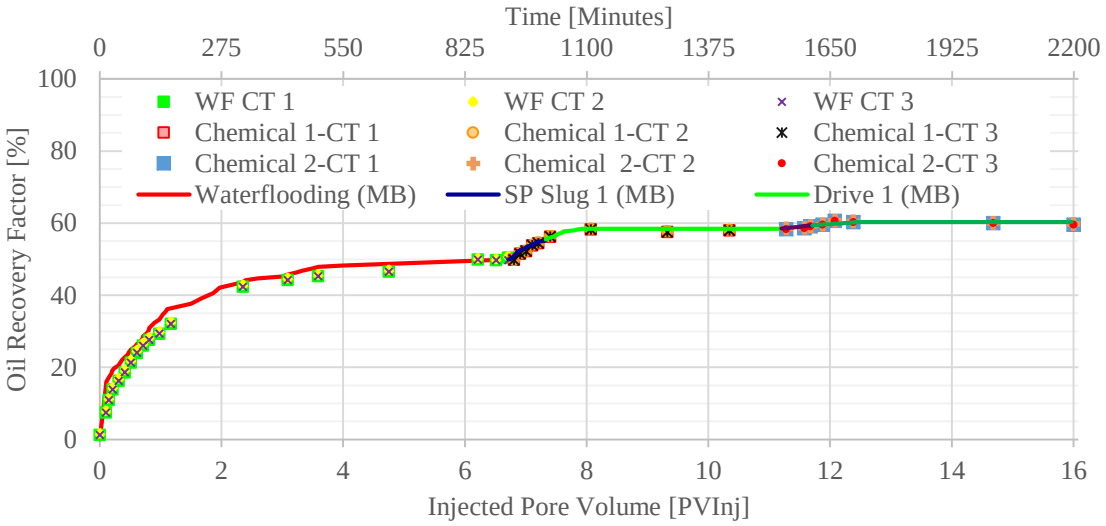

Figure 5.59 Comparison of Oil Recovery Factor obtained through Volumetric Material Balance (MB) and CT for SP process as Tertiary oil Recovery Method.

5.3.11 Other comparisons of tests results

5.3.11.1 Test 1 and Test 2

Wcut and WOR of both tests are analyzed aiming to stand out the principal differences between both processes. Figure 5.60 and Figure 5.61 present the Wcut comparisons showing a reduction of the amount of produced water as result of a better mobility ratio of the SP process. These results are evidenced for a delay in the breakthrough of the chemical injected fluid when comparing the SP and the WF. The lower Wcut continues until approximately 5 PV of the SP blend injection. After that, the Wcut tends to be very similar for both processes, because the majority of the recoverable oil had already produced.

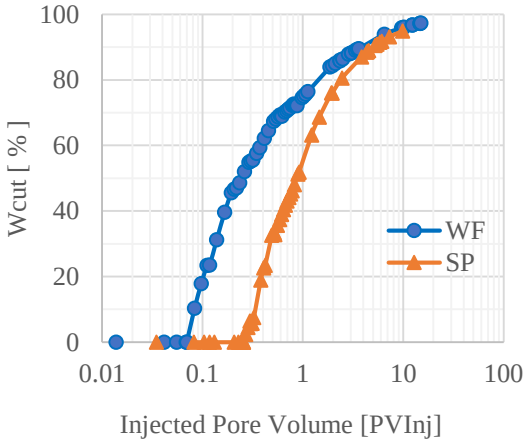

Figure 5.60 Wcut comparison between WF (Test 1) and SP (Test 2).

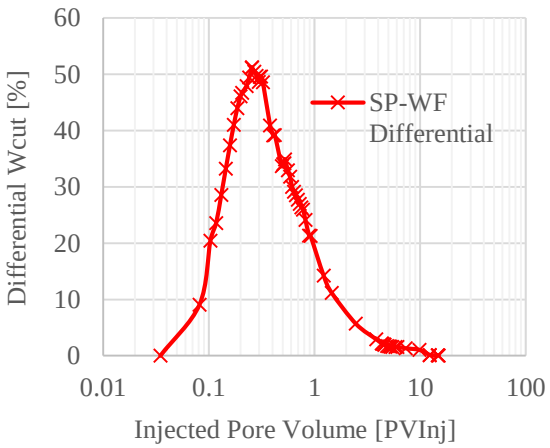

Figure 5.61 Differential between WF (Test 1) and SP (Test 2)

Figure 5.62 shows a comparison of WOR for both oil recovery methods. The WOR is reduced during all the process because two benefits of the SP process are acting simultaneously, i.e., there is a reduction of produced water while oil production increases.

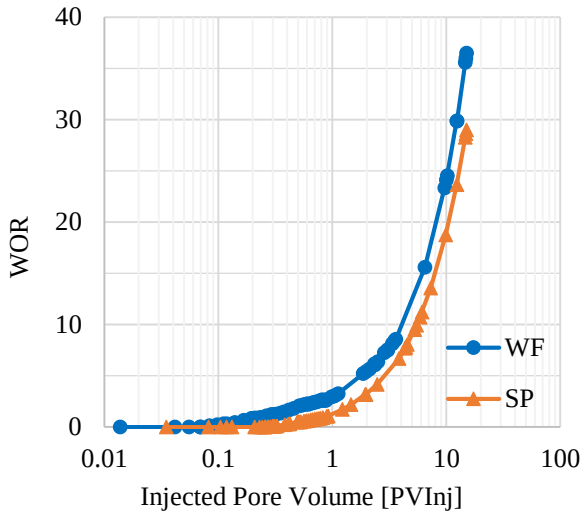

Figure 5.62 WOR comparison between WF and SP

5.3.11.2 Test 2 and Test 3

Figure 5.63 presents the SP blend comparative results between test 2 (Secondary oil recovery method) and test 3 (Tertiary oil recovery method) performance as a function of the total mobilized oil (TMO) of each test.

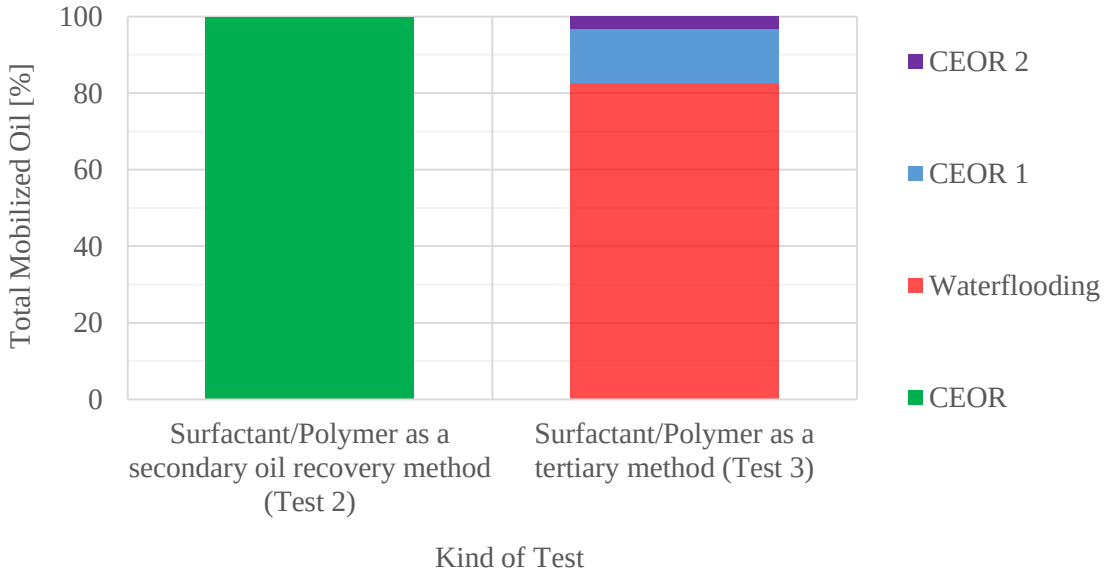

Figure 5.63 Process efficiency in function of total mobile oil for test 2 and test 3.

Only the injection of CEOR 1 in test 3 allowed to reach a 96.8% of TMO. It confirmed that the slug size determined in Item 5.3.6 corresponds to an appropriate quantity of chemical to achieve a high efficiency during the CEOR process.

6 CONCLUSIONS AND SUGGESTIONS

6.1 Conclusions

Based on the performed work and the literature support, the author can highlight the following conclusions:

Respect to objective *characterize the rheological behavior of the polymer solution to be used* in this work:

- The polymer solutions studied were mainly affected by the divalent cations content than by the range of the investigated temperature. However, both factors generated a detrimental effect on polymer rheological and viscoelastic behavior.
- The polymer solution with synthetic Brine II (without divalent content) presented a more extended Linear Viscoelastic Region and higher viscosity values. Therefore, it shows the best rheological and viscoelastic performance.

According to the objective *design the surfactant solution to be employed during the core flooding tests* and aiming to understand the interactions among fluids and chemical products, it is concluded that:

- The observed phase behavior corresponds to a transition Winsor II→I without finding some Winsor III microemulsion. The Bancroft Rule was used as qualitative verification tool of the type of formed microemulsion and confirmed the phase behavior observed. This behavior corresponds to a reversal status of the surfactant. Therefore, some criteria for the selection of optimal salinity were proposed that based on the condition where the transition Winsor II to I occurs.
- Regarding the lowest interfacial tension reduction at the target salinity, the surfactant concentration to be used was 0.5 [%wt] of SDS. Although similar IFT values were obtained using 2 [%wt] of SDS, the highest microemulsion viscosity value was obtained at this surfactant concentration. Therefore, it is discarded.

Respecting, the displacement efficiency of the tailor-made chemical solution and in agreement with the objective *design surfactant-polymer flooding and evaluate its performance with core flooding tests supported by computed tomography* is possible to address the following conclusions:

- The Surfactant-Polymer Blend used as a secondary and tertiary oil recovery method provided an improvement in the oil recovery factor of 17 and 10 percentage points compared to the conventional waterflooding.
- The surfactant-polymer blend generates a better mobility ratio, that was evidenced by the delay of the breakthrough respect to the waterflooding.
- The water-oil ratio during the Chemical Enhanced Oil Recovery processes diminished due to the improvement of displacement efficiency and mobilization of the residual oil saturation.
- Chemical Enhanced Oil Recovery methods are more efficient when they are applied in early stages during the field development as a strategy of field management.

Finally, to improve the understanding of the fluids dynamics through computed tomography and by the objective *evaluate and analyze the obtained results through core flooding tests and compare the material balance with the Computed Tomography results* is concluded that:

- The use of the CT scanner during core-flooding tests is a powerful tool to determine the porosity and saturation profiles along the rock sample. Also, visualization inside of the rock (2D and 3D) improves the two-phase flow dynamic understanding through the porous media.
- A limitation of the mathematic expressions used to determine the saturation profiles by CT data was identified when conducting the Surfactant-Polymer process as a secondary oil recovery method (Swi and High So) at the tested conditions. For this case, the computed tomography is a reliable and accurate tool only when the displacement performance corresponds to a two-phase process. i.e., when a minimum amount of microemulsion is present inside the rock, and therefore, the water and oil volumes in each pixel is accurately quantified by the CT. That occurs at lower and higher amounts of the chemical blend injected since at the begging of the flooding process, there is not enough chemical blend to interact with the oil, while at long term, the low remaining oil limits the interactions between the fluids.
- For the CEOR processes evaluation as tertiary oil recovery methods the CT was an accurate tool to determine the fluids saturation inside the rock.

6.2 Suggestions

- Evaluate Surfactant-Polymer process as Enhanced Oil Recovery technique using the CT scanner in both energies (High and Low energy) aiming to identify three-phase flow to obtain saturation profiles with a high microemulsion content.
- Repeat the optimum salinity selection using the criteria proposed by this work.
- Perform the history matching through small-scale simulation aiming to represent the physical phenomena related to the Surfactant-Polymer process and the injection schemes tested in this work.

REFERENCES

ABBAS, M. An Extension of Johnson , Bossler and Neumann JBN Method for Calculating Relative Permeabilities. 2016.

ABIDIN, A. Z.; PUSPASARI, T.; NUGROHO, W. A. Polymers for Enhanced Oil Recovery Technology. Procedia Chemistry, v. 4, p. 11–16, 2012.

AL-BAHAR, M. A. et al. Evaluation of IOR Potential within Kuwait. Abu Dhabi International Conference and Exhibition, 2004.

ALMEIDA, M. L. DE. Estabilidade de emulsões de água-em-óleo na presença de campo elétrico externo. p. 90, 2014.

ALVESTAD, J. et al. Coreflood experiments with surfactant systems for IOR: Computer tomography studies and numerical modelling. Journal of Petroleum Science and Engineering, v. 7, n. 1–2, p. 155–171, 1992.

BARNES; HUTTON; WALTERS. An Introduction to Rheology. [s.l: s.n.]. v. 3

BATAWEEL, M. A.; NASR-EL-DIN, H. A. Rheological Study for Surfactant-Polymer and Novel Alkali-Surfactant- Polymer Solutions. n. 1, p. 1–16, 2012.

BATENBURG, D. W. VAN et al. SPE175407 Visualization of Oil Mobilization in ASP Core Floods Using X-ray CT Imaging. SPE Kuawait Oil & Gas Show and Conference held in Mishref, Kuwait, 11-14 October 2015, 2015.

BENNETT, K. E. et al. Microemulsion Rheology: Newtonian and Non-Newtonian Regimes. SPE Annual Technical Conference and Exhibition, 1981.

BRASHEAR, J. P.; V. A. KUUSKRAA. The Potential and Economics of Enhanced Oil Recovery. Journal of Petroleum Technology, v. 30, n. 9, p. 1231–1239, 1995.

BRITISH PETROLEUM. BP Statistical Review of World Energy 2017. British Petroleum, n. 66, p. 1–52, 2017.

CARCOANA, A. N. Enhanced Oil Recovery in Rumania. SPE/DOE, v. SPE-10699-, 1982.

CHAKRAVARTHY, D. et al. Application of X-Ray CT for Investigation of CO and WAG Injection in Fractured Reservoirs. Petroleum Society's 5th Canadian International Petroleum Conference, p. 1–14, 2004.

COLES, M. .; MUEGGE, E. . The Use of Attenuation Standards for CT Scanning. 1995

DAKE, L. P. Fundamentals of Reservoir EngineeringEnvironmental science technologyAmsterdam, The NetherlandsElsevier B.V., , 2008.

DEHGHANPOUR, H.; KURU, E. A New Look at the Viscoelastic Fluid Flow in Porous Media

- A Possible Mechanism of Internal Cake Formation and Formation Damage Control. Spe, n. 1985, 2009.

DODA, A. Effect of viscoelasticity and alkali on heavy oil EOR performance using HPAM, “AA-NVP” co- and cross-linked polymers. [s.l: s.n.].

DONALDSON, E. C.; LORENZ, P. B.; THOMAS, R. D. The Effects of Viscosity and Wettability on Oil and Water Relative Permeabilities. Fall Meeting of the Society of Petroleum Engineers of AIME, 1966.

DONALDSON, E. C.; WAQI, A. Wettabillty. Houston, Texas: Gulf Publishing Company, 2008.

DOS SANTOS, R. L. A.; BEDRIKOVESTSKY, P.; HOLLEBEM, C. R. Optimal Design and Planning for Laboratory Corefloods. Society of Petroleum Engineers, v. SPE 39038, 1997.

ELMOFTY, O. Surfactant enhanced oil recovery by wettability alteration in sandstone reservoirs. 2012.

EZEKWE, N. Petroleum Reservoir Engineering Practice. Boston: Pearson Eduacation, Inc, 2011.

GHOSH, K.; MAITI, S. N. Melt Rheological Properties of Silver-Powder-Filled Polypropylene Composites. Polymer-Plastics Technology and Engineering, v. 36, n. 5, p. 703–722, 1997.

GHOULAM, M. BEN et al. Quantitative effect of nonionic surfactant partitioning on the hydrophile-lipophile balance temperature. Langmuir, v. 20, n. 7, p. 2584–2589, 2004.

GOODLETT, G. .; HONARPOUR, M. M.; CHUNG, F. T. The Role of Screening and Laboratory Flow Studies in EOR Process Evaluation. Spe, p. 28, 1986.

GOODWIN, J. W. Colloids and Interfaces with Surfactants and Polymers – An Introduction. [s.l: s.n.]. v. 7

GREEN, D. W. et al. Surfactant Flooding. [s.l: s.n.].

GREEN, D. W.; WILLHITE, G. P. Enhanced Oil Recovery. Richardson, Texas: Society of Petroleum Engineers Inc, 1998.

HEALY, R. N.; REED, R. L. Physicochemical Aspects of Microemulsion Flooding. Society of Petroleum Engineers Journal, v. 14, n. 5, p. 491–501, 1974.

HEALY, R. N.; REED, R. L.; STENMARK, D. . Multhiphase Microemulsion Systems. Dallas: Society of Petroleum Engineers Journal, 1976

HERNANDES DE LEON, I. B. Recuperação avançada de óleo viscoso por injeção de polímero em diferentes temperaturas. 2015.

HICKS, P. J. X-Ray Computer-Assisted Tomography for Laboratory Core Studies. Journal of Petroleum Technology, v. 48, n. 12, p. 1120–1122, 1996.

HOLMBERG, K.; JÖNSIN, B.; KRONBERG, B. Surfactants And Polymers In Aqueous Solutions. [s.l: s.n.]. v. 14

HOVE, A.; NILSEN, V.; LEKNES, J. Visualization of Xanthan Flood Behavior in Core Samples by Means of X-Ray Tomography. SPE Reservoir Engineering, v. 5, n. 4, 1990.

HUH, C. Interfacial tensions and solubilizing ability of a microemulsion phase that coexists with oil and brine. Journal of Colloid And Interface Science, v. 71, n. 2, p. 408–426, 1979.

HUIFEN, X. et al. Effect of Elastic Behavior of HPAM Solutions on Displacement Efficiency Under Mixed Wettability Conditions. Society of Petroleum Engineers, 2004.

HUNT, P. K.; ENGLER, P.; BAJSAROWICZ, C. Computed Tomography as a Core Analysis Tool: Applications, Instrument Evaluation, and Image Improvement Techniques. Journal of Petroleum Technology, v. 40, n. 9, p. 1203–1210, 1988.

JIANG, H. et al. The Effect of Elasticity on Displacement Efficiency in the Lab and Results of High Concentration Polymer Flooding in the Field. Spe, n. 1, p. 1–6, 2008.

KREMESEC, V. J.; TREIBER, E. Effect of System Wettability on Oil Displacement by Micellar Flooding. 1978.

LAKE, L. W. Enhanced Oil Recovery. Facsimile ed. Englewood Cliffs: Prentice-Hall, 1991.

LEVITT, D. B.; POPE, G. A. Selection and Screening of Polymers for Enhanced-Oil Recovery. Society of Petroleum Engineers, n. April, p. pp.1-18. SPE-113845, 2008.

LIU, S. et al. Favorable Attributes of Alkaline-Surfactant-Polymer Flooding. SPE Journal, v. 13, n. 1, p. 5–16, 2008a.

LIU, S. et al. ASP Process: Wide Range of Conditions for Good Recovery. SPE Symposium on Improved Oil Recovery, p. 1–18, 2008b.

LLAVE, F. M. et al. Phase Behavior and Oil recovery investigations using mixed and alkaline-Enhanced surfactant systems. Bartlesville, Oklahoma: [s.n.].

LONDON, M. et al. Waterflooding Experiments with X-ray CT Imaging. SPE Heavy Oil Conference, p. 1–15, 2014.

LOPES, L. F.; SILVEIRA, B. M. O.; MORENO, R. B. Z. L. Rheological Evaluation of HPAM fluids for EOR Applications. International Journal of Engineering & Technology IJET-IJENS, v. 14, n. 3, p. 35–41, 2014.

LOPEZ SALINAS, J. L. et al. Viscometer for Opaque, Sealed Microemulsion Samples. SPE International Symposium on Oilfield Chemistry, v. m, 2009.

LORENZ, P. B.; BROCK, S. Surfactant and Consurfactant properties of mixed and polysulfonated surfactant by phase volume measurements. Bartlesville, Oklahoma: [s.n.].

MAITI, S. N.; MAHAPATRO, P. K. Melt rheological properties of nickel powder filled

polypropylene composites. Polymer Composites, v. 9, n. 4, p. 291–296, 1988.

MAMUDU, A.; TAIWO, O. A.; OLAFUYI, O. Cubic Spline and Graphical Techniques for Determining Unsteady State Relative Permeabilities in Field Cores. 2016.

MAMUDU, A.; TAIWO, S.; OLAFUYI, O. Comparative Approach to Relative Permeability Predictions. n. August, 2017.

MELO, M. A. et al. Evaluation of Polymer Injection Projects in Brazil. Latin American and Caribbean Petroleum Engineering Conference, p. 17. SPE-94898, 2005.

MELO, M. A. DE et al. Polymer Injection Projects in Brazil : Dimensioning , Field Application and Evaluation. SPE/DOE Thirteenth Symposium on Improved Oil Recovery, p. 11, 2002.

MELO, M. DE; LUCAS, E. Characterization and Selection of Polymers for Future Research on Enhanced Oil Recovery. Chemistry & Chemical Technology, v. 2, n. 4, p. 295–303, 2008.

MELROSE, J. C. Role of Capillary Forces In Detennining Microscopic Displacement Efficiency For Oil Recovery By Waterflooding. Journal of Canadian Petroleum Technology, v. 13, n. 4, p. 9, 1974.

MENDONÇA, J. L. G. DE; COCHAR GUTIERRE, T. M. OS AQUÍFEROS BOTUCATU E PIRAMBÓIA NO ESTADO DE SÃO PAULO: NOVOS MAPAS DE ISÓBATAS DO TOPO, ESPESSURA E NÍVEL D'ÁGUA. X Congresso Brasileiro de Águas Subterrâneas 1. Anais...1998

MOORE, T. F.; SLOBOD, R. L. Displacement of Oil by Water-Effect of Wettability, Rate, and Viscosity on Recovery. Fall Meeting of the Petroleum Branch of AIME, 1955.

MORROW, N. R. Interplay of Capillary, Viscous and Buoyancy Forces in the Mobilization of Residual Oil. Journal of Canadian Petroleum Technology, v. 18, n. 3, p. 35–46, 1979.

MULLER, G. Thermal stability of high-molecular-weight polyacrylamide aqueous solutions. Polymer Bulletin, v. 5, n. 1, p. 31–37, 1981.

NAJAFABADI, N. F. et al. Formulations for a three-phase, fully implicit, parallel, EOS compositional surfactant-polymer flooding simulator. Journal of Petroleum Science and Engineering, v. 86–87, p. 257–271, 2012.

NASR-EL-DIN, H. A et al. Viscosity Behavior of Alkaline, Surfactant, Polyacrylamide Solutions Used for Enhanced Oil Recovery. Spe Oilfield Chem. Int. Symp. (Anaheim, Calif, 2/20-22/91) Proc., p. 293–306, 1991.

NEEDHAM, R. B.; CO, P. P.; DOE, P. H. Polymer Flooding Review. Journal of Petroleum Technology, n. December, p. 1503–1507, 1987.

NISHIMI, T. The formation of middle-phase microemulsions of polar oils. Macromolecular Symposia, v. 270, n. 1, p. 48–57, 2008.

PACHÓN CONTRERAS, Z. DEL P. et al. Petroleum Sulfonates Preparation and Evaluation for Chemical Enhanced Oil Recovery in Colombian Oil Fields. Ciencia, Tecnología y Futuro, v. 5, p. 55–73, 2014.

PERTTAMO, E. K. Characterization of Associating Polymer (AP) Solutions. Department of Physics and Technology, Centre for Integrated Petroleum Research, v. Master, n. May, p. 145, 2013.

POLLARD, J. M.; SHI, A. J.; GÖKLEN, K. E. Solubility and partitioning behavior of surfactants and additives used in bioprocesses. Journal of Chemical and Engineering Data, v. 51, n. 1, p. 230–236, 2006.

POPE, G. A. et al. The effect of several polymers on the phase behavior of micellar fluids. Society of petroleum engineers journal, v. 22, n. 6, p. 816–830, 1982.

REED, R.; HEALY, R. Some physicochemical aspects of microemulsion flooding: a review. Improved Oil Recovery by Surfactant and Polymer Flooding, p. 383–437, 1977.

REICHENBACH-KLINKE, R. et al. Hydrophobic Associative Copolymer with Favourable Properties for the Application in Polymer Flooding. SPE International Symposium on Oilfield Chemistry., p. 1–11, 2011.

RICHARD PASHLEY; KARAMAN, M. Applied Colloid and Surface Chemistry. Appliied Colloid and Surface Chemistry, v. 143, p. 188, 2004.

RIOS, V. D. E. S. Recuperação de Óleo por Injeção de Polímeros – Abordagens Experimental, Analítica e Numérica em Pequena Escala. 2014.

ROSEN, M. J. Surfactants and interfacial phenomena. [s.l: s.n.]. v. 40

RUCKENSTEIN, E. Microemulsions, Macroemulsions, and the Bancroft Rule. Langmuir, v. 12, n. 26, p. 6351–6353, 1996.

SAGI, A. R. et al. Laboratory Studies for Surfactant Flood in Low-Temperature Low-Salinity Fractured Carbonate Reservoir. SPE International Symposium on Oilfield Chemistry, 8-10 April, The Woodlands, Texas, USA, n. April, 2013.

SALAGER, J. L. Physio-Chemical Properties of Surfactant-Water-Oil Mixtures: Phase Behavior, Microemulsion Fomration and Interfacial Tension. [s.l.] University of Texas at Austin, 1977.

SALTER, S. J. Optimizing Surfactant Molecular Weight Distribution I. Sulfonate Phase Behavior and Pysical Properties. 1983.

SAMANTA, A. et al. Effects of alkali, salts, and surfactant on rheological behavior of partially hydrolyzed polyacrylamide solutions. Journal of Chemical and Engineering Data, v. 55, n. 10, p. 4315–4322, 2010.

SAMANTA, A. et al. Surfactant and Surfactant-Polymer Flooding for Enhanced Oil Recovery. Advances in Petroleum Exploration and Development, v. 2, n. 1, p. 13–18, 2011.

SANABRIA, F. C. B. Avaliação da injeção de surfactantes como método de recuperação avançada em reservatórios de arenito. p. 134, 2013.

SANDERSEN, S. B. Enhanced Oil Recovery with Surfactant Flooding. [s.l.] Technical University of Denmark, 2012.

SCHRAMM, L. L. Surfactants, Fundamentals and Applications in the Petroleum Industry. [s.l: s.n.].

SHAMEEM, S.; KHAMEES, A. Dual-Energy CT-Scanning Applications in Rock Characterization. Proceedings of SPE Annual Technical Conference and Exhibition, 2004.

SHANDRYGIN, A.; LUTFULLIN, A. Current Status of Enhanced Recovery Techniques in the Fields of Russia. SPE Annual Technical Conference and Exhibition, n. September 2008, p. 21–24, 2008.

SHARMA, B. C.; BRIHGAM, W. E.; CASTAINER, L. M. CT Imaging Techniques for Two-Phase and Three-Phase In-Situ Saturation Measurements. Tulsa: [s.n.].

SHENG, J. J. Modern Chemical Enhanced Oil Recovery. [s.l.] Elsevier, 2011.

SHENG, J. J. Enhanced Oil Recovery Field Case Studies. [s.l.] Elsevier, 2013.

SHENG, J. J. Status of surfactant EOR technology. Petroleum, v. 1, n. 2, p. 97–105, 2015.

SHENG, J. J.; LEONHARDT, B.; AZRI, N. Status of Polymer-Flooding Technology. Journal of Canadian Petroleum Technology, v. 54, n. 2, p. 116–126, 2015.

SHUPE, R. D. Chemical Stability of Polyacrylamide Polymers. Journal of Petroleum Technology, v. 33, n. 8, p. 1513–1529, 1981.

SILVEIRA, B. M. O.; LOPES, L. F.; MORENO, R. B. Z. L. Rheological Approach of HPAM Solutions under Harsh Conditions for EOR Applications. n. 3, p. 1–8, 2016.

SORBIE, K. S. Polymer-improved oil recovery. New York: Springer Science & Business Media., 2013.

SOTO, D.; SUAREZ, A. Sand-Selective Optimization Methodology reduces Water Cut and Improves Production in Mature Fields : San Francisco , Colombia. 2011.

STOLL, W. M. et al. Alkaline / Surfactant / Polymer Flood : From the Laboratory to the Field. SPE Reservoir Engineering, v. 14, n. 6, p. 702–712, 2011.

STOSUR, G. J. et al. The Alphabet Soup of IOR, EOR and AOR: Effective Communication Requires a Definition of Terms. SPE International Improved Oil Recovery Conference in Asia, v. SPE 84908, p. 1–3, 2003.

SUAREZ, A. F. et al. Beating the Marginal Well Performance in a Mature Field: San Francisco

Field in Colombia. SPE Latin American and Caribbean Petroleum Engineering Conference, 2005.

TABER, J. J.; MARTIN, F. D.; SERIGHT, R. S. EOR Screening Criteria Revisited - Part 1: Introduction to Screening Criteria and Enhanced Recovery Field Projects. SPE Reservoir Engineering, v. 12, n. 3, p. 189–198, 1997.

TELES, E. O. et al. Reactivation of Mature Oilfields: A Multifaceted Production Management. International Journal of Materials, Mechanics and Manufacturing, v. 4, n. 1, p. 36–39, 2015.

THAKUR, S.; BEHBEHANI, S.; DERNAIKA, M. Advanced Rock Characterization by Dual-Energy CT Imaging : A Novel Method for Complex Reservoir Evaluation. 2014.

THURSTON, G. B.; SALAGER, J. L.; SCHECHTER, R. S. Effects of salinity on the viscosity and birefringence of a microemulsion system. Journal of Colloid And Interface Science, v. 70, n. 3, p. 517–523, 1979.

TIAB, D.; DONALDSON, E. C. Petrophysics. p. 889, 2004.

URBISSINOVA, T. S.; TRIVEDI, J. J.; KURU, E. Effect of elasticity during viscoelastic polymer flooding: A possible mechanism of increasing the sweep efficiency. Journal of Canadian Petroleum Technology, v. 49, n. 12, p. 49–56, 2010.

VIDAL PRADA, J. C. Factibilidad del uso de álcalis orgánicos como sustitutos de álcalis inorgánicos para recobro químico de crudo de los cmapos Dina cretáceo y San Francisco. [s.l: s.n.].

VINEGAR, H. J.; WELLINGTON, S. L. Tomographic imaging of three-phase flow experiments. Review of Scientific Instruments, v. 58, n. 1, p. 96–107, 1987.

WANG, D. et al. Viscous-Elastic Fluids Can Mobilize Oil Remaining After Water-Flood By Force Parallel To the Oil-Water Interface. Spe Asia Pacific Impr. Oil Recovery Conf. [Apiorc 2001] (Kuala Lumpur, Malaysia, 10/8-9/2001) Proc., 2001.

WANG, D. et al. The Influence of Viscoelasticity on Displacement Efficiency - From Micro-To Macroscale. SPE annual techinical conference, 2007.

WANG, S.; AYRAL, S.; GRYTE, C. Computer-Assisted Tomography for the Observation of Oil Displacement in Porous Media. Society of Petroleum Engineers Journal, v. 24, n. 1, p. 53–55, 1984.

WANG, Y. et al. Optimized Surfactant IFT and Polymer Viscosity for Surfactant- Polymer Flooding in Heterogeneous Formations. SPE Improved Oil Recovery Symposium, p. 1–11, 2010.

WELLINGTON, S. L.; VINEGAR, H. J. X-Ray Computerized Tomography. Journal of Petroleum Technology, v. 39, n. 8, p. 885–898, 1987.

WEVER, D. A. Z.; PICCHIONI, F.; BROEKHUIS, A. A. Polymers for enhanced oil recovery: A paradigm for structure-property relationship in aqueous solution. Progress in Polymer Science (Oxford), v. 36, n. 11, p. 1558–1628, 2011.

WITHJACK, E. M. Computed Tomography for Rock-Property Determination and Fluid-Flow Visualization. SPE Formation Evaluation, n. December, p. 696–704, 1988.

WITHJACK, E. M.; DEVIER, C.; MICHAEL, G. The role of x-ray computer tomography in core analysis. SPE Western Regional/AAPG Pacific Section Joint Meeting, n. SPE Paper #83467, p. 12, 2003.

WU, F.-T.; CAETANO-CHANG, M. R. Estudo mineralógico dos arenitos das formações Pirambóia e Botucatu no Centro-Leste do Estado de São Paulo. Revista do Instituto Geológico, v. 13, n. 1, p. 58–68, 1992.

WYATT, K.; PITTS, M.; SURKALO, H. SPE 113126 Economics of Field Proven Chemical Flooding Technologies. Technology, n. April, p. 19–23, 2008.

ZHANG, D. L. et al. Favorable Attributes o f Alkali-Surfactant-Polymer Flooding. 2006.

ZHANG, Z.; LI, J.; ZHOU, J. Microscopic Roles of “Viscoelasticity” in HPMA polymer flooding for EOR. Transport in Porous Media, v. 86, n. 1, p. 199–214, 2011.

ZHOU, G.; WILLETT, J. L.; CARRIERE, C. J. Temperature dependence of the viscosity of highly starch-filled poly(hydroxy ester ether) biodegradable composites. Rheologica Acta, v. 39, n. 6, p. 601–606, 2000.

ZHU, D. et al. Aqueous hybrids of silica nanoparticles and hydrophobically associating hydrolyzed polyacrylamide used for EOR in high-temperature and high-salinity reservoirs. Energies, v. 7, n. 6, p. 3858–3871, 2014.